ADDIS ABABA UNIVERSITY

ADDIS ABABA INSTITUTE OF TECHNOLOGY

SCHOOL OF CIVIL AND ENVIRONMENTAL ENGINEERING

Fire Resistance of Concrete Filled Steel Tube Column under Axial Load

A Thesis in Structural Engineering

By Bereket Adamu

May, 2021

Addis Ababa

A Thesis

Submitted in Partial Fulfillment of the Requirements for the Degree of Master of Science

APPROVAL

The undersigned have examined the thesis entitled '**Fire Resistance of Concrete Filled Steel Tube Columns under Axial Load**' presented by **Bereket Adamu**, a candidate for the degree of **Master of Science in Structural Engineering** and hereby certify that it is worthy of acceptance.

Dr. Bedilu Habte		
Advisor	Signature	Date
Dr. Abreham Gebre		
Internal Examiner	Signature	Date
Dr. Esayas G/Yohannes		
External Examiner	Signature	Date
Dr. Ing. Mebruk Mohammed		
Chairman	Signature	Date

UNDERTAKING

I certify that research work titled “Fire Resistance of Concrete Filled Steel Tube Column under Axial Load” is my work. The work has not been presented elsewhere for assessment. Where material has been used from other sources it has been properly acknowledged/referred.

Bereket Adamu Abebe		
Name of Student	Signature	Date

.

ACKNOWLEDGMENTS

First and foremost, I would like to thank the almighty God for his unending blessings and gave me health to carry out this research.

I am very grateful to express my deepest gratitude to my advisor Dr. Ing. Bedilu Habte for his unreserved assistance, constructive and timely comments at all stages of my work.

Finally, I have no words to express my warm feeling of appreciation and thanks to my family, friends, and colleagues for their lovely encouragement to complete this work.

TABLE OF CONTENTS

LIST OF TABLES

LIST OF FIGURES

LIST OF SYMBOLES

CFST	Concrete filled steel tube
αi	Sensitivity factor
CoV	Coefficient of variation
D	Diameter of the column
D/t	Diameter to thickness ratio
EC2	Eurocode 2 Part 1-2 (EN 1992-1-2)
EC3	Eurocode 3 Part 1-2 (EN 1993-1-2)
EC4	Eurocode 4 Part 1-2 (EN 1994-1-2)
FEM	Finite element modeling
FR	Fire-resistance
F-F	Fixed-Fixed boundary condition
P-F	Pinned-Fixed boundary condition
fc	Compressive cylinder strength of concrete at room temperature
fy	Yield strength of structural steel at room temperature
hj	Thermal gap conductance
L	Length of the column
q	Heat flux
T	Temperature
t	The thickness of the steel tube
n = N/NRd	Axial load level
λ	Slenderness ratio
Ui	Uncertainty Coefficient
αc	Concrete thermal expansion coefficient
αs	Steel thermal expansion coefficient

ABSTRACT

Concrete-filled steel tube (CFST) structural sections are an effective, sustainable and attractive option in multi-story buildings and are becoming increasingly common in modern construction practice around the world. Whilst the analysis and design of these elements at ambient temperatures is well understood but their response to higher temperatures is still under study. This paper concerns to analyze the effect of different parameters on the fire resistance of the CFST column under axial load. The research is conducted using non-linear finite element analysis software (ABAQUS 2020). Latin Hypercube Sampling (LHS) technique is applied to see the effect of five parameters: Diameter to steel tube thickness ratio (D/t), compressive strength of concrete (f_c), load ratio (n), the yield stress of steel (f_y), and slenderness ratio (λ) on the axial deformation and fire resistance of CFST column. The effect of cross-sectional shape and support conditions is also investigated. From this analysis, it was found that the load ratio, slenderness ratio, and diameter to thickness ratio have a moderate effect on the result of fire resistance and axial deformation. Among these, the slenderness ratio is the most influential parameter on fire resistance and axial deformation determination. Whereas, from the case of support condition, Fixed-Fixed supported CFST columns have higher fire resistance than pinned-fixed supported CFST columns.

Key Words: Concrete filled steel tube column; Fire resistance; 3-D finite element model

CHAPTER 1 INTRODUCTION

1.1 Background

Composite structures in the general definition consist of two or more different materials with significantly different properties in such a manner that the materials directly interact with each other. The combination of concrete and steel in a single structural member gives an advantage for the good qualities and a recognized strategy in the building industry at this time. Concrete-filled steel tubular (CFST) columns are one type of composite column so that the combined action of steel and concrete gives a special structural property. In this case, the compressive strength of the concrete element increases due to the passive confinement that the steel tube generates on the concrete core. At the same time, the effect of local buckling of the steel tube is modified due to the filling of the concrete core which keeps it from getting failure soon. A concrete-filled steel tubular (CFST) structure consists of a steel tube of circular, square, rectangular, or elliptical cross-section filled with plain or reinforced concrete. CFST columns have many positive rewards at normal temperature for the building industry: high load-bearing capacity with smaller cross-section size, beautiful appearance, high stiffness and ductility, high seismic resistance, and reduced construction cost and time since no form work is required.

Fire safety has become a significant concern in building design especially after the break down of the World Trade Center twin towers. Different researches were studied on the fire resistance of the CFST column. The fire resistance of the concrete-steel tubular column increases due to the influence of the concrete infill and can achieve an elevated temperature without external fire protection.

In this study, the analysis effect of fire on CFST column under axial load is investigated by varying different parameters with material property and geometrical section variations.

1.2 Statement of the problem

In recent times our world has higher exposure to fire attacks due to human civilization as well as their consequence on building structures. The structural behavior of columns under fire becomes essential since it concerns the safety of the building and people inside in case

of fire event occurs. Since steel structures are much sensitive to fire attack than concrete structures it is necessary to evaluate the effect of fire on concrete-filled steel tube structures as they are used for high rising buildings. This research presents Fire resistance of concrete-filled steel tubular column under axial load.

1.3 Objective

1.3.1 General objective

The main objective of this paper is to analyze the fire resistance of Concrete filled steel tubular (CFST) columns with different parameters using the global three-dimensional Finite element simulation software (ABAQUS 2020).

1.3.2 Specific objectives

- To study the effect of cross-section and support condition on the fire resistance of CFST column.
- To study the effect of outer diameter to Steel tube thickness ratio (D/t) of the cross-section, compressive strength of concrete (fc), load ratio (μ), yield strength of steel (fy), and slenderness ratio (λ) on the fire resistance of CFST column under axial load.

1.4 Scope of the research

This research generally relies on the analysis part of the fire resistance of the CFST column. Slender columns with a circular and square cross-section and fixed-fixed and pinned-fixed columns are considered. The effect of five parameters: diameter to steel tube thickness ratio (D/t), Compressive strength of concrete (fc), Loading ratio (n), yielding stress of steel (fy) and slenderness ratio (λ) are taken to see the impact of geometry and material condition. In this research, no physical test has been carried out. Experimental data are taken from literature and no reinforcement is provided on the filled concrete (Plain concrete is filled in the steel tube). The design phase is not studied in this paper.

1.5 Methodology of the study

The following methods are applied to accomplish the objective of the research.

i. Data collection for numerical Analysis of CFST columns is done by defining proper values for parameters from previous works.
ii. Buckling mode shape is analyzed as a first model to account for imperfection on the stress analysis stage.
iii. Heat transfer analysis of the CFST column is conducted using the FEM simulation package called ABAQUS.
iv. Non-linear stress analysis of CFST columns is done by taking the input value of nodal temperatures as filled input value which is done from the heat transfer analysis and adding imperfection of the column from the first model.
v. Fire resistance duration of the column with axial deformation versus times plot are extracted from the above steps and verified with previous works of literature for comparison.
vi. A parametric study is conducted to access their effect on fire resistance of CFST column.
vii. Finally, a conclusion is made based on the results, and recommendations are put for further study.

1.6 Organization of the Thesis

The first chapter is the introduction part. In this chapter, the general background of the study is presented. The statement of the problem, the objective of the research, scope, and limitation of work, and the methodology are included. The second chapter concerns a Literature review regarding the fire resistance of concrete-filled steel tube column will be presented. Chapter three deals with the thermal and mechanical properties of materials used in calculations and the finite element modeling methods. The fourth chapter deals with the verification of the finite element modeling and the sampling technique used to explore the effect of different parameters. The fifth chapter concerns the parameteric nad sensitivity analysis on the output results of non-linear finite element model taken from LHS sampling technique. Finally, in chapter six conclusion and recommendation will be covered.

CHAPTER 2 LITERATURE REVIEW

2.1 General

In the previous years, Concrete Filled Steel Tube (CFST) columns become widely useful in the construction of high-rise buildings due to their fine-looking appearance and they become popular with architects and structural engineers. This is due to their appreciable advantages such as high load resistance capacity and ductility, high earthquake resistance, and reduction in cross-section, attractive visual aspect, very fast construction, and cost-saving appearance in building construction technology, and relatively higher fire resistance without using external protection. CFST columns can reach higher fire resistance times without external protection due to the temperature drop-down effect of the core concrete infill that holds the go-up temperature in the cross-section and the coverage of the steel tube protects the core concrete from direct vulnerability and keeping on its wholeness. However, the main drawback of the CFST column is that the steel tube is exposed, thus leading to a lower fire resistance compared to concrete-encased steel composite columns or even conventional RC columns.

2.2 Advantage of CFST columns on Building structures

As previously stated, the Concrete Filled Steel Tube (CFST) column section supplies a lot of benefits that make this technology attractive for architects and structural designers (Lu, Han, and Zhao, 2010)(Han et al. 2013). The usefulness of CFST columns to new designs has become an important issue in the previous decades mainly due to the following advantages of these types of composite elements over other classic structural members.

Economic advantage

- This technology allows a higher efficiency in the construction process because the steel tube can bear a substantial amount of construction loads before pumping concrete.
- No additional formwork is needed for concrete pouring since the steel tube acts simultaneously as formwork and external reinforcement for the concrete core. Likewise, equipment used for casting normal concrete structures can be employed and no extra machinery is needed.

- Problems related to connections rarely appear as a result of the modern assembly techniques currently used in structural engineering. Therefore, these helps and allows prefabrication on the plant and a fast and dry assembly on site.
- The hardening of concrete does not block the construction process. The time for assembly and erection is short without and delay which implies waiting time and reduced costs.

Structural advantages

- The steel tube applies passive confinement to the concrete core and increases its load-bearing capacity. In addition to these inward local buckling of steel tube is improved due to the support of the concrete core.
- CFST columns have higher seismic resistance than unfilled steel hollow sections due to their higher energy absorption and ductility during an earthquake.
- The influence of the concrete core makes the steel tube section highly rigid and higher load-bearing capacity. Therefore, even slender columns can resist higher loads without increasing the external dimension. To escalate these effects, reinforcing bars can be applied.

Architectural advantage

- The overall functional floor area increases due to the reduced dimension of the column cross-section for a certain design load.
- The visible steel tube allows different kinds of architectural designs with different surface finishing's because of the reduction in the external surface area of the column and more off it decreases the coating cost under painting and corrosion protection.

Fire resistance advantages

- The Fire resistance of steel tubular columns increases due to the influence of the core concrete infill.
- The use of reinforcement enhances the fire resistance of the CFST column without the need for external fire protection as shown in Figure 2-1 for circular hollow section (CHS) and square hollow section (SHS).

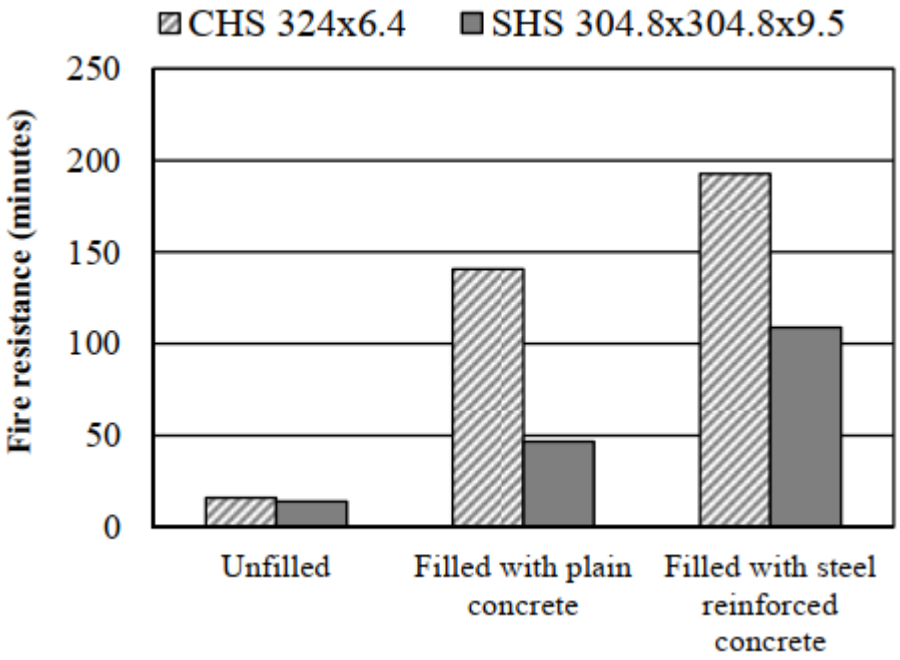

Figure 2-1: Fire resistance enhancement achieved by filling steel hollow section column with concrete (Adapted from (Lu, Han and Zhao, 2010))

2.3 Previous researches on fire resistance of concrete-filled steel tube columns

Many types of research are done to conduct the consequence of different parameters on the fire resistance characteristics of CFST columns. It has been determined that the fire resistance increases with increased compressive strength of concrete and cross-sectional dimension. The cross-sectional geometry of the column has a vital effect on the fire resistance of the CFST column. This increase in fire resistance is due to the high load-carrying capacity of the column with an increase in cross-sectional size. In addition to the cross-sectional size the concrete core takes a longer time to reach the critical temperature at which the column will collapse ((Espino's, Romero and Hospitaler, 2012); (Han et al., 2013); (Kodure, 1998)). Concrete strength delivers a moderate effect on fire resistance on CFST columns. Other parameters like Load level, steel ratio, and slenderness ratio have inverse proportionality with fire resistance of CFST column.

It has been determined that for columns with higher fire resistance especially for stocky columns, the steel tube thickness has inversely proportional with fire resistance of the column (Kodure, 1998) and (Espinos, Romero and Hospitaler, 2012). At the time of fire

exposure, firstly the steel tube holds the enforced load or applied load due to its high expansion. When the temperature rises the steel tube strength gradually decreases and the load is transferred to the concrete. In these times the inside temperature in the concrete is still relatively low because of the external protection of steel tube and low thermal conductivity of concrete. Now the concrete gets responsible for carrying the entirely load till the column fails. As the steel tube thickness increases there is an indication of an increase in load transferred to the concrete, which results to a reduction in fire resistance of the column.

However, for lower fire resistance (below one hour) columns especially for slender columns, an increase in steel tube thickness results in a fire-resistance increase. This type of CFST column starts failure too soon due to global and local buckling of the steel tube. More so during the failure of the column the tube is still contributed importantly in load carrying and therefore as the steel tube thickness increases the column adds its strength by substituting the concrete with high strength material of steel tube and its help's by retarding happening of local buckling.

Due to the reason that the steel tube shell of the square CFST column is more subjected to local buckling than circular CFST column, the circular columns have higher fire resistance than square columns according to (Lie and Stringer, 1993). Local buckling decreases the containment of concrete and permits the occurrence of spalling. Additionally, unequal distribution of temperature field arises in the shape of square CFST columns during the fire and gives bigger internal stress in concrete than circular CFST columns. And this internal stress reduces the load-resistance capacity of the square CFST column.

According to (Kodur, 2007) the type of concrete affects fire resistance. Two types of aggregates are used to develop concrete mixture, carbonate aggregates, and siliceous aggregates. Carbonate aggregates have fire resistance 10-20% more than siliceous aggregate concrete. This is due to the higher heat capacity of carbonate aggregate than siliceous aggregate which takes place in an endothermic reaction in carbonate aggregate around $700^{\circ}C$, which delays the increase in temperature of concrete during fire exposure.

One of the most effective way to improve the fire resistance of CFST column if covering with fire protection coating. (Han et al., 2003) reported 11 CFST fire tests on square and rectangular columns with and without fire protection. It was clear to found that the fire

protection causes a delay in the temperature field within the cross-section. And this delay increases by increasing the protection thickness. Although fire protection has a significant effect in improving the fire resistance of CFST columns, it also has some drawbacks: fire protection takes a high price, care must be taken while applying, and also frequent maintenance is required. One of the main disadvantages of using fire protection is that it reduces the usable floor area as a result of increasing the column width.

To improve the fire resistance of CFST columns and to overcome fire protection disadvantages, researchers tried two different ways other than fire protection. The first method is to use fiber-reinforced concrete (FC) or reinforced concrete (RC) as infill for the steel tube instead of plain concrete (PC). According to (Kodur and Lie, 1995) RC has a significant effect in increasing the fire resistance of CFST columns than FC, especially in eccentrically loaded columns.

While simulating the response of a structure exposed to fire, it is predominant to accurately and efficiently estimate the temperature growth within structural members (Gardner and Ng 2006). This is due to the reason that heat has a substantial influence on the mechanical properties (e.g., strength, modulus of elasticity, and deformation capacity) of structural components. Generally, the higher the temperature the more quickly the material deteriorates. An overestimate of temperature within a structure will lead to an increase in the thickness of insulating material and it causes more material to be used to safely resist the load. Then again, an underestimate of temperature may lead to dangerous structural design.

In the previous years, Experimental tests have been carried on to inquire about the fire resistance of CFST columns (Lie, T.T. and Chabot, 1992). In the meantime, numerical models have been formulated by several researchers to carry out nonlinear heat transfer analysis and stress analysis of CFST columns under fire (Lie and Stringer, 1993), (Hong and Varma, 2009), and (Espinos et al., 2010). In these models, specific heat and thermal conductivity of steel and concrete materials were in general determined by using empirical models presented in (Eurocode 4 part 2, 2005). The influence of specific heat and thermal conductivity is generally not negligible on heat transfer as long as thermal contact conductance at the steel-concrete interface and moisture content of concrete are considered and various values are recommended but Eurocode gives a better result.

2.4 Material properties at higher temperatures

Material properties and stress-strain diagrams of concrete and steel can be affected by higher temperatures. This section focuses on the thermal and mechanical properties of concrete and steel at a higher temperature.

2.4.1 Concrete

i. Density

Generally, the density of concrete decreases with an increase in temperature. At higher temperatures, the concrete density (ρc) mainly depends on its material composition, moisture content, the nature of curing, and temperature change. The density of concrete with limestone ingredients stays constant from normal temperature conditions up to a temperature between 600°C and 900°C until the limestone de-carbonates, which depends on the heating conditions (Schneider, 1981). After de-carbonation, the density of concrete decreases highly due to loss of water and loss of carbon dioxide in the processes of de-carbonation, then due to the expansion of concrete density of concrete continues to decrease since the volume of concrete increases with constant weight.

Euro code (2005) assumes the concrete density as temperature-dependent but many analytical models assume a constant value for a concrete density as 2300 kg/m3. According to Euro code 2 (2005), the density of concrete is affected by the loss of water and it remains constant up to 115°C and decreases with an increase in temperature as shown in Figure 2-2 below.

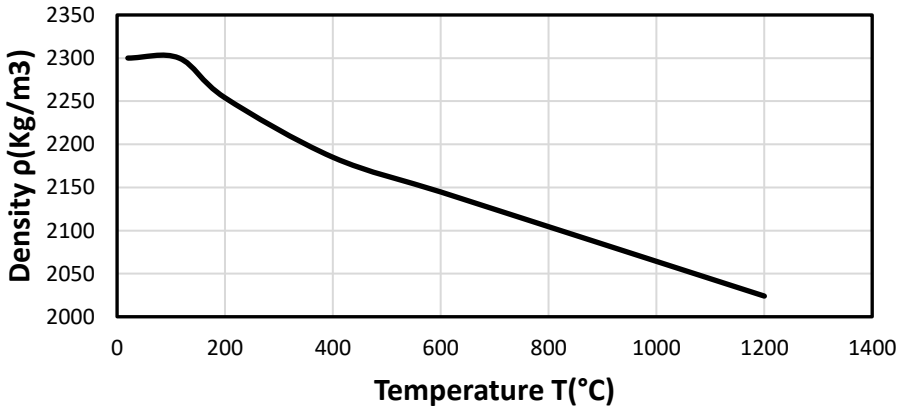

Figure 2-2 Density of concrete with variation of Temperature according to Euro code 2

ii. Thermal conductivity

Thermal conductivity can be defined as the ratio of heat flow rate to a temperature gradient, which represents a uniform flow of heat through concrete with unit thickness over a unit area subjected to a unit temperature difference among the two face to face sides. Since concrete contains moistures with different forms so that the type and amount of moisture have a substantial influence on the thermal conductivity of concrete (Kodur and Khaliq, 2011). According to (Vangeem *et al.*, 1997) concrete strength doesn't affect the thermal conductivity of concrete.

The factors that affect concrete thermal conductivity are hardened cement paste, pore volume distribution, and water content. With low temperature, the wet concrete owns higher thermal conductivity. At higher temperatures, the concrete thermal conductivity increases slightly but decreases as the temperature reaches 100°C, then it keeps decreasing as more cracking develops (Naus, 2006).

According to (Eurocode 2 part 2, 2005) thermal conductivity of concrete is modeled by showing upper and lower conductivity limits. For CFST columns the upper limit values are recommended as these values are close to the test results obtained on composite sections. Figure 2-3 shows the different values of thermal conductivity for the upper and lower limits.

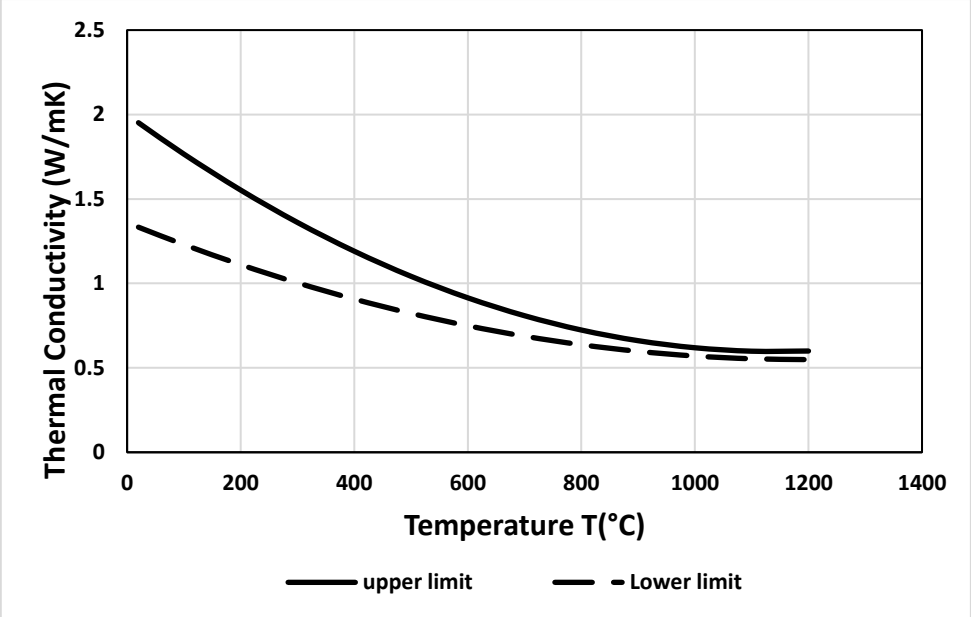

Figure 2-3 Models of thermal conductivity according to (Eurocode 2 part 2, 2005)

iii. Specific heat

Specific heat is defined as the amount of heat required per unit mass to change the temperature of the material by 1°C, and it is generally expressed in terms of heat capacity which is the product of density and specific heat. Specific heat is highly affected by moisture content, aggregate type, and density of concrete (Kodur and Khaliq, 2011).

At higher temperatures, the chemically bound water within the concrete is loosed step by step as free water, which vaporizes as part of a gas mixture. Additional heat is absorbed by the concrete during the phase change procedure and it affects the development of temperature in the concrete. When conducting heat transfer analysis, the specific heat of concrete should be revised to shine this effect, and otherwise, a complex coupled thermo-hydro-mechanical analysis is conducted but it is a difficult and time taking procedure.

When modeling to simulate concrete specific heat the (EN 1992-1-2, 2004) uses one model for all types of aggregate and the effect of water content is taken into account. It shows a peak value of specific heat in the interval between 100°C and 115°C. Figure 2-4 shows the variation of specific heat with temperature according to (EN 1992-1-2, 2004) with different values of moisture contents.

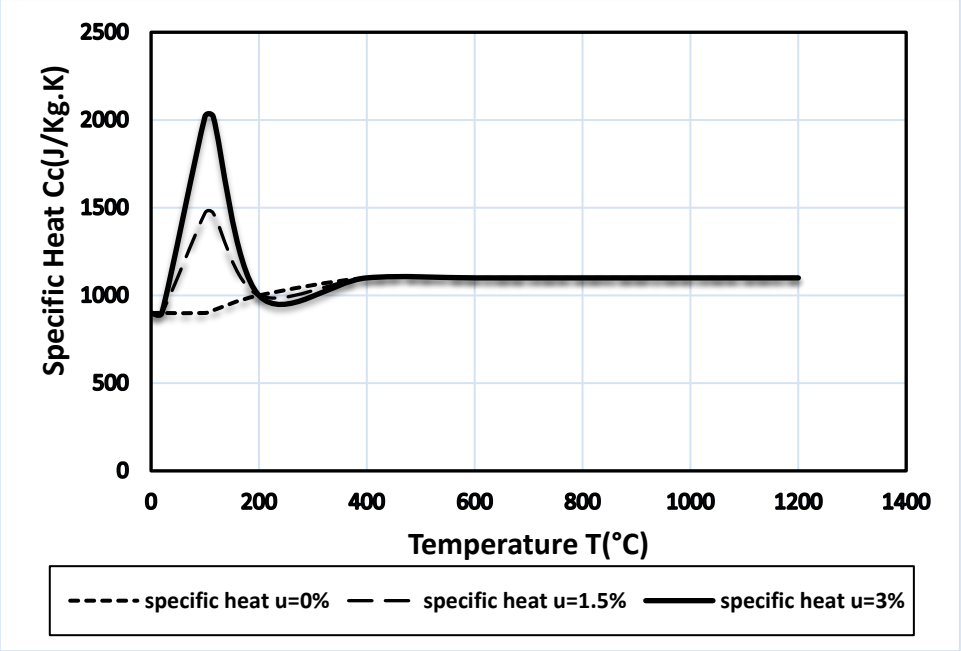

Figure 2-4 model for concrete specific heat with temperature according to (Eurocode 2 part 2, 2005)

iv. Thermal expansion

The coefficient of Thermal expansion is an important factor that affects the performance of concrete in fire conditions which represents the change of volume due to the variation of temperature. It is expressed as a change in length per degree of temperature change. The use of coefficient of Thermal expansion is looked at the amount of structural movement and thermal stress resulting from temperature change that can lead to breaking into fragments and cracking.

Due to the interaction of the two components of concrete (cement paste and aggregate), the expansion of concrete is complicated each of which has its effect on the thermal expansion coefficient. A large difference in thermal expansion of hardened cement paste and aggregate can lead to micro stresses and micro cracking that disrupt the concrete microstructure. Observations of thermal expansion of concrete can be affected by various external effects that come with the temperature change. As an example, additional volume changes are caused by a change in moisture content, chemical reactions that lead to dehydration and conversion, creep, and micro-cracking that results from non-uniform thermal stress (Naus, 2006).

Some researchers use a constant value for concrete thermal expansion as was stated (Espinos et al., 2010) and (Hong and Varma, 2009) and they both take the coefficient of

thermal expansion as $\alpha c = 6x10^{-6}$ °C. According to (Eurocode 2 part 2, 2005) the concrete thermal expansion coefficient is temperature-dependent with both siliceous and calcareous aggregates and generally, the thermal expansion of siliceous aggregates is higher than calcareous aggregates as demonstrated in Figure 2-5.

From different kinds of literature it was determined that the major factors that affect the thermal expansion of concrete can be summarized as:

- The type of aggregate and its content (especially coarse aggregate)
- Moisture content
- Temperature

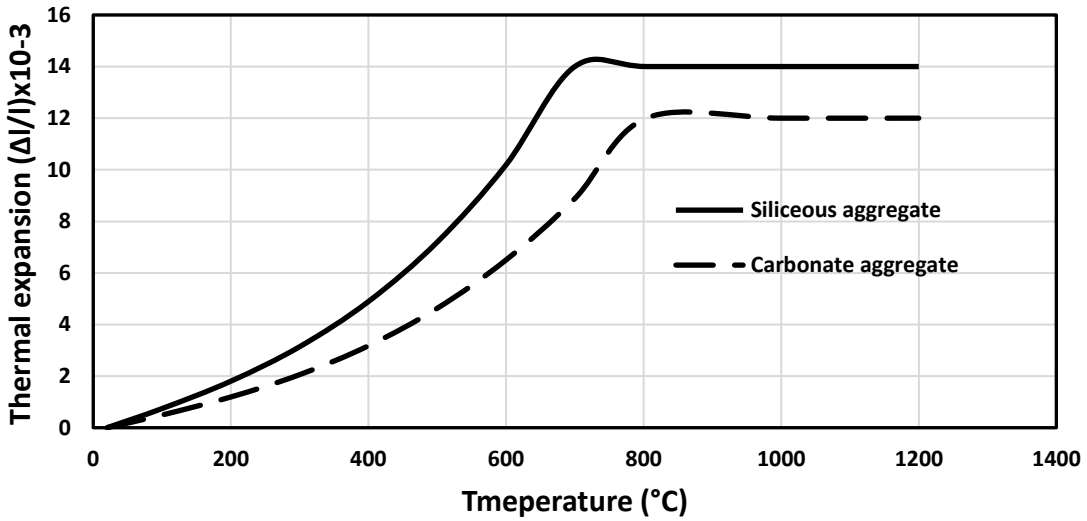

Figure 2-5 Thermal expansion of siliceous and calcareous aggregates according to EC 2 part 1.2 2005

v. Stress-strain curve

At elevated temperature, the stress-strain curve of concrete is different from the curve from that at normal temperature. With an increase in temperature modules of elasticity of concrete decreases and makes the concrete soft during a fire before the peak load is reached. Concrete has a larger ultimate strain than at ambient temperature and as the peak load is reached the descending curve part becomes bigger than at normal temperature conditions (Castillo, 1987).

The type of aggregate affects the fire resistance behavior of concrete and according to (Cheng et al, 2004) carbonate aggregates have higher fire resistance than siliceous aggregates. The compressive strength of concrete has also an effect on the fire resistance

of concrete. It has been found that high-strength concrete loses more strength than normal strength particularly at temperatures below 400°C. This is because the cement past has a trend to shrink as absorption and the water is driven out but the aggregate expands and loss of bond in concrete mixture occurs during higher temperatures. Above 400°C high strength concrete losses its compressive strength more rapidly. During this time dehydration of cement paste results in disintegration. Since there is thermal expansion above 100°C with this higher temperature the cement paste tends to shrink and the aggregate expands and their bond is weakened resulting in the reduction of concrete strength (Castillo, 1987)

(Eurocode 2 part 2, 2005) is used to model the simulation of the compressive strength of concrete during fire exposure. Figure 2-6 shows concrete strength at different elevated temperatures for these models.

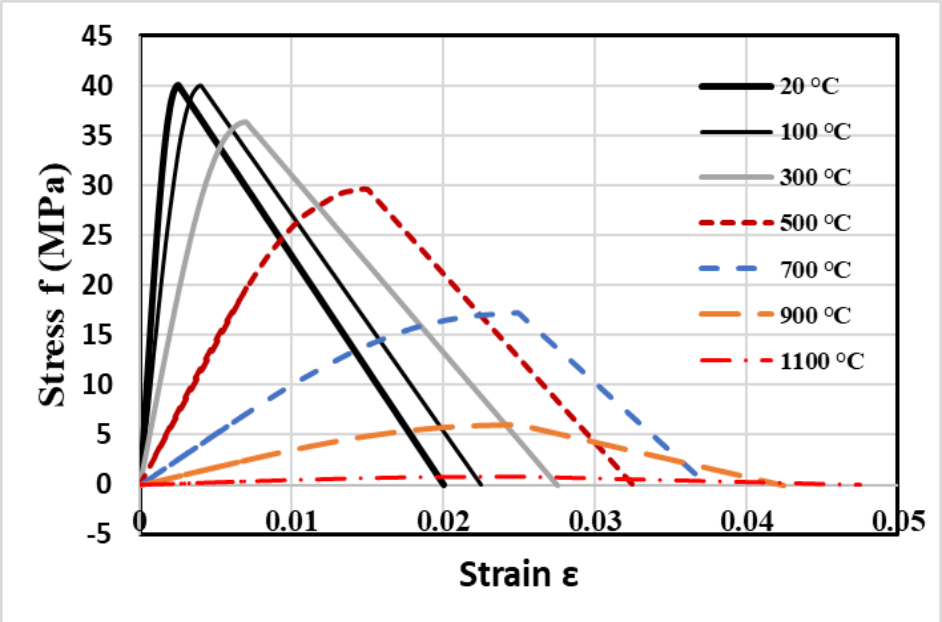

Figure 2-6 Euro Code 2 stress-strain model for concrete at elevated temperature

2.4.2 Steel

i. Density

According to (Schneider, 1981) the density of steel decreases with 13% of its ambient temperature with increasing temperature. His study was supported by the experimental result presented for steel grade S 533. But available numerical studies on (Eurocode 3 part 2, 2005) consider steel density as temperature-independent, and uses a constant value of 7850 Kg/m3. It was reasonable because the steel reaches its melting point at 1600°C.

ii. Thermal conductivity

The thermal conductivity of steel is higher than concrete. Steel thermal conductivity at 20°C decreases with increasing alloying constituents. Steel with low-alloyed metal decreases its thermal conductivity with an increase in temperature up to 800°C. While the thermal conductivity of high-alloyed steel increases with an increase in temperature. This is due to the reason that the order of crystal lattice decreases with an increase in the part of alloying constituents and influences the electronic part of the thermal conductivity (Schneider, 1981).

According to EC3, the thermal conductivity of steel decreases with an increasing temperature up to 800°C, and then it remains constant after 800°C. Figure 2-7 illustrates the thermal conductivity of steel with temperature according to EC3.

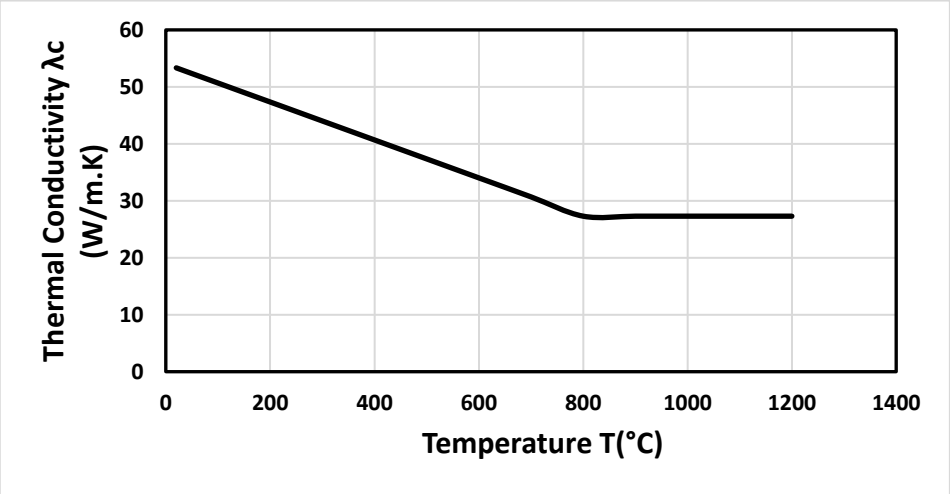

Figure 2-7 Thermal conductivity of steel according to (Eurocode 3 part 2, 2005)

iii. Specific heat

According to (Eurocode 3 part 2, 2005) the specific heat of steel material slightly increases with an increase in temperature. This increase in specific heat with temperature comes due to the movement of individual atoms in steel farther apart from their initial state and these achieve a higher energy state.

As shown in Figure 2-8 below a peak value of specific heat of steel occurred at a temperature around 750°C which is related to a phase change that occurred due to the movement of atoms. Due to this process, a large amount of heat is absorbed and that causes a peak value for the specific heat of steel.

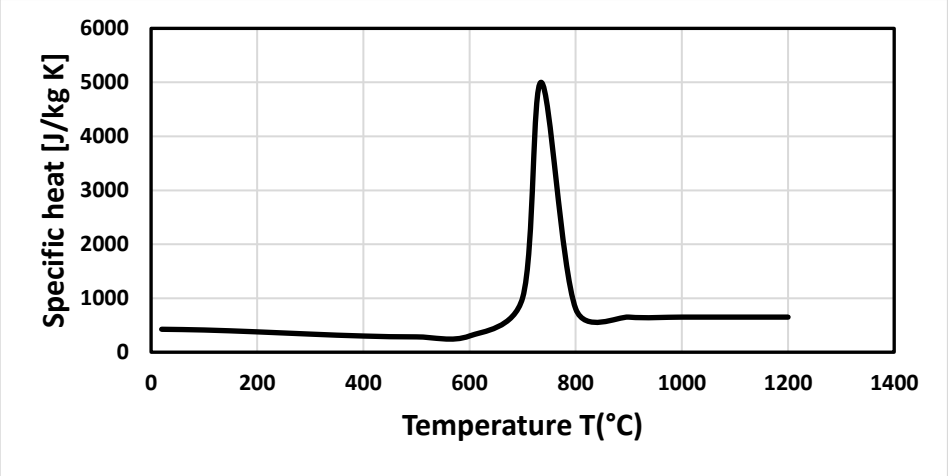

Figure 2-8 Specific heat of steel with varying temperature according to (Eurocode 3 part 2, 2005)

iv. Thermal expansion

The thermal expansion of steel according to the model proposed by (Eurocode 3 part 2, 2005) increases with an increase in temperature but stays constant around temperature values from 750°C to 860°C. The thermal expansion will be affected by the type of steel strength. Normal strength steel has higher thermal expansion than higher- strength steel and it is also predicted by Euro code with the different chemical composition of higher-strength and normal-strength steel. Figure 2-9 shows the thermal expansion model of steel proposed by Euro code 3(2005).

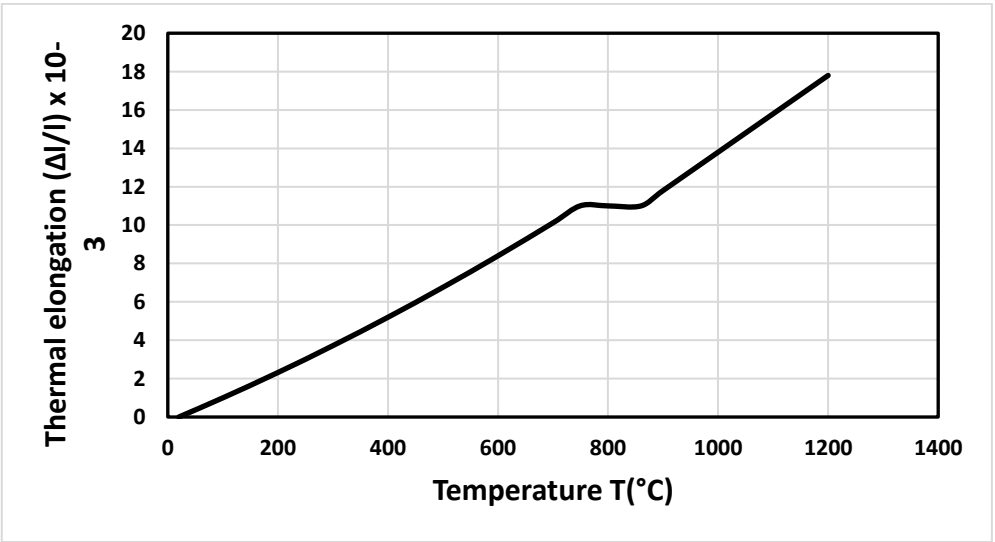

Figure 2-9 Thermal expansion of steel with temperature according to (Eurocode 3 part 2, 2005)

v. Stress-strain curve

The stress-strain curve of steel at higher temperatures is different from that at normal temperature conditions. The modulus of elasticity, yield stress, and ultimate stress values decreases with an increase in temperature. The yield strength decreases with an increase in temperature due to the movement of atoms and the undermining of the strength of steel material in the factories. (Cooke, 1988) presents that the yield strength of steel decreases with an increase in temperature and 0.2% proof stress is taken instead of the yield stress point and (Chen et al., 2006) found that the reduction factor of 0.2% proof strength and the modulus of elasticity is the same with normal-strength steel up to 540°C. Above 540°C the situation is different so that the reduction factor of 0.2% proof strength and modulus of elasticity for higher-strength steel is less than for normal strength steel.

According to Euro code 3, the two limits in the stress-strain curve of steel are distinguished as proportionality limit and yield point. The proportionality limit occurs at the end of the linear part of the stress-strain curve, after which the point that relates to the stress-strain curve remains elastic but becomes non-linear. The yield point in Euro code 3 of the stress-strain diagram is the point after which the stress-strain becomes both inelastic and non-linear. The main aim to introduce the proportionality limit in Euro code 3 at higher temperatures is to capture the behavior of the creep effect. The nonlinearity after the proportional limit indicates that the stress induces more strain than in the linear-elastic range. These simplify the stress-strain curve of steel in Euro code 3 to partially account for the higher temperature effect on creep strain so that as the temperature rises the range of proportionality limit becomes less on the stress values and it involves on the strain side. The figure below shows the variation of the stress-strain curve with temperature according to Euro code 3.

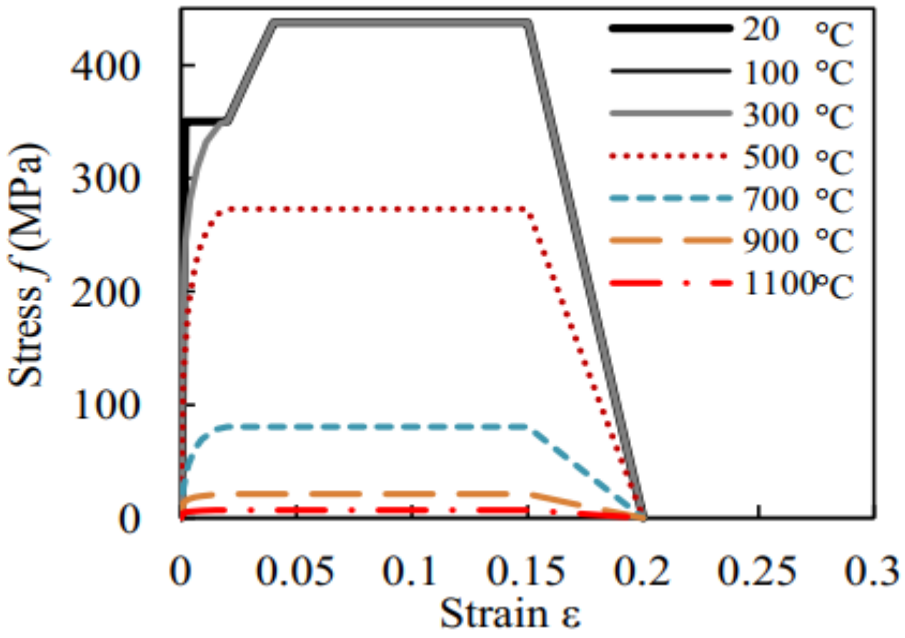

Figure 2-10 Stress-strain plot of steel at different elevated temperatures based on EC 3

CHAPTER 3 METHODOLOGY

3.1 Introduction

Abaqus finite element software (Abaqus, 2020) was used to model the fire resistance of the CFST column. There are two methods to simulate the fire resistance of the CFST column using ABAQUS. These are summarized in the following two paragraphs.

The first one is sequentially coupled thermal stress analysis, in which the thermal stress is independent of the stress analysis but the stress analysis is dependent on the thermal analysis. First thermal stress is conducted and the nodal temperature values are extracted from this step and are assigned to the stress analysis as a predefined field. In this method, the computing time is saved but less accurate than the second method. This is because the stress analysis doesn't take into consideration the change of temperature distribution, which is caused by the change in the size of the gap between the steel tube and concrete core due to the effect of the applied loading.

The second method is the fully coupled thermal analysis. In this method, both the thermal and stress analysis are strongly interdependent. Therefore, it is clear that in these methods the temperature distribution is affected by the gap between the steel tube and concrete core. As the gap between the steel tube and the concrete core widens the heat conductance decreases during loading of the column so that which causes a convergence problem. This method is accurate but it is time-consuming and it may require several days of computing time.

From the above two methods of computing the fire response of the CFST column, it is decided to use the first method called sequentially coupled thermal stress analysis to formulate the FE model because of its saving in computing time. This method also gives accurate and reasonable results as presented in studies by (Espinos et al., 2010) and (Han et al., 2013). To overcome the convergence problem, the element and mesh size in this method must be the same for both the thermal and stress analysis.

This chapter concerns the analysis of heat transfer and the stress analysis in CFST columns. The non-linear FE procedure is used to develop a numerical model using ABAQUS (2020).

3.2 Heat transfer analysis

3.2.1 Fire Analysis

From the many building codes described worldwide, there is an internationally acceptable Temperature time curve which is specified in ISO 834 standard (ISO 1980) or ASTM E119-883 that characterizes the continuous growth of gas temperature along with time with a reduced rate. This curve becomes a standard practice that is used in the testing laboratories to find out the fire resistance of structural elements and it doesn't represent the real fire condition. The standard ISO 834 curve according to (Eurocode 1 part 2, 2002), section 3.2.1 is calculated using the following equation.

$$\theta g = 20 + 345\log_{10}(8t + 1) \qquad \textbf{Equation 3-1}$$

Where: θg is the gas temperature in the compartment in [°C]

t is time in [min]

According to (ASTM E119-88) (Standard method of Fire test of building construction and materials), the standard temperature-time curve is calculated by using the following approximated equation.

$$\theta g = 20 + 750[1 - \exp(-3.79533\sqrt{t})] + 170.1\sqrt{t} \qquad \textbf{Equation 3-2}$$

Where: θg is the gas temperature in the compartment in [°C]

t is time in [hours]

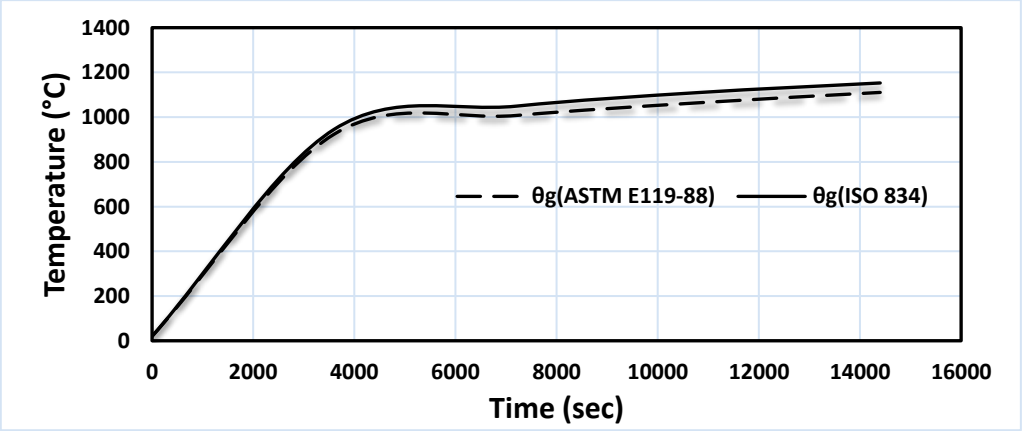

Figure 3-1 The two types of fire curves

According to the above Figure 3-1, The ISO 834 curve and the ASTM E119-88 curve give almost the same result. The ASTM E119-88 fire curve is used to validate the experimental result and the ISO 834 curve is applied in the parametric evaluation of FEM simulation.

3.2.2 Mechanism of heat transfer analysis

The heat transfer model is designed to find the nodal temperature distribution with a specified time at which the fire resistance of the CFST member wants to be verified.

The heat transfer of the structural member can be applied to the CFST column by two mechanisms, the first is the net heat flux which is a combination of the convective and radiation heat transfer mechanism and the second is the conductive heat transfer mechanism. The net heat flux transfers heat from the fire to the exposed surface and the conductive heat transfers heat from the structural element itself which is evaluated through the equation by using (Eurocode 1 part 2, 2002) and the overall mechanism is explained in Figure 3-2.

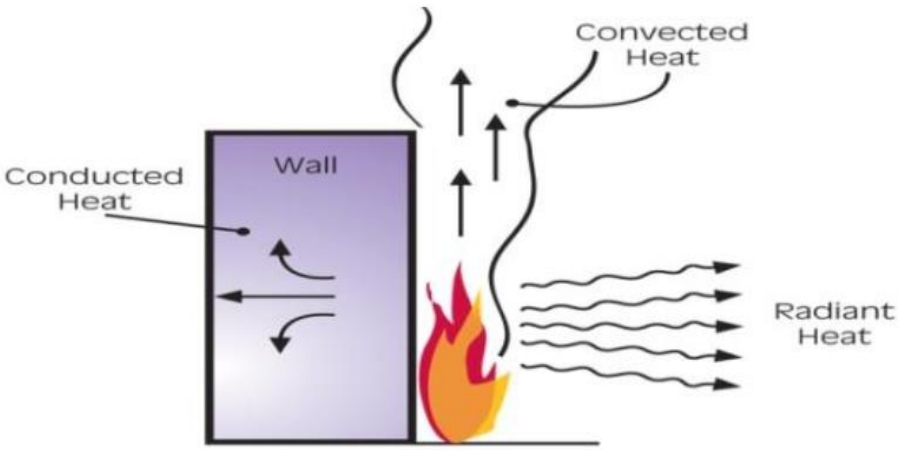

Figure 3-2 Heat Transfer of a Structural member

The net heat flux on the exposed surfaces according to (Eurocode 1 part 2, 2002) is composed of the convective heat flux and radiation heat flux as expressed in the following equation:

$$h'_{net} = h'_{net,c} + h'_{net,r} \, (W / m^2) \qquad \textbf{Equation 3-3}$$

Convective heat transfer is the transfer of heat between places by the movement of fluids, in free or natural convection and it is a process that transfers heat by mass transferring mechanisms. The net convective heat flux part can be calculated as follows.

$$h'_{net,c} = \alpha c(\theta g - \theta m)(W / m^2)$$ **Equation 3-4**

Where: αc is the coefficient of heat transfer by convection equals to 25 (W/m^2K)

θg is the gas temperature in the vicinity of the fire exposed member [°C]

θm is the surface temperature of the member [°C]

Radiation is the transfer of energy to a body using the emission or absorption of electromagnetic radiation. Thermal radiation propagates through the vacuum. The net radiation heat flux $h'_{net,r}$ is determined using the following equation:

$$h'_{net,r} = \phi \varepsilon_m \varepsilon_f \sigma[(\theta r + 273)^4 - (\theta_m + 273)^4](W / m^2)$$ **Equation 3-5**

Where: ϕ is the configuration factor equal to 1

ε_m is the emissivity of the member equal to 0.7

ε_f is the emissivity of the fire equal to 1

σ is the Stephan-Boltzmann constant, equal to 5.67 x 10-8 W/m^2K^4

θ_r is the effective radiation temperature of the fire environment [°C]

θ_m is the surface temperature of the member [°C]

Conduction is the transfer of heat from one point to another due to the temperature difference between two bodies. The conductive heat transfer between the contact surfaces is assumed to be calculated as follows according to (Eurocode 1 part 2, 2002).

$$q = k(\theta_A - \theta_B)$$ **Equation 3-6**

Where:

q is the heat flux per unit area crossing the interface from point A on one surface to point B on the other,

θ_A is the temperature of the points on the slave surface (in this case concrete core) [°C]

θ_B is the temperature of the points on the master surface (in this case Steel tube) [°C]

k is the gap conductance.

3.2.3 Temperature field analysis model

3.2.3.1 Material properties

To simulate the heat transfer finite element model, for the thermal properties of concrete Eurocode 2 part 2 (Eurocode 2 part 2, 2005) is used to specify density, thermal conductivity, and specific heat of concrete. While for steel tube Euro code 3 part 2 (Eurocode 3 part 2, 2005) is applied to specify density, thermal conductivity, and specific heat of steel.

3.2.3.2 Thermal contact at the steel tube interface

In the previous researches, it is widely believed that an air gap may be developed in the interface between steel and concrete. This is due to two main reasons, the first one is the initial gap between the concrete and steel may already exist due to the shrinkage of concrete, and the second reason, since steel, have a larger coefficient of thermal expansion than concrete there exists a delay in temperature rise within the concrete core. Due to these the steel and concrete are not in perfect contact and therefore thermal contact conductance (hj) can be used to shine the resistance of heat in the interface.

Different values for the thermal contact conductance (hj) have been suggested by some researchers. (Espinos et al., 2010) suggest the value of hj as a constant value of 200 W/m^{2}K in his sensitivity analysis, and (Lu, Han, and Zhao, 2010) used a constant value of 100 W/m^{2}K while other researchers such as (Hong and Varma, 2009) assumed that the temperature at the steel tube-concrete interface are equal and these would result in a higher value of hj, and these is the case to use “TIE” constraint in ABAQUS.

In these research a constant value of 200 W/m^{2}K is applied and it gives better result with the experimental data from the literature.

3.2.3.3 Boundary condition and element type

In the simulation of the thermal stress analysis of structural members, the sequentially coupled thermal stress analysis is adopted and validated by various tests (Espinos et al., 2010). In this type of analysis, the structural response of a member at higher temperatures

depends on the value of the temperature fields, but the thermal response doesn't depend on the structural response. Due to the above reason, the effect of the axial load, end restraint and also load eccentricity on the development of the temperature field of CFST columns is not considered in the heat transfer analysis.

In this research, the general-purpose finite element software ABAQUS (2020) was used to develop the heat transfer analysis. 3-D finite element models are used in which the eight-node continuum (DC3D8) heat transfer elements are used to model both the concrete core and the steel tube.

3.3 Modeling of stress analysis

To model the stress analysis the step must be divided in two. In the first step, the axial load is applied on the CFST column at normal temperature conditions and the second step considers loading from the first step and the temperature distribution from the heat transfer analysis which is applied to the stress analysis as a predefined field through the second step. In addition, geometric non-linearity is included in the stress analysis to account for the imperfection of the column by conducting a buckling mode shape analysis as a first model.

3.3.1 Material properties

a) Concrete

To account for the effect of material non-linearity, Concrete damage plasticity in ABAQUS (2020) is applied to define the compressive and tensile behavior of concrete. In this model, the plasticity, compressive and tensile behavior of concrete need to be defined. The plasticity of concrete is defined by taking the values as follows. The ratio of the second stress invariant on the tensile meridian with the compressive meridian (KC) is set to 2/3; the ratio of compressive strength under biaxial loading to uniaxial concrete compressive strength (fbo/fc') is equal to 1.16; flow potential eccentricity (e) equal to 0.1; a value of zero for viscosity parameter and the value of dilation angle is set to 40°. These values were decided based on a sensitivity analysis done by (Tao, Wang and Yu, 2013)

The compressive stress-strain and reduction factor of concrete is taken according to EC 2 (2005). The stress-strain relationship is indicated in the equation below and the plot is given in

Figure **3-3** below.

For $\varepsilon \le \varepsilon_{c,\theta}$

$$\sigma = \frac{3\varepsilon f_{c,\theta}}{\varepsilon_{c1,\theta}(2+(\frac{\varepsilon}{\varepsilon_{c,\theta}})^3)} \qquad \textbf{Equation 3-7}$$

For $\varepsilon_{c,\theta} \le \varepsilon \le \varepsilon_{cu,\theta}$ linear or non-linear models are permitted (the linear model was chosen)

Where $\varepsilon_{c,\theta}$ is the strain at compressive strength $f_{c,\theta}$ and $\varepsilon_{cu,\theta}$ is the ultimate strain

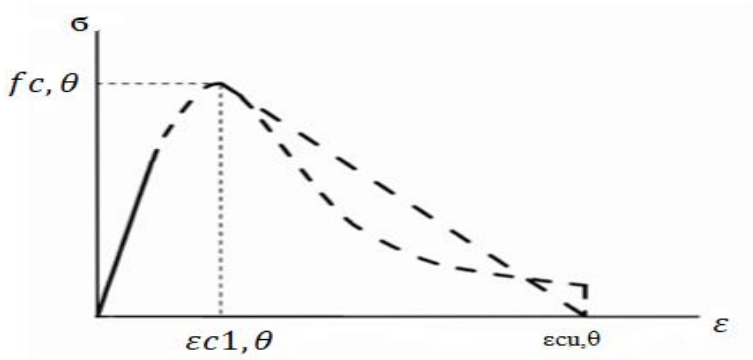

Figure 3-3 Stress-strain curve for concrete at elevated temperatures (EC 2 2005)

To account for the tensile behavior of concrete the "GFI" option was chosen by entering the tensile stress and the fracture energy. Fracture energy was calculated in Eq. (3-8) after (Tao, Wang and Yu, 2013) with ambient temperature. According to the test report of (Gao, 2013) the fracture energy is independent of temperature variation. The fracture energy at ambient temperature GF in N/m is given by

$$G_F = (0.0469 d_{\max}^2 - 0.5 d_{\max} + 26)(\frac{f_c'}{10})^{0.7} \qquad \textbf{Equation 3-8}$$

Where $d_{\max}$ is the maximum aggregate size of concrete (mm) and f_c' is the concrete cylinder strength in (MPa).

The default value of $d_{\max}$ is 20mm if it is not reported as a reference according to (Tao, Wang and Yu, 2013)

The tensile stress of concrete is calculated in accordance with (CEB-FIP, 1990) using the equation below, and to consider the influence of temperature on the tensile stress, the tensile strength at higher temperature is calculated by taking the reduction factor given in Euro code 2 (2005) as shown on Figure 3-4 below.

$$f_t = 1.4 \times (0.1 \times f_c')^{(2/3)}$$ **Equation 3-9**

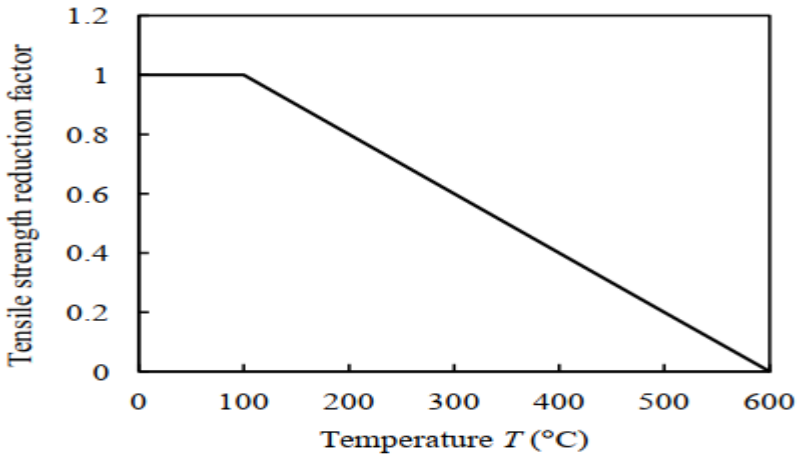

Figure 3-4 Concrete tensile stress reduction factor with higher temperature (Eurocode 2 part 2, 2005)

The thermal expansion of concrete was proposed according to Euro code 2 (2005) for siliceous and carbonate aggregate as given by the following equations.

Thermal expansion of siliceous aggregates is given by the equation below.

$$\varepsilon_c(\theta) = -1.8\times10^{-4} + 9\times10^{-6}\theta + 2.3\times10^{-11}\theta^3 \quad for\ 20^\circ C \le \theta \le 700^\circ C$$
$$\varepsilon_c(\theta) = 14\times10^{-3} \quad for\ 700^\circ C \le \theta \le 1200^\circ C$$

Equation 3-10

Thermal expansion of calcareous aggregates is given by the equation below.

$$\varepsilon_c(\theta) = -1.2\times10^{-4} + 6\times10^{-6}\theta + 1.4\times10^{-11}\theta^3 \quad for\ 20^\circ C \le \theta \le 805^\circ C$$
$$\varepsilon_c(\theta) = 12\times10^{-3} \quad for\ 805^\circ C \le \theta \le 1200^\circ C$$

Equation 3-11

In this research a constant calue of 6×10^{-6} is used for the thermal expansion of concrete and siliceous aggregates are used to model the CFST column.

b) Steel

To define the structural and thermal behavior of steel, Carbon steel was selected instead of stainless steel because of its availability and most commonly used in construction. Therefore, the mechanical Properties and thermal expansion of carbon steel at high temperatures have been defined according to EC3 part 1-2. The general stress-strain curve can be obtained from the following table of equations:

Table 3-1 Eurocode 3 parameters and equations for carbon steel properties

Strain Range ε	Stress σ	Tangent modules
$\varepsilon \le \varepsilon_p,\theta$	$\varepsilon E_a,\theta$	E_a,θ
$\varepsilon_p,\theta \le \varepsilon \le \varepsilon_y,\theta$	$f_p,\theta - c + (b/a)[a^2 - (\varepsilon_y,\theta - \varepsilon)^2]^{0.5}$	$\frac{b(\varepsilon_y,\theta - \varepsilon)}{a[a^2 - (\varepsilon_y,\theta - \varepsilon)^2]^{0.5}}$
$\varepsilon_y,\theta \le \varepsilon \le \varepsilon_t,\theta$	f_y,θ	0
$\varepsilon_t,\theta \le \varepsilon \le \varepsilon_u,\theta$	$f_y,\theta[1-(\varepsilon - \varepsilon_t,\theta)/(\varepsilon_u,\theta - \varepsilon_t,\theta)]$	-
$\varepsilon = \varepsilon_u,\theta$	0	-
Parameters	$\varepsilon_{p,}\theta = f_p,\theta/E_a,\theta \quad \varepsilon_y,\theta = 0.02 \quad \varepsilon_t,\theta = 0.15 \quad \varepsilon_u,\theta = 0.2$	
Functions	$a^2 = (\varepsilon_y,\theta - \varepsilon_p,\theta)(\varepsilon_y,\theta - \varepsilon_p,\theta + c/E_a,\theta$ $b^2 = (\varepsilon_y,\theta - \varepsilon_p,\theta)E_a,\theta + c^2$ $c = \frac{(f_y,\theta - f_p,\theta)^2}{(\varepsilon_y,\theta - \varepsilon_p,\theta)E_a,\theta - 2(f_y,\theta - f_p,\theta)}$	

Where:

f_y,θ is effective yield strength.

f_p,θ is the proportional limit:

E_a,θ is the slope of the linear elastic range.

ε_p,θ is the strain at the proportional limit.

ε_y,θ is yield strain.

ε_t,θ is limiting strain for yield strength

ε_u,θ is ultimate strain.

Table 3.1 in EC3 Part 1-2 section 3.2.1 gives the reduction factor for the parameter fy, fp, and Ea for a certain temperature. The variation of these reduction factors with temperatures is illustrated in Figure 3-5 below. For temperatures below 400 °C an alternative Strain hardening formula indicated in the equation below may be used for the stress-strain curve of carbon steel as given in Annex A of EC 3 Part 2 provided that local or member buckling does not lead to premature failure.

$$
\begin{aligned}
&for\ 0.02 < \varepsilon < 0.04 && \sigma_a = 50(f_u,\theta - f_y,\theta)\varepsilon + 2 f_y,\theta - f_u,\theta \\
&for\ 0.04 \le \varepsilon \le 0.15 && \sigma_a = f_u,\theta \\
&for\ 0.15 < \varepsilon < 0.2 && \sigma_a = f_u,\theta[1 - 20(\varepsilon - 0.15)] \\
&for\ \varepsilon \ge 0.2 && \sigma_a = 0
\end{aligned}
$$

Equation 3-12

Where f_u,θ is the ultimate strength at elevated temperatures, allowing for strain hardening and it is determined based on the equation below with temperature variation.

$$
\begin{aligned}
&for\ \theta_a < 300^\circ C && f_u,\theta = 1.25 f_y,\theta \\
&for\ 300^\circ C \le \theta_a < 400^\circ C && f_u,\theta = f_y,\theta(2 - 0.0025\theta_a) \\
&for\ \theta_a \ge 400^\circ C && f_u,\theta = f_y,\theta
\end{aligned}
$$

Equation 3-13

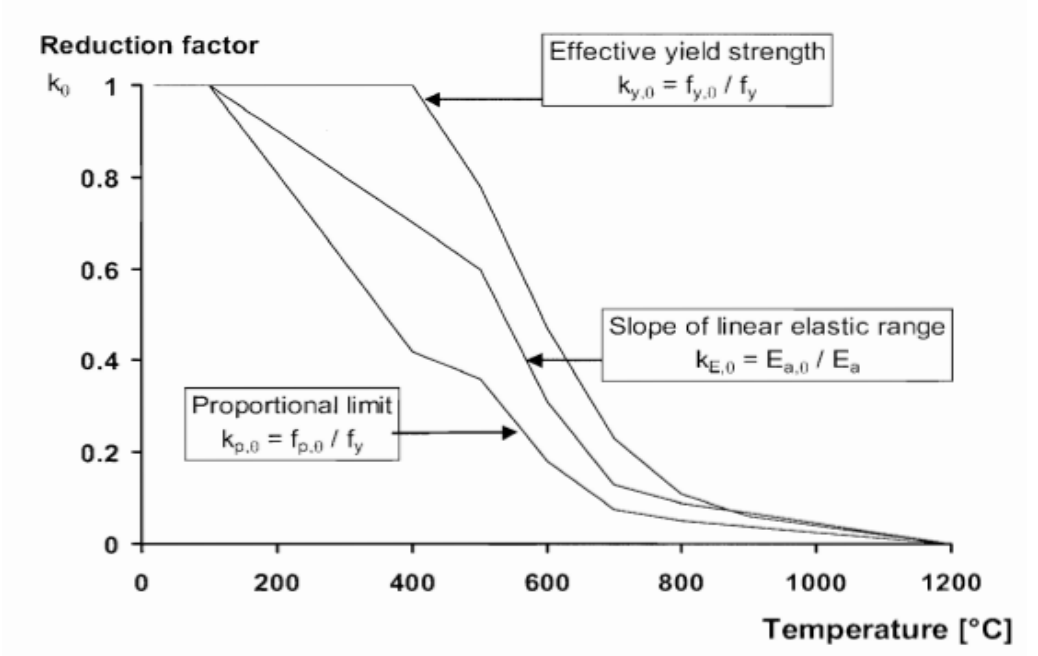

Figure 3-5 Reduction factors for the stress-strain relationship of carbon steel at elevated temperatures according to EC 3 Part 2

For the elastic part, the elastic modulus and Poisson's ratio were defined, the Poisson's ratio was taken equal to 0.3, the elastic modulus of steel at high temperatures were obtained from table 3.1 in EC3 Part 1-2 section 3.2.1.

The thermal elongation of steel (*Δl/l*) was determined according to EC 3 as shown in the equation below.

$$\begin{aligned} &for\ 20^{\circ}C \le \theta_a < 750^{\circ}C && \Delta l/l = 1.2\times10^{-5}\theta_a + 0.4\times10^{-8}\theta_a^{\,2} - 2.416\times10^{-4} \\ &for\ 750^{\circ}C \le \theta_a \le 860^{\circ}C && \Delta l/l = 1.1\times10^{-2} \\ &for\ 860^{\circ}C \le \theta_a \le 1200^{\circ}C && \Delta l/l = 2\times10^{-5}\theta_a - 6.2\times10^{-3} \end{aligned}$$

Equation 3-14

Where l is the length at 20 °C; Δl is the temperature-induced elongation, and θ_a is the steel temperature in °C.

3.3.2 Steel concrete interaction

The interaction between the steel tube and the concrete core is defined as a 'contact' interaction option in ABAQUS 2020 between the inner surface of the steel tube and the outer surface of the concrete core. The inner surface of the steel tube was chosen as a

'master surface' and the outer concrete core was chosen as a 'slave surface'. The mechanical properties of these 'contact' interactions were defined in both the tangential and normal directions. For the behavior of tangential direction, a 'friction' model is used to simulate the contact pair by taking a friction coefficient of 0.3. these value was used by (Espinos et al., 2010) and found it to be suitable for CFST columns. For the behavior of normal direction, a 'hard contact' option was used. These imply that the pressure acts between the two surfaces when both the steel tube and the concrete core come in contact and the pressure value is zero when there is no contact between the two surfaces.

3.3.3 Boundary condition and element type

Generally, three-dimensional modeling to simulate the fire behavior of the CFST column was developed using ABAQUS finite element package. In order to account for the difference in thermal expansion of steel and concrete, the upper boundary condition was modeled by defining a rigid plate at the upper end of the column. The plate is controlled by a reference point located at its centroid. The pinned or fixed-boundary condition was assigned to this reference point. A frictionless contact interaction was defined between the loading plate and the top of concrete, and a coupling constraint was assumed between the reference point and the top of the steel tube. Three-dimensional smoothing was allowed for the curved part in order to overcome convergence problems. At the bottom end of the column, a pinned or fixed-boundary condition was applied depending on the support type to a reference point located at the centroid of the bottom end. This reference point was coupled with the bottom end of the column so that they had the same deformation.

In the stress analysis model, the same element meshing was adopted as for the thermal analysis model. Solid element (C3D8R) was used for the concrete core and steel tube while Rigid element (R3D4) was used for the top-loading plate.

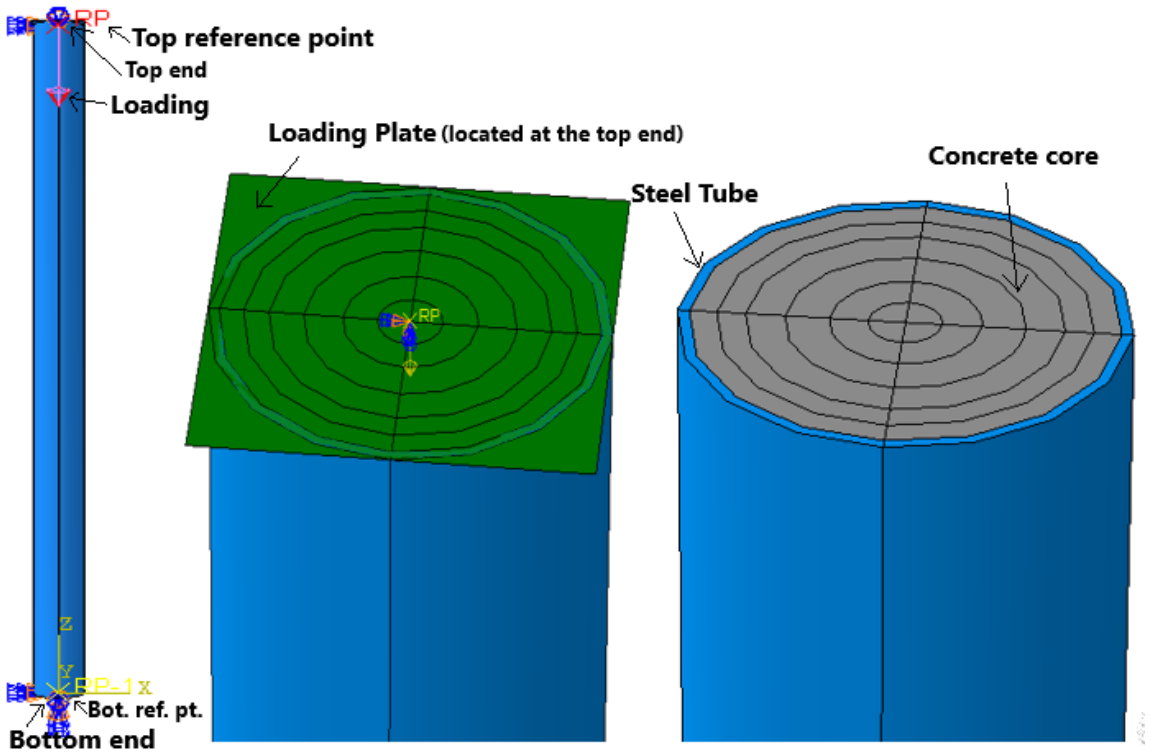

Figure 3-6 Typical FE modeling for stress analysis

3.3.4 Addition of initial imperfection

In order to represent the initial geometric imperfection of the CFST column in the finite element model to predict the overall buckling of the columns, the deformed shape of the column first buckling mode was obtained, and afterward amplified by means of an imperfection factor for each of the geometries under studied. Generally, the geometric imperfection of the member is specified as the first buckling mode shape multiplied by the magnitude. Since the actual column specimens were not reported, the assumed value of imperfection was considered. Larger imperfection magnitude reduces the failure time of the CFST column. The initial geometric imperfection equal to L/1000, where L is the column length, gives better result in comparison of the FE models and the test results, and the same result was obtained by the previous investigation. This value of L/1000 was used in the verification and parametric studies.

3.4 Failure criteria on fire resistance of CFST column

The failure criteria for axially loaded elements specified in ISO 834 standard (ISO 834-1, 1999) was adopted to identify the ultimate state of the column specimen in the fire. ISO 834 standard failure criteria is either the axial shortening exceeding 0.01L mm or the

deformation rate exceeding 0.003L mm/min, Where L is the length of the specimen in mm. the criteria for elapsed time from the beginning of the temperature rise phase to the time of failure was recorded using the axial deformation time curve. The time at which this failure happens is defined as the fire resistance (FR) of the column.

3.5 Finite element mesh

Meshing technique can be done on individual parts and then assembled or vice-versa. In this analysis, the whole models were meshed individually and then assembled for further processing. The mesh size of the parts was based on the mesh convergence studies and hence element size across the cross-section was as D/15 for a circular column or B/15 for the square column, where D and B are the overall diameter of the circular tube and the overall width of the Square tube, respectively. The FE method discretizes the CFST column as per the given discretization value by itself. Some of the representative mesh for the assembled CFST columns are shown below for both circular and square cross-sections.

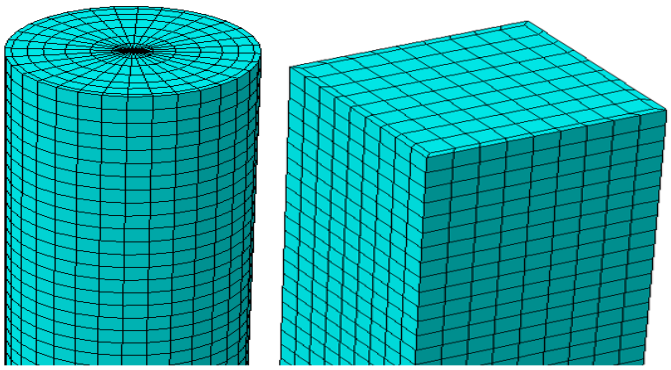

Figure 3-7 Sample mesh for Circular and square CFST column

3.6 Material compatibility between steel grade and concrete class

For the CFST column subjected to compressive load, it is necessary to ensure that yielding of the steel section occurs before the concrete core reaches its maximum stress. Otherwise, the full plastic resistance of the composite section cannot be achieved due to the brittle failure of high-strength concrete after reaching the maximum stress. Hence, the selections of steel grade and concrete class must ensure that the yield strain of steel is smaller than the compressive strain of concrete at the peak stress. The yield strain of steel and the strain

of concrete at peak stress may be calculated according to (EN 1992-1-1, 2004) and (EN 1993-1-1, 2005) as follows:

Steel yield strain (‰):

$$\varepsilon_y = \frac{f_y}{E_a} \qquad \textbf{Equation 3-15}$$

Concrete strain at peak stress (‰):

$$\varepsilon_{c1} = 0.7 f_{cm}^{0.31} < 2.8 \qquad \textbf{Equation 3-16}$$

Where $f_{cm} = f_{ck} + 8$ is the mean compressive strength of concrete at 28 days, in N/mm^2.

Ea = 210GPa is the elastic modulus of the steel tube.

Hence the maximum steel strength can be determined according to the concrete characteristic strength with strength class up to C90/105 using the following expression:

$$f_y \leq 0.7 E_a (f_{ck} + 8)^{0.31} \qquad \textbf{Equation 3-17}$$

Where,

f_y is the characteristic yield strength of steel

f_{ck} is the characteristic cylindrical compressive strength of concrete

Ea is the modulus of elasticity of steel

Since the maximum yield stress of steel used in this research is S355 and the minimum compressive strength of concrete used is C25/30, To check the compatibility we have calculated the yield strain of steel 1.69 and the strain of concrete at peak stress with a value of 2.07. Therefore, the value of the yield strain of steel is less than the strain of concrete at peak stress in all samples.

Therefore, according to material compatibility, the steel grade S235, S275 and S355 are compatible with the concrete grade ranging from C25/30 to C50/60.

Chapter 4 FINITE ELEMENT ANALYSIS

4.1 Analytical study of the finite element model

Part

The part module is the first step to conduct any application on finite element modeling. In this step, the geometry of the column is created by defining a 3-D deformable solid section for steel and concrete and a 3-D discrete rigid planar shell section for the loading plate. The cross-sectional modeling was sketched and then partition techniques are applied to become ready for assembly.

Property

In the property module, the material properties were defined, the cross-section is created and then the material was assigned with a solid section for both steel and concrete. In heat transfer analysis, the density, elasticity, thermal conductivity, and specific heat of both concrete and steel with temperature variation were inserted based on the recommended values. While in stress analysis, for concrete the elastic of concrete, density of concrete, thermal expansion, and the concrete damage property of concrete was defined, and for steel tube, the density of steel, modulus of elasticity of steel, thermal expansion, and plastic behavior of steel was defined with temperature variation based on the recommended values as discussed in chapter three.

Assembly

In this module, the geometry of the column was composed of steel tube and concrete core in the instance option. Loading plate was applied only in the buckling analysis and stress analysis models by translating the center of the loading plate from the origin into the upper centroid of the cross-section.

Step

FE provides various analysis procedures to analyze the behavior of different models providing different needs. In this research, three types of analysis steps are applied for the whole model. “Linear perturbation, Buckle” can be used to analyze linear analysis and to

predict the buckling shape of the column. The second is the "heat transfer" step which conducts the thermal analysis by giving the total time for the application of fire on the column. The third and the last step is the "static general step". In this step, the application of load and fire is simultaneously applied in order to predict the fire resistance capacity of the column. The time for the static general step is equal to the heat transfer step and the amount of the value of the total time depends on the capacity in which the column can safely resist the applied and fire load.

Interaction

In the stress analysis surface to surface, the interaction was defined by applying a friction coefficient of 0.25 and a normal hard contact interaction property for the steel (master surface) to the concrete core (slave surface). In heat transfer analysis two interaction properties were defined by specifying thermal conductance of 200 W/m^2K and a film coefficient of 25 W/m^2K and a surface to surface interaction between steel tube and concrete was made by using the interaction property of thermal conductance value and a convection and radiation interaction. Load were applied by specifying the temperature-time variation of the fire load based on ISO834 fire curve.

In stress analysis, a coupling constraint was applied by defining a reference point at the centroid of the cross-section in both ends. In the bottom end, both the steel and concrete are coupled with the reference plate to act together since no load is applied here. While in the upper end, the loading plate was coupled with the top steel tube cross-section. But the interaction between concrete core and loading plate was defined by surface to surface interaction with a frictionless contact behavior. In heat transfer analysis there is no constraint applied since no load is specified in both end conditions.

Load

Loads and boundary conditions must be applied to the geometry of the model to predict the accurate result. In this analysis for each of the two ends, two different types of boundary conditions were used. Which are fixed-fixed and pinned-fixed. In both cases, the compressive load was applied in the Z -direction on the top-loading plate. While the opposite end condition was remaining fixed from transition and rotation. In buckling analysis, a unit load is applied and in the stress analysis, a load is applied based on its assumed load ratio. While in the heat transfer analysis no-load and boundary condition are

applied but instead, a fire load is applied as convection and radiation in the interaction module. In this module, the values of nodal temperature were defined in the stress analysis as a predefined field by selecting "from results and output databases" and inserting the job file done in the heat transfer analysis.

Meshing

The meshing procedure is the one that discretizes the geometry of the column into small pieces of elements. In the module different techniques are used to mesh the part and the whole assembly. In the model, parts are independently meshed and then assembled for further job analysis. Details about meshing are given in the methodology section.

4.2 Validation of the Finite element model

As experiments were not performed in this study, the use of simulation software, ABAQUS was necessary. To validate the finite element models, the experimental test conducted by (Lie, T.T. and Chabot, 1992) is used to simulate the accuracy of the CFST columns in terms of temperature fields, axial deformation, and fire resistance time. The length of the column was 3810 mm from this only the middle 3048 mm was exposed to fire. Figure 4-1 shows the deformed shape of CFST column C08 from the test result and FE output in terms of axial deformation. The unit system used in Abaqus is in the SI unit. Therefore, axial deformation is measured in meter, and time is measured in sec. While the test result was reported with length in mm and time in min. Therefore, to report all output results for verification and parametric studies, Abaqus model results are converted into test result units. The material and geometry used for C08 is shown in table 4.1 below.

Table 4-1 Material data for validation of C08

Parameter	Value	Unit
Cylindrical compressive strength, f_c	35.5	N/mm^2
Steel yield strength, f_y	350	N/mm^2
Length of column, L	3.81	m
External diameter, D	168.3	mm
Steel tube thickness, t	4.78	mm
Load ratio, n	0.23	
Test load	218	KN
End condition	Fixed-Fixed	

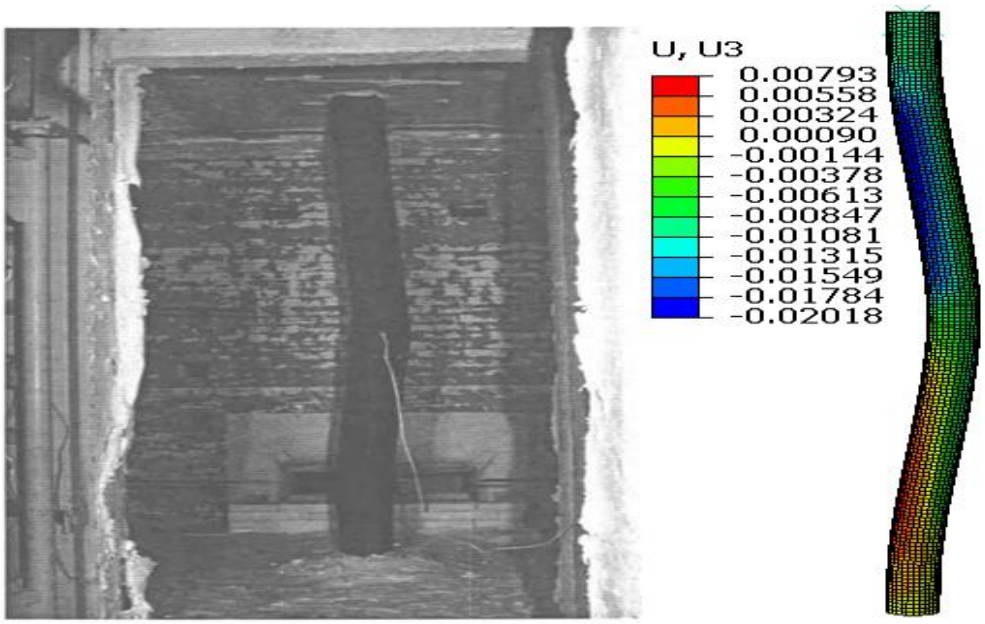

Figure 4-1 Deformed shape of CFST column C08 from test result and Abaqus output

4.2.1 Temperature field Verification

In the heat transfer analysis model, the value of nodal temperatures was found after a certain time amount of fire exposure. The temperature-time curves predicted by the FE model are used to compare to the test results. From the comparison, it shows that the finite element models almost matched with the measured temperature field of test results at the outer location on the cross-section of the columns. However, the measured test curves and predicted values show small difference at point 2 around 100 °C. This is due to the fact that evaporation of water could not be considered in the FEM and there is some gap developed throughout the curve at points 1 and 2 due to the material data variations between the Euro code and the experimental procedure.

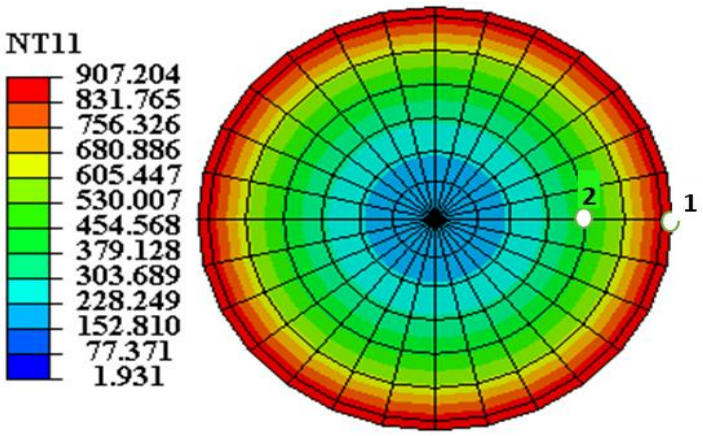

Figure 4-2 Temperature gradient for C08 column from Abaqus output

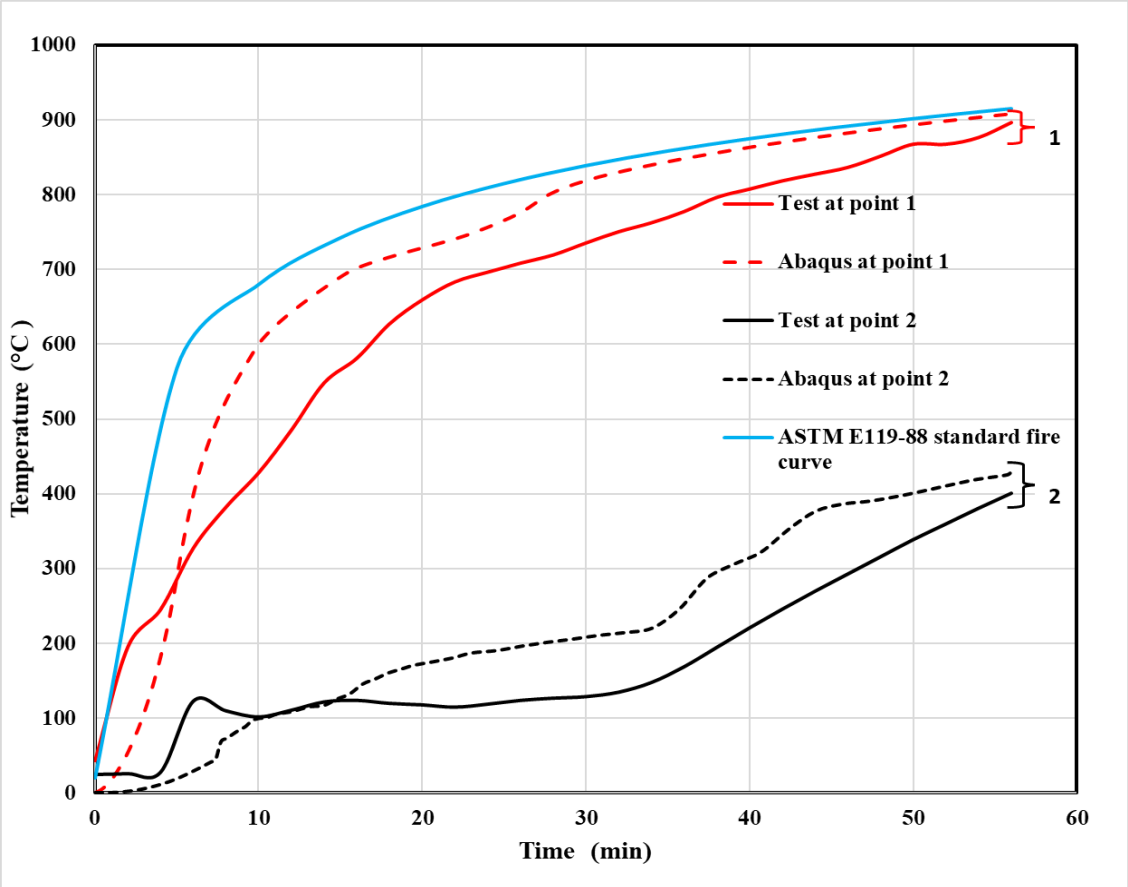

Figure 4-3 Temperature time curve of C08 column from test result and Abaqus output at the outer surface

4.2.2 Axial Deformation and Fire resistance time verification

It can be noticed from the numerical result that the predicted curves have higher expansion compared to the test result. Two reasons may be used to explain this case. On one hand, the distribution of temperature is not even in the test scenario so that the maximum difference in temperature was high. meanwhile, the thermal and mechanical properties at elevated temperatures were not measured for the steel and concrete, which might be different from the actual values. The adoption of nominal values specified in design codes likely affects the prediction accuracy of the FE modeling.

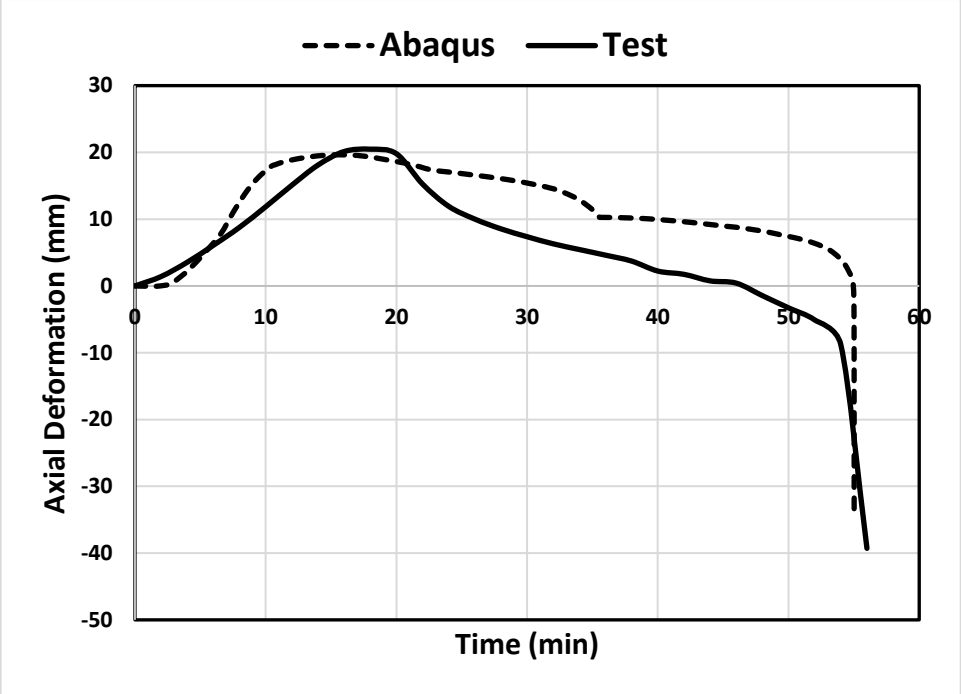

Figure 4-4 Comparison of axial deformation time plot for C08 column from test result and Abaqus output

From the experiment, it was found that the maximum axial deformation was 20.48 mm and the fire resistance time has been 56 minutes and from the finite element model, it was found that the maximum axial deformation was 19.64 mm and fire resistance time of 55 minute which has a 4.27% error from maximum axial deformation and 1.82% error from the fire resistance time. Both samples showed buckling as the failure mode and it can be observed that the finite element model result is in good arrangement with the experimental result. The similarity of failures can be seen in Figure 4-1 above. Hence, we concurred that the finite element software could give good results during the prediction of axial deformation and fire resistance time for further course of action.

4.3 Sampling Method

In order to carry out the three-dimensional finite element analysis, the input combinations are generated using the Latin Hypercube sampling (LHS) method. LHS is a sampling method designed to accurately recreate the input distribution through sampling in fewer trials when compared to the Monte Carlo method, which needs thousands of trials in which the distribution of each variable is assumed to be normal. In the LHS method, the cumulative distribution function of each factor is divided into intervals of equal

probability, and the sampling is done by taking one input value from each interval. LHS is a sampling technique used to force the samples drawn to correspond more closely with the input distribution and thus converges faster on the true statistics of the input distribution (Netsanet Bezu, 2018).

In these cases, the 32 combinations of random variables of the LHS table are found to be sufficient and considered in the determination of axial deformation and fire resistance of the CFST column. The statistical variation and the 32x5 combinations of random variables are shown in Table 4-2 and Table 4-3 respectively. The value of the length of column, the external diameter and the thickness of the steel tube is shown in appendix A as calculated according to Euro code specifications.

In the LHS layers, a range of values with a confidence level of 95% is considered. The minimum and maximum values of each random variable are fixed by considering the actual conditions where a particular CFST column exhibits. That is, material and dimensions are considered to account for the behavior of different CFST columns with fire exposure specimens in which conducting experimental investigation is difficult. These combinations are set systematically using the LHS sampling method.

Table 4-2 statistical variations of random samples

Variables	Observation	Mean	Standard deviation
D/t	32	35	17.735
fc'(MPa)	32	37.5	7.565
n	32	0.45	0.151
fy (MPa)	32	295	36.31
λ	32	1.05	0.454

Table 4-3 32x5 LHS Layer outputs of Random Variables

Label	Diameter to thickness ratio D/t	Cylindrical compressive strength of concrete fc, MPa	Load ratio n	Steel yield strength fy, (MPa)	Slenderness ratio, λ
C1	50.80	48.39	0.35	355.00	0.78
C2	22.17	42.74	0.51	235.00	1.36
C3	22.85	47.58	0.26	275.00	0.93
C4	16.83	35.48	0.68	275.00	0.83
C5	44.45	29.03	0.20	275.00	1.03
C6	26.71	45.97	0.59	355.00	1.80

Label	Diameter to thickness ratio D/t	Cylindrical compressive strength of concrete fc, MPa	Load ratio n	Steel yield strength fy, (MPa)	Slenderness ratio, λ
C7	42.96	39.52	0.25	275.00	0.35
C8	16.20	25.00	0.38	355.00	1.27
C9	20.32	32.26	0.57	355.00	0.64
C10	36.56	40.32	0.54	275.00	1.17
C11	11.11	45.16	0.41	355.00	1.12
C12	38.74	26.61	0.36	355.00	0.40
C13	15.28	34.68	0.31	275.00	0.49
C14	40.49	28.23	0.65	235.00	1.41
C15	63.50	37.10	0.52	275.00	0.92
C16	51.41	43.55	0.67	235.00	1.32
C17	30.50	50.00	0.55	275.00	0.54
C18	25.40	44.35	0.43	355.00	0.30
C19	56.44	25.81	0.46	275.00	1.07
C20	61.13	46.77	0.70	275.00	0.88
C21	31.75	36.29	0.23	355.00	0.98
C22	28.22	33.87	0.28	275.00	1.75
C23	57.13	38.71	0.30	235.00	1.25
C24	48.80	37.90	0.60	355.00	0.59
C25	48.90	30.65	0.64	275.00	0.45
C26	33.66	29.84	0.44	235.00	0.69
C27	43.33	31.45	0.49	355.00	1.65
C28	54.78	41.94	0.22	355.00	1.51
C29	34.93	49.19	0.39	275.00	1.70
C30	61.00	41.13	0.47	275.00	0.74
C31	13.64	33.06	0.62	275.00	1.56
C32	9.84	27.42	0.33	235.00	1.22

4.3.1 Scaling factor of input parameters

The range of input variables for the model varied by taking into consideration some essential points which will be helpful in the parametric study of the fire resistance of CFST columns. The diameter to thickness ratio ranges from 10 to 60 to cover all classes of the cross-section. The cylindrical compressive strength of concrete fc’ varied from C25/30 to C50/60 which covers the range of normal strength concrete in order to know the effect of compressive strength on the fire resistance of the CFST column. To see the effect of applied axial force on the fire resistance of the column the loading ratio ranges from 25% to 70% of the plastic axial load resistance of the column. The steel yield strength ranges from S235 to S355 to investigate the effect of normal steel yield strength on the fire

resistance of the column. Finally, the slenderness ratio ranges to cover the allowed limits of the slender columns according to the EC 4-1-1 2005.

4.3.2 Sensitivity Analysis

Sensitivity analysis is the analysis of the effect of input quantity variables (independent variables) on the output quantity variables (dependent variables). It answers the question of which quantities are dominant, and therefore particular attention has to be paid when (i) preparing the input values; (ii) conceiving and organizing the control variables; (iii) considering and deciding on the improvement of technological procedures and economic criteria are also included in cases (ii) and (iii). Furthermore, it has the potential to differentiate by means of sensitivity analysis which quantities are in a rather low influential position; and therefore, they can be considered only in a deterministic way (as non-random ones). This can contribute to simplify and accelerate both the calculation and modeling process (Kala and Kala, 2006). While range is the simplest measure of spread for a given data, it doesn't consider a very reliable measure because it is highly sensitive to the sample size and it is very sensitive to extreme values. Therefore, the coefficient of variation, COV is used to quantify the spread of the data points. This statistic is defined as the ratio of the standard deviation to the mean. As such it gives a normalized measure of the spread. It is often expressed in the form of a percent as shown in the equation below.

Coefficient of variation (COV)

$$CoV = \frac{\sigma_i}{\bar{x}} \times 100\% \qquad \textbf{Equation 4-1}$$

The sensitivity factor αi is a kind of an index to estimate the contribution of the uncertainty of xi to the uncertainty of the function f. Since the objective function f is given, the effect of random variables can be determined as follows in the equation below.

Sensitivity factor

$$\alpha_i = \frac{\partial f}{\partial i} \times \frac{\overline{x_i}}{\overline{f}} \qquad \textbf{Equation 4-2}$$

the uncertainty coefficients were calculated by multiplying the coefficient of variation and the sensitivity factor as shown in the equation below. The uncertainty analysis states the percentage contribution of the variables. If the Ui value is positive then the variables have a positive contribution. That means an increase of those particular variables results in an

increased value of the dependent variable and if it is negative, it has a negative contribution which means decreasing those particular variables results in an increased value of the dependent variable.

Uncertainty analysis,

$$U_i = CoV_i * \alpha_i \qquad \textbf{Equation 4-3}$$

where i is random variable index

CHAPTER 5 PARAMETERIC STUDY AND SENSITIVITY ANALYSIS

5.1 Introduction

In order to evaluate the effect of different parameters such as cross-sectional diameter, steel tube thickness, loading ratio, and slenderness ratio it requires the generation of different models with a random sampling of probabilistic inputs generated using Latin Hypercube sampling (LHS) software. Deterministic studies of boundary condition (support condition) and cross-section type (Circular vs square) were also conducted. The results obtained from the finite element analysis are discussed in terms of the axial deformation curve and the fire resistance time. Also, by using sensitivity/uncertainty analysis, the percentage contribution of the five variables; D/t, fc, n, fy and λ are discussed.

5.2 Deterministic based studies

The following values are considered to see the effect of cross-section and support conditions.

Table 5-1 values used to see the effect of cross-section and support condition

Parameter	Value	Unit
Cylindrical compressive strength, fc	30	N/mm2
Steel yield strength, fy	275	N/mm2
Load ratio, n	0.4	
Length of the column, L	3	m
Ea	210,000	N/mm2
Viscosity of concrete	0.2	
Viscosity of steel	0.3	
Heated length	Full length	

5.2.1 Effect of cross-section type

In order to see the effect of cross-section type on the fire resistance of the CFST column, six samples are selected. These two samples have an equal cross-sectional area of steel tube section as we see on Table 5-2 below, two samples have an equal cross-sectional area of concrete core section as we see on Table 5-3 below and the other two samples have an

equal total cross-sectional area as we see on Table 5-4 below, for the case of circular and square section types. While other parameters are taken based on Table 5-1 above.

Table 5-2 Case A Columns with an equal cross-sectional area of steel tube, As

Features	Group 1			Group 2		
	CCFST	SCFST	CCFST/SCFST	CCFST	SCFST	CCFST/SCFST
Size(mm)	189.6x5	150x150x5		253.3x5	200x200x5	
As(mm2)	2899.69	2900	1.000	3900.29	3900	1.000
Ac(mm2)	25333.93	19600	1.293	46491.56	36100	1.288
Atotal(mm2)	28233.62	22500	1.255	50391.85	40000	1.260

Table 5-3 Case B Columns with an equal cross-sectional area of the concrete core, Ac

Features	Group 3			Group 4		
	CCFST	SCFST	CCFST/SCFST	CCFST	SCFST	CCFST/SCFST
Size(mm)	134.1x5	120x120x5		224.1x6.3	200x200x6.3	
As(mm2)	2027.898	2300	0.882	4310.705	4881.24	0.883
Ac(mm2)	12095.77	12100	1.000	35132.63	35118.76	1.000
Atotal(mm2)	14123.67	14400	0.981	39443.33	40000	0.986

Table 5-4 Case C Columns with the equal total cross-sectional area, Atotal

Features	Group 5			Group 6		
	CCFST	SCFST	CCFST/SCFST	CCFST	SCFST	CCFST/SCFST
Size(mm)	180.5x6.3	160x160x6.3		203.1x4.5	180x180x4.5	
As(mm2)	3447.772	3873.24	0.890	2807.641	3159	0.889
Ac(mm2)	22140.7	21726.76	1.019	29589.73	29241	1.012
Atotal(mm2)	25588.47	25600	1.000	32397.37	32400	1.000

The results of the above three cases: case A, case B, and case C is plotted in Figure 5-1, Figure 5-2, and Figure 5-3 below.

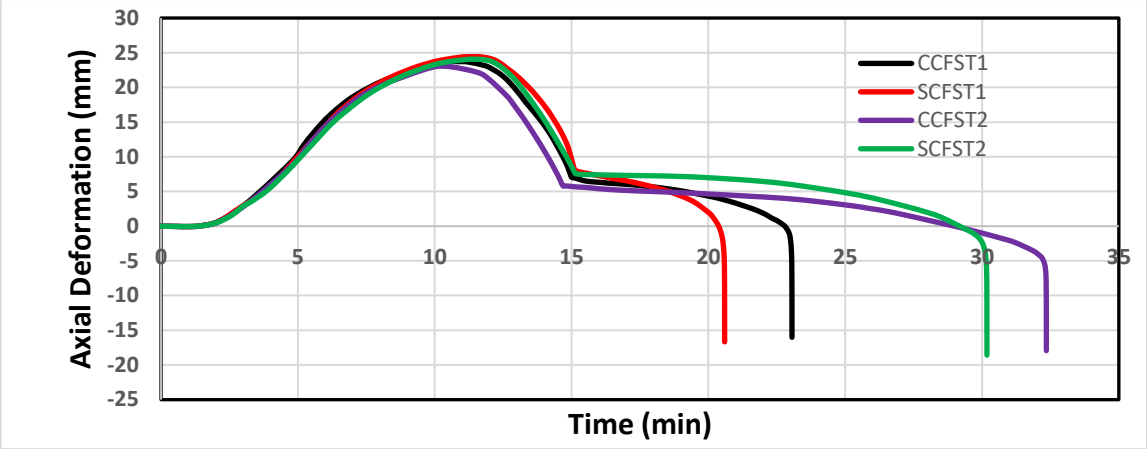

Figure 5-1 Axial deformation Vs time plot of Case A

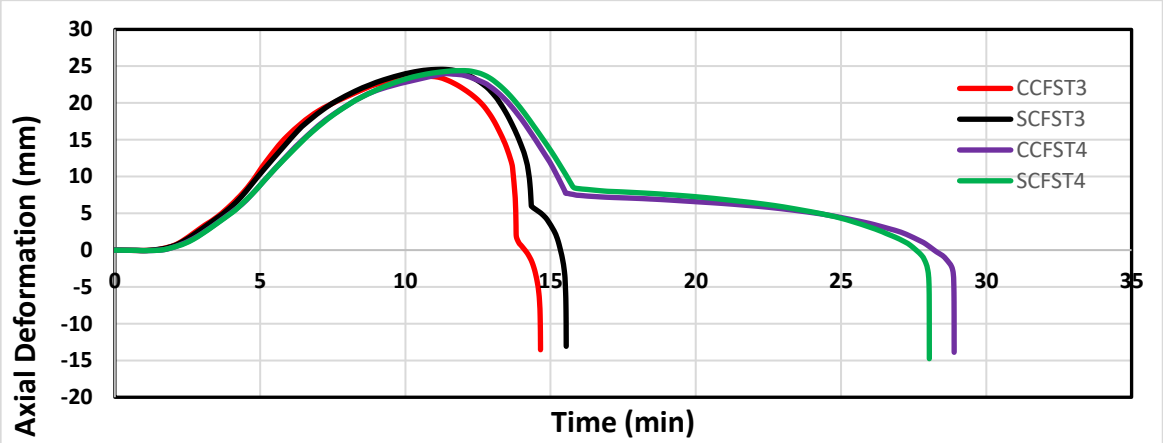

Figure 5-2 Axial deformation Vs time plot of Case B

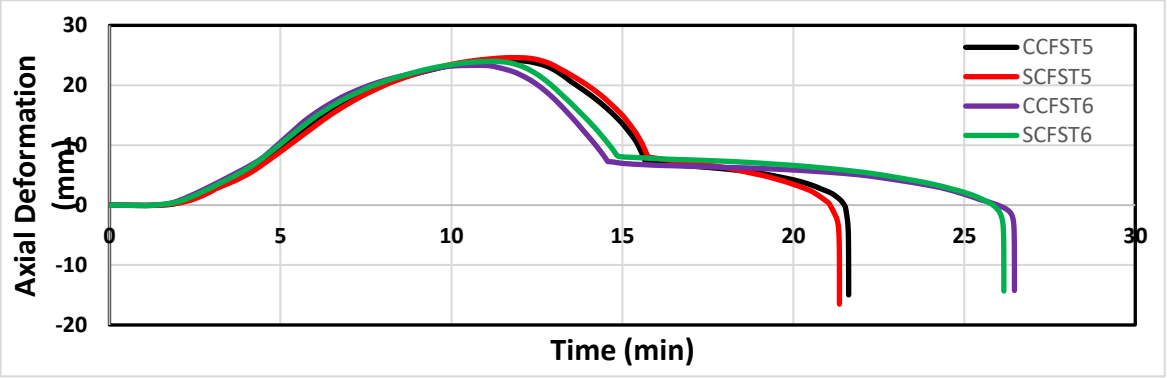

Figure 5-3 Axial deformation Vs time plot of Case C

According to case A the area of steel tube cross-section is equal for each of the two samples and the resulting axial deformation time plot is shown from Figure 5-1 above, for both group 1 and group 2 samples the fire resistance of the circular CFST column is higher than square CFST column. This is due to the reason that the square column has a larger outer surface that is exposed

to fire and the edge of the square column has higher exposure as indicated in Figure 5-4 below. Therefore, the heat transfer in the circular column is slower.

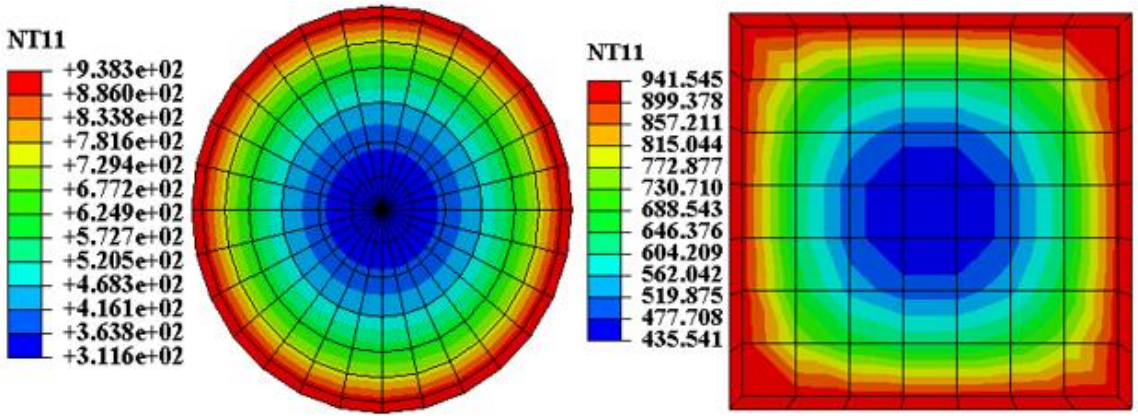

Figure 5-4 Nodal temperature output for Case A group 1 columns

The result of case B is shown from Figure 5-2 above and we see that in group 3 the fire resistance of the square column is higher than the circular column. In this case, even if the cross-sectional area of concrete is equal for both circular and square, the moment of inertia of the square column is slightly higher than the circular column, which provides high resistance to global buckling for the square column. While the fire resistance of the circular column is higher than the square column for group 4 samples. From this we can say that at a small cross-section with an equal area of concrete square columns resist more than circular but as the cross-section increases circular columns resist more than the square column. However, more research should be done to better understand the effect of cross-sectional shape on fire resistance.

According to case C, the total cross-section of circular and square section column is equal for both groups, group 5 and group 6. From the result shown in Figure 5-3 above we can see that the fire resistance of the circular CFST column is higher than the square CFST column.

Generally, the fire resistance based on the effect of cross-section needs more research by including their plastic resistance of the cross-sections under axial load.

5.2.2 Effect of support condition

To understand the effect of the nature of the end condition on the fire resistance of the CFST column two support conditions; Pinned-Fixed and Fixed-Fixed are considered for three paired samples. While other values of parameters are specified according to Table 5-1 above.

Table 5-5 List of samples taken to see the effect of support condition

Case	Outer diameter, D (mm)	Steel tube thickness, t (mm)
1	168.3	5
2	219.1	8
3	323.9	10

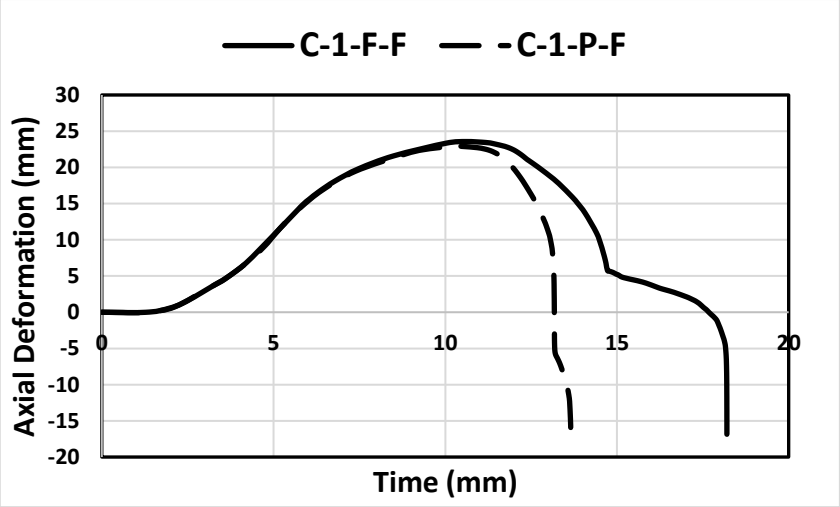

Figure 5-5 Axial deformation vs time plot for case 1 support condition

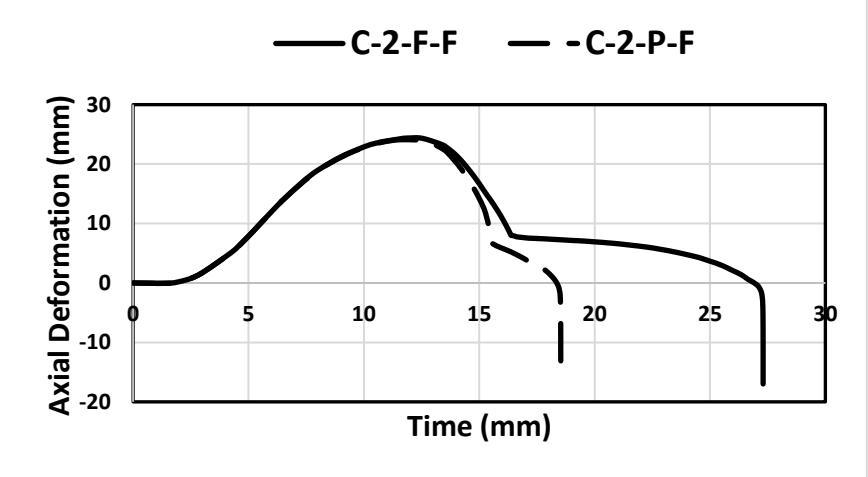

Figure 5-6 Axial deformation vs time plot for case 2 support condition

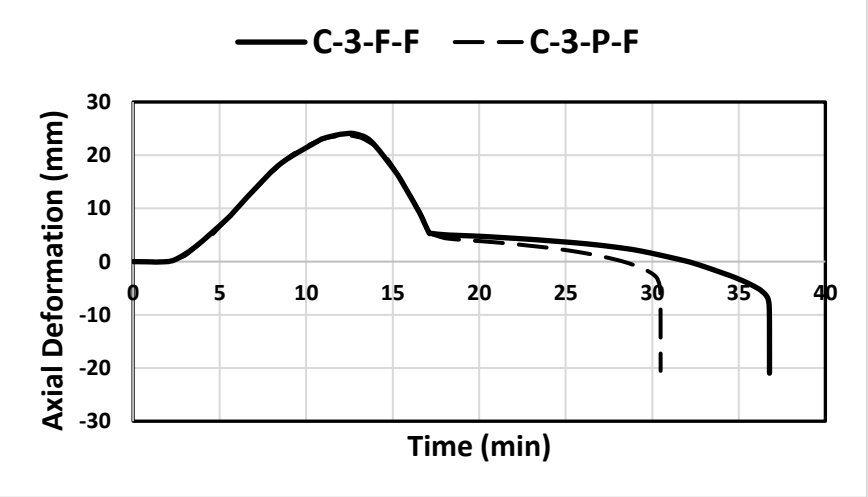

Figure 5-7 Axial deformation vs time plot for case 3 support condition

From the above three figures, it is obvious to see the effect of support condition on the overall effect of CFST column under fire exposure. Both fixed-fixed and pinned fixed column has the same effect on the axial deformation but on the fire resistance time amount, fixed-fixed support condition is much more than pinned-pinned support condition.

5.3 Parametric study

To conduct the effect of five parameters: Outer diameter to Steel tube thickness ratio (D/t) of the cross-section, compressive strength of concrete (fc), load ratio (μ), yield strength of steel (fy), and slenderness ratio (λ), a probabilistic generated input parameter was taken by using Latin Hypercube Sampling (LHS) technique as discussed in chapter four. And know the investigation of those parameters is discussed from the result of Finite element output.

5.3.1 Column Geometry

The column cross-section chosen for this parametric study was circular section as it is commonly used in most of the construction industry. The support condition is a fixed-fixed boundary condition to make it applicable for building construction.

5.3.2 Evaluation of the finite element method

From the 32 configurations, the detailed discussion of three representative samples is presented as follows.

The fire behavior of column C-7 is indicated in Figure 5-8 below. The column axial displacement vs time curve is measured at the top loading plate. The vertical gap between the steel tube and the concrete core is illustrated in the figure.

From Figure 5-8, it can be concluded that the CFST column passes through four stages before it fails. The four stages are discussed below.

Stage 1 (O-A): Both the steel tube and the concrete core begin to expand due to the thermal expansion of materials. As the steel tube expands more than the concrete core, a vertical gap is formed between the top of the steel tube and the top of the concrete surface as indicated by section O-A. at this stage, the steel tube carries most of the applied load.

Stage 2 (A-B): The steel gradually loses its ability to support the load as it degrades with temperature rise over time. As a result, the steel tube begins to contract, often accompanied by local bulging of the steel section. Then the concrete starts gradually to take part in carrying the load.

Stage 3 (B-C): At these stages, there is no longer a vertical gap between the top surface of the concrete and the top surface of the steel tube as shown in Figure 5-8 (b). The concrete core now carries the greatest proportion of the applied load and losses its strength slowly than the steel tube because of its lower thermal conductivity and higher heat capacity and therefore causes the temperature to rise more slowly. Another reason is that the concrete core loses its strength more slowly than the steel tube for temperatures below 700 °C according to EC 2 (2005) and EC 3 (2005).

Stage 4 (C-D): Over time, the strength of the concrete decreases as its temperature increases, and the rate at which the column contacts progressively increases until sudden failure occurs.

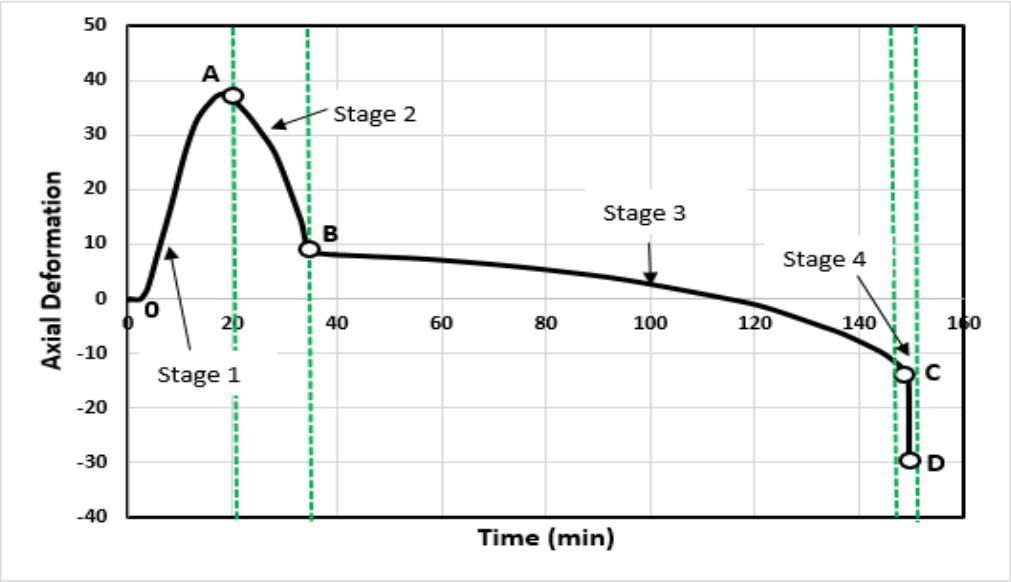

a) Axial Deformation vs time plot for C-7

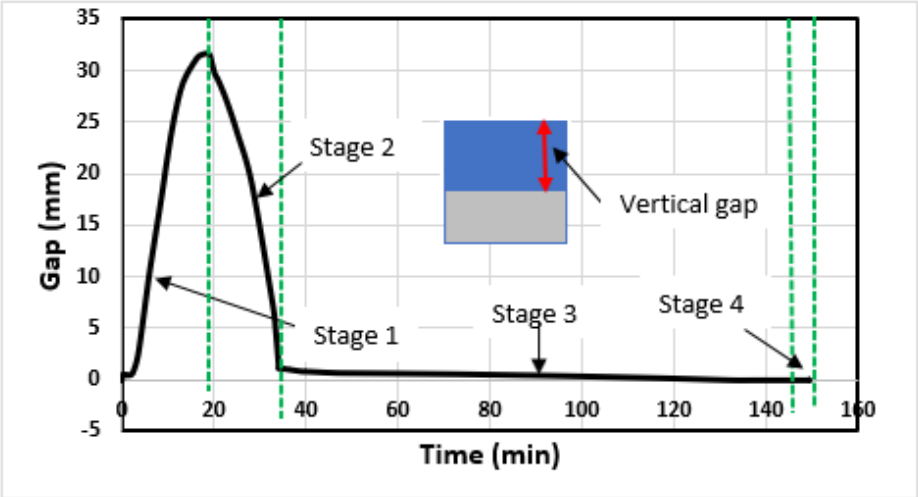

b) Vertical gap vs time plot for C-7

Figure 5-8 Fire behavior of CFST column for sample C-7

The CFST column C-16 passes through three stages before it fails as indicated in Figure 5-9 below. The three stages are discussed using the paragraph below.

Stage 1 (0-A): Both the steel tube and concrete core begin to expand due to the thermal expansion of materials. The vertical gap is formed between the steel tube and concrete core as indicated in Figure 5-9 (b). At this stage, the steel tube carries more load than the concrete core.

Stage 2 (A-B): The steel gradually loses its ability to support the load as it degrades with temperature rise over time. As a result, the steel tube begins to contract, often accompanied by local bulging of the steel section. Then the concrete starts gradually to take part in carrying the load.

Stage 3 (B-C): At these stages, there is no longer a vertical gap between the top surface of the concrete and the top surface of the steel tube as shown in Figure 5-8 (b). The concrete core now carries the greatest proportion of the applied load and losses its strength slowly than the steel tube for the reason discussed above.

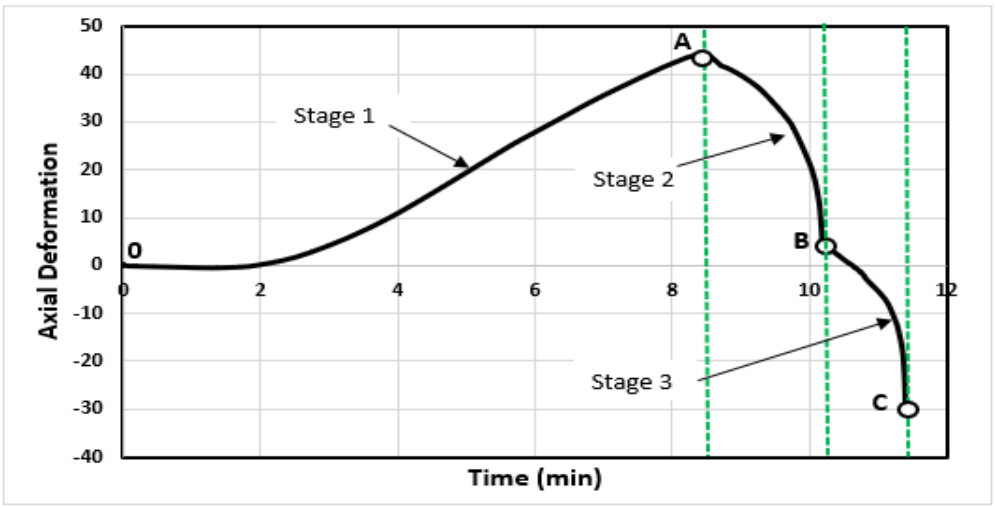

a) Axial Deformation vs time plot for C-16

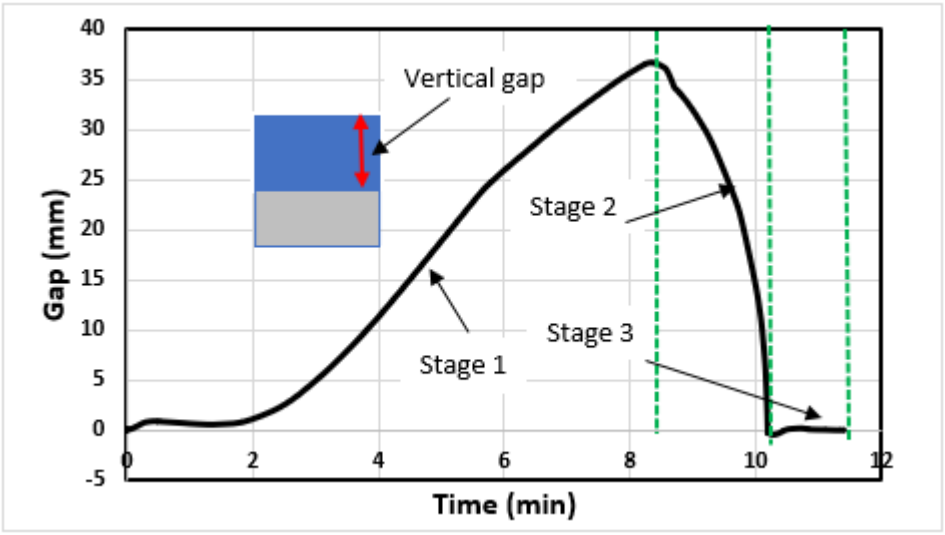

b) Vertical gap vs time plot for C-16

Figure 5-9 Fire behavior of CFST column for sample C-16

The CFST column C-2 passes through two stages before it fails as indicated in Figure 5-10 below. The two stages are discussed using the paragraph below.

Stage 1 (0-A): Similar to the first case, both the steel tube and the concrete core begin to expand by thermal expansion. As the steel tube expands more than concrete, a vertical gap is formed between the top of the steel tube and the top of the concrete surface.

Stage 2 (A-B): In this stage, the column fails due to the steel tube failure and overall buckling before the concrete takes part in carrying the load. This is clearly shown in Figure 5-10 below.

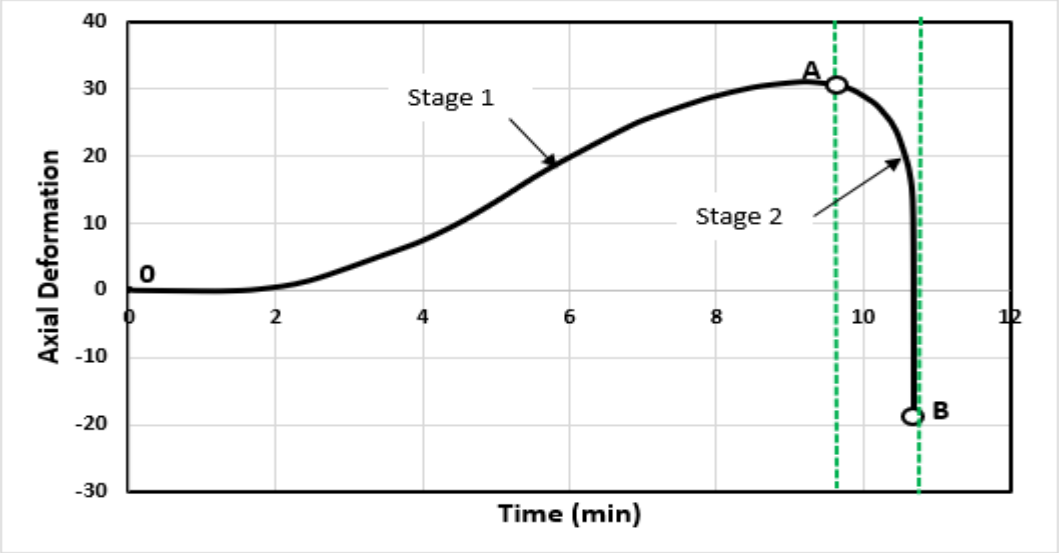

a) Axial Deformation vs time plot for C-2

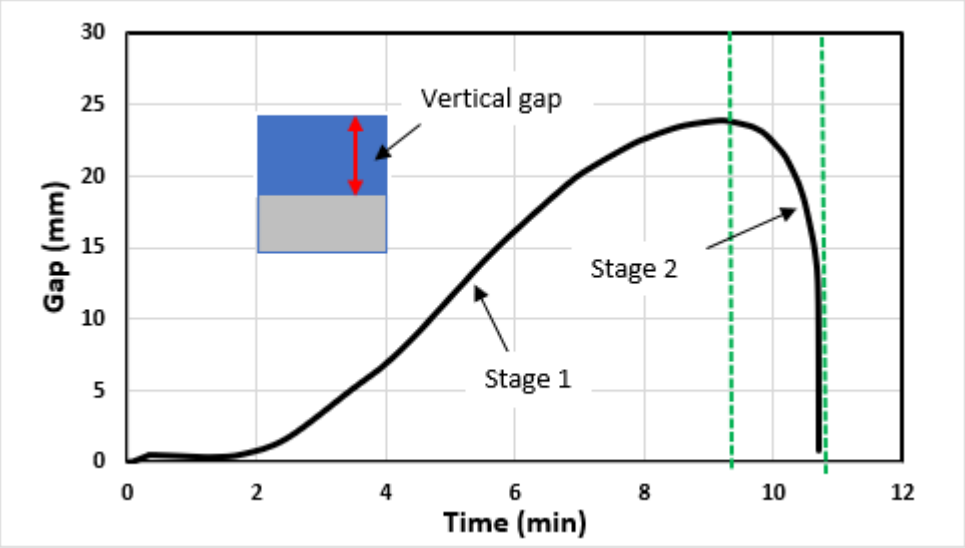

b) Vertical gap vs time plot for C-2

Figure 5-10 Fire behavior of CFST column for sample C-2

The summary output of the finite models for the 32 combinations is shown in table 5-6 below and the deformed shape of the C-13 and C-18 columns are plotted in the figure 5-11 below.

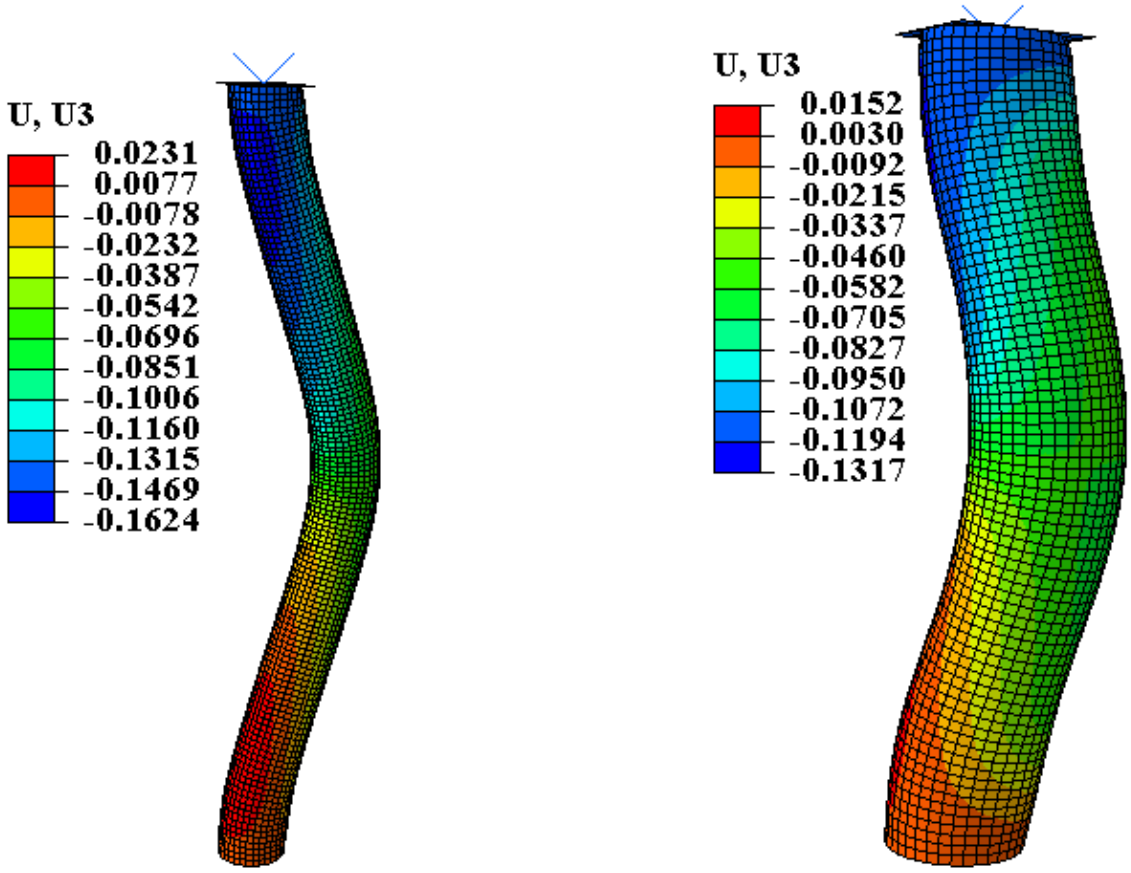

a) Deformed shape of C-13 b) deformed shape of C-18

Figure 5-11 Deformed shape of column C-13 and C-18

Table 5-6 Summary of the results for the 32 LHS samples obtained from Abaqus

Sample No.	Axial Deformation U3 (mm)	Fire Resistance Time FR (min)	Failure Mode
C-1	50.90	57.80	Buckling
C-2	31.00	10.69	Buckling
C-3	76.73	34.89	Buckling
C-4	24.95	14.54	Buckling
C-5	35.69	26.16	Buckling
C-6	37.83	9.87	Buckling
C-7	37.87	149.55	Buckling
C-8	69.95	16.11	Buckling
C-9	44.57	26.78	Buckling
C-10	67.68	14.13	Buckling
C-11	33.88	15.61	Buckling
C-12	13.68	49.53	Buckling
C-13	26.69	39.62	Buckling
C-14	62.61	10.31	Buckling
C-15	61.57	44.95	Buckling
C-16	44.03	11.39	Buckling
C-17	50.65	48.00	Buckling

Sample No.	Axial Deformation U3 (mm)	Fire Resistance Time FR (min)	Failure Mode
C-18	19.56	86.09	Buckling
C-19	54.10	15.61	Buckling
C-20	21.83	22.74	Buckling
C-21	79.64	26.48	Buckling
C-22	52.85	12.83	Buckling
C-23	74.81	19.58	Buckling
C-24	51.05	60.21	Buckling
C-25	16.74	39.95	Buckling
C-26	21.59	24.71	Buckling
C-27	58.29	11.28	Buckling
C-28	44.03	17.97	Buckling
C-29	32.57	11.00	Buckling
C-30	50.37	43.75	Buckling
C-31	48.24	11.09	Buckling
C-32	38.02	14.56	Buckling

Based on the result above all columns failed due to buckling because of their higher slenderness. Samples with a low value of slenderness ratio also failed finally by buckling. This is due to the reason that this type of cross-section like CFST columns are vulnerable to local plastic hinge formation between local buckling that occurs due to the high ductility of the CFST column when we compared to other sections and showing bulging and tearing of steel tube as is also referred in (Khandaker et al., 2021).

All samples can be matched with the above-discussed column under three categories. Column samples C-1, C-3, C-5, C-9, C-12, C-15, C17, C-18, C-20, C-21, C-23, C-24, C-25, C-26 and C-30 shows their behavior like C-7. Column samples C-4, C-10, C-13, C-19, and C-28 show their behavior like C-16. While column sample C-6, C-8, C-11, C-14, C-22, C-27, C-29, C-31, and C-32 shows their behavior like C-2.

5.3.3 Sensitivity analysis

Sensitivity Analysis, Axial Deformation

Using equations 4-1, 4-2, and 4-3, the coefficient of Variation, sensitivity factor, and uncertainty are obtained. From this, it can be observed that the load ratio n, the slenderness ratio λ, and the diameter to thickness ratio D/t govern the axial deformation of the CFST column.

Table 5-7 Sensitivity analysis parameters for axial deformation

	αi	COVi	Ui	%
D/t	0.12843	45%	0.057393	20%
fc	0.000608	20%	0.000123	0%
n	-0.20949	34%	-0.07044	-25%
fy	0.027028	16%	0.004266	2%
λ	0.351645	43%	0.150525	53%

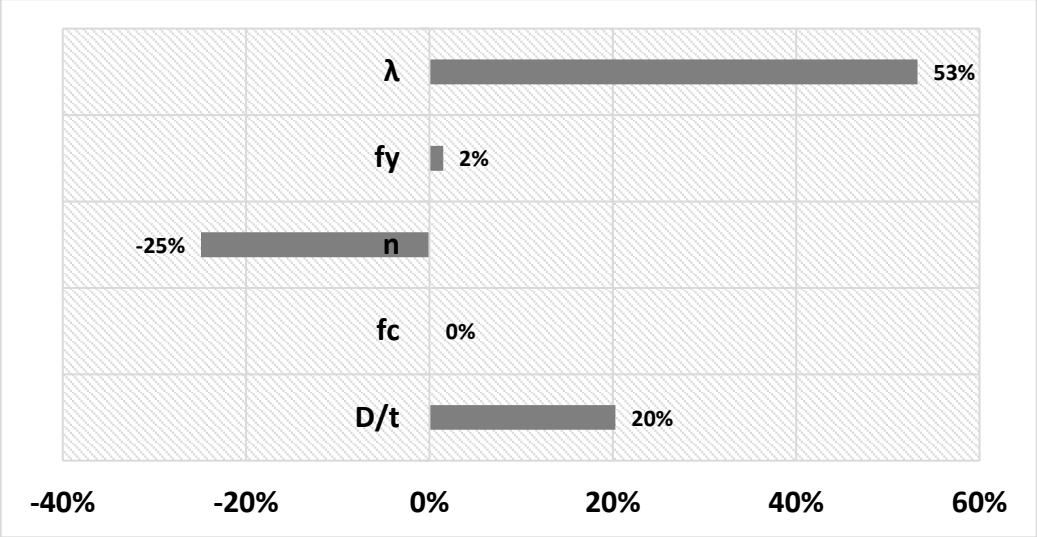

Figure 5-12 Sensitivity analysis for axial deformation

Sensitivity Analysis, Fire Resistance

Using equations 4-1, 4-2, and 4-3, the coefficient of Variation, sensitivity factor, and uncertainty are obtained. From this, we can see that the slenderness ratio λ, the load ratio n and the diameter to thickness ratio D/t govern the fire resistance of the CFST column.

Table 5-8 Sensitivity analysis parameters for fire resistance

	αi	COVi	Ui	%
D/t	0.180004	45%	0.08044	15%
fc	0.168284	20%	0.033949	6%
n	-0.2411	34%	-0.08107	-15%
fy	0.161352	16%	0.025466	5%
λ	-0.70877	43%	-0.3034	-58%

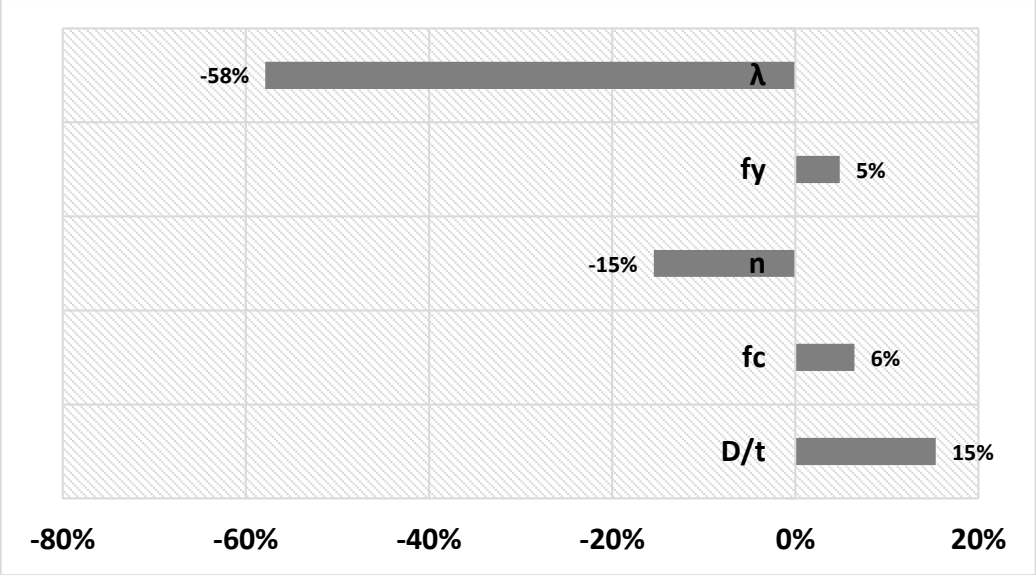

Figure 5-13 Sensitivity analysis for Fire resistance

From the sensitivity analysis, it can be seen that the slenderness ratio has a positive impact on the axial deformation and a negative contribution to the fire resistance of the column. The load ratio has a negative contribution to both the axial deformation and the fire resistance of the column. While the diameter to thickness ratio has a positive contribution to both the axial deformation and fire resistance.

As we can see from the above two charts, the influence of the compressive strength of concrete and the yield strength of steel is much less than the other parameters. From the axial deformation chart yield strength of steel has some amount of positive contribution while the effect of compressive strength of concrete is almost null. In the case of fire resistance, both of them have some positive contribution but the effect of compressive strength of concrete is better than the yield strength of steel.

CHAPTER 6 CONCLUSIONS AND RECOMMENDATIONS

6.1 Conclusion

This thesis presents a numerical study on the fire resistance of the CFST column under axial load. Some conclusions drawn from the outcome of this thesis are summarized as follows:

- A non-linear finite element model on the fire resistance of concrete-filled steel tube columns has been developed and verified against test results.
- From the effect of the support condition, it is seen that fixed-fixed support has higher fire resistance than pinned-fixed boundary conditions.
- The results of a parametric study by FE modeling reveal that sectional dimension, slenderness ratio, and load level have a significant effect on the fire resistance of the CFST column.
- During the sensitivity analysis, it was seen that the slenderness ratio, diameter to steel tube thickness ratio, and yield stress of steel have a direct relationship with axial deformation while the load ratio has an inverse relationship with axial deformation of CFST column under fire. Whereas the compressive strength of concrete does not affect the axial deformation.
- The fire resistance has a direct relationship with the diameter to steel tube thickness ratio, the yield stress of steel, and compressive strength of concrete, and an inverse relationship with load ratio and slenderness ratio.

6.2 Recommendation

The following recommendations are given for further work

- The design guideline for the fire resistance of the CFST column should be assessed based on these analyses using EC and other works of literature.
- Further studies should be conducted in order to see the effect of cross-section on the total capacity of the CFST column in terms of plastic resistance under fire conditions.

- Further study is required to account for bending effect in addition to compression on the fire resistance behavior of CFST column
- CFST column with external fire protection should be studied to investigate the importance of fire protection on fire resistance.
- CFST column with fiber-reinforced concrete (FC) or reinforced concrete (RC) as filling for steel tube should also be studied instead of plain concrete (PC) filling to investigate their importance in enhancing fire resistance.
- Preloading of the column should be investigated in order to see its effect on the fire resistance of the CFST column.

REFERENCES

Abaqus (2020) 'Analysis User's Guide Volume I: Introduction, Spatial Modeling, Execution & Output', I.

ASTM E119-88 (no date) 'ASTM E119: Standard Test Methods for Fire Tests of Building Construction and Materials', 552(1).

Castillo (1987) 'Carlos CASTILLO - Effect of transient high temperature on high strength concrete.pdf'.

CEB-FIP (1990) 'CEB FIP model code 1990 ing.pdf'.

Chen et al. (2006) 'Behavior of high strength structural steel at elevated temperatures', *Journal of Structural Engineering*, 132(12), pp. 1948–1954. doi: 10.1061/(ASCE)0733-9445(2006)132:12(1948).

Cheng et al (2004) 'Stress-strain curves for high strength concrete at elevated temperatures', (1), pp. 84–94.

Cooke, G. M. E. (1988) 'An introduction to the mechanical properties of structural steel at elevated temperatures', *Fire Safety Journal*, 13(1), pp. 45–54. doi: 10.1016/0379-7112(88)90032-X.

EN 1992-1-1 (2004) 'EN 1992-1-1 (2004) (English): Eurocode 2: Design of concrete structures - Part 1-1: General rules and rules for buildings', 1(2004).

EN 1992-1-2 (2004) 'EN 1992-1-2 (2004) (English): Eurocode 2: Design of concrete structures - Part 1-2: General rules - Structural fire design', 2(2004).

EN 1993-1-1 (2005) 'EN 1993-1-1 (2005) (English): Eurocode 3: Design of steel structures - Part 1-1: General rules and rules for buildings', 1(2005).

Espinos, A., Romero, M. L. and Hospitaler, A. (2012) 'Simple calculation model for evaluating the fire resistance of unreinforced concrete filled tubular columns', *Engineering Structures*, 42, pp. 231–244. doi: 10.1016/j.engstruct.2012.04.022.

Espinos et al. (2010) 'Advanced model for predicting the fire response of concrete filled tubular columns', pp. 1–67. doi: 10.1016/j.jcsr.2010.03.002.

Eurocode 1 part 2 (2002) 'Eurocode 1: Actions on structures - Part 1-2: General actions - Actions on structures exposed to fire [Authority: The European Union Per Regulation 305/2011, Directive 98/34/EC, Directive 2004/18/EC]', 2(2011).

Eurocode 2 part 2 (2005) '"Design of concrete structures, Part 1-2, General rules, structural fire design."BS EN 1992-1-2:2004, British Standards Institution, London.', 1(2005).

Eurocode 3 part 2 (2005) 'Design of steel structures - Part 1-2: General rules - Structural fire design [Authority: The European Union Per Regulation 305/2011, Directive 98/34/EC, Directive 2004/18/EC]', 1(2005).

Eurocode 4 part 2 (2005) '"Design of composite steel and concrete structures, part 1.2 General rules, Structural fire design". BS EN 1994-1-2:2005. British Standards Institution, London.', 2(2011).

Gao (2013) 'Finite element modeling of reinforced concrete beams exposed to fire', *Engineering Structures*, 52, pp. 488–501. doi: 10.1016/j.engstruct.2013.03.017.

Han et al. (2003) 'An experimental study and calculation on the fire resistance of concrete-filled SHS and RHS columns', *Journal of Constructional Steel Research*, 59(4), pp. 427–452. doi: 10.1016/S0143-974X(02)00041-X.

Han et al. (2013) 'Fire performance of concrete filled stainless steel tubular columns', *ENGINEERING STRUCTURES*, 56, pp. 165–181. doi: 10.1016/j.engstruct.2013.05.005.

Hong, S. and Varma, A. H. (2009) 'Analytical modeling of the standard fire behavior of loaded CFT columns Analytical modeling of the standard fire behavior of loaded CFT columns', 65(1), pp. 54–69. doi: 10.1016/j.jcsr.2008.04.008.

ISO 834-1 (1999) 'Fire-Resistance tests - Elements of building construction', 1999.

Kala, Z. and Kala, J. (2006) 'Sensitivity Analysis of Lateral Buckling Hot-Rolled Steel Beams', pp. 9–14.

Khandaker et al. (2021) 'Axial Load Behavior of Ultrahigh Strength Concrete-Filled Steel Tube Columns of Various Geometric and Reinforcement Configurations', *Infrastructures*, 6(5), p. 66. doi: 10.3390/infrastructures6050066.

Kodur and Lie (1995) 'FIRE PERFORMANCE OF CONCRETE-FILLED HOLLOW STEEL COLUMNS'.

Kodur, V. (2007) 'Guidelines for Fire Resistant Design of Concrete-Filled Steel HSS Columns - State-of-the-Art and Research Needs', 7, pp. 173–182.

Kodur, V. and Khaliq, W. (2011) 'Effect of Temperature on Thermal Properties of Different Types of High- Effect of Temperature on Thermal Properties of Different Types of High-Strength Concrete', (June), pp. 10–11. doi: 10.1061/(ASCE)MT.1943-5533.0000225.

Kodure, V. 1998 (1998) 'DESIGN EQUATIONS FOR EVALUATING FIRE RESISTANCE OF SFRC-FILLED HSS COLUMNS By V.', (June), pp. 671–677.

Lie, T.T. and Chabot, M. (1992) 'Experimental Studies on the Fire Resistance of Hollow Steel Columns Filled with Plain Concrete'.

Lie and Stringer, 1994 (1993) 'Calculation of the fire resistance of steel hollow structural section columns filled with plain concrete', (1992), pp. 1992–1995.

Lu, H., Han, L. and Zhao, X. (2010) 'Fire performance of self-consolidating concrete filled double skin steel tubular columns : Experiments', *Fire Safety Journal*, 45(2), pp. 106–115. doi: 10.1016/j.firesaf.2009.12.001.

Naus, D. J. (2006) *The Effect of Elevated Temperature on Concrete Materials and Structures - A Literature Review*.

Netsanet Bezu (2018) 'Parametric Study of Shear Strength of Reinforced Concrete Beams A Thesis in Structural Engineering " Parametric Study of Shear Strength of Reinforced Concrete Beams "'.

Schneider (1981) 'Effect of Temperature on Steel and Concrete for PCRV's', 67, pp. 245–258.

Tao, Z., Wang, Z. Bin and Yu, Q. (2013) 'Finite element modelling of concrete-filled steel stub columns under axial compression', *Journal of Constructional Steel Research*, 89, pp. 121–131. doi: 10.1016/j.jcsr.2013.07.001.

Vangeem, M. G. *et al.* (1997) 'Thermal Properties of Commercially Available High-Strength Concretes Thermal Properties of Commercially Available', (2031).

APPENDIX

Appendix A

Result output values using Latin hypercube sampling method

Sample No.	Result output values					Adjusted values				
	D/t	fc (MPa)	n	fy (MPa)	λ	D/t	fc (MPa)	n	fy (MPa)	λ
C1	50.26	48.39	0.35	320.16	0.78	50.80	48.39	0.35	355.00	0.78
C2	21.74	42.74	0.51	235.00	1.36	22.17	42.74	0.51	235.00	1.36
C3	23.42	47.58	0.26	273.71	0.93	22.85	47.58	0.26	275.00	0.93
C4	16.71	35.48	0.68	258.23	0.83	16.83	35.48	0.68	275.00	0.83
C5	45.23	29.03	0.20	277.58	1.03	44.45	29.03	0.20	275.00	1.03
C6	26.77	45.97	0.59	343.39	1.80	26.71	45.97	0.59	355.00	1.80
C7	41.87	39.52	0.25	262.10	0.35	42.96	39.52	0.25	275.00	0.35
C8	18.39	25.00	0.38	331.77	1.27	16.20	25.00	0.38	355.00	1.27
C9	20.06	32.26	0.57	324.03	0.64	20.32	32.26	0.57	355.00	0.64
C10	36.84	40.32	0.54	300.81	1.17	36.56	40.32	0.54	275.00	1.17
C11	11.68	45.16	0.41	339.52	1.12	11.11	45.16	0.41	355.00	1.12
C12	38.52	26.61	0.36	335.65	0.40	38.74	26.61	0.36	355.00	0.40
C13	15.03	34.68	0.31	289.19	0.49	15.28	34.68	0.31	275.00	0.49
C14	40.19	28.23	0.65	254.35	1.41	40.49	28.23	0.65	235.00	1.41
C15	62.00	37.10	0.52	296.94	0.92	63.50	37.10	0.52	275.00	0.92
C16	51.94	43.55	0.67	246.61	1.32	51.41	43.55	0.67	235.00	1.32
C17	30.13	50.00	0.55	265.97	0.54	30.50	50.00	0.55	275.00	0.54
C18	25.10	44.35	0.43	327.90	0.30	25.40	44.35	0.43	355.00	0.30
C19	55.29	25.81	0.46	308.55	1.07	56.44	25.81	0.46	275.00	1.07
C20	58.65	46.77	0.70	312.42	0.88	61.13	46.77	0.70	275.00	0.88
C21	31.81	36.29	0.23	347.26	0.98	31.75	36.29	0.23	355.00	0.98
C22	28.45	33.87	0.28	293.06	1.75	28.22	33.87	0.28	275.00	1.75
C23	56.97	38.71	0.30	238.87	1.25	57.13	38.71	0.30	235.00	1.25
C24	46.90	37.90	0.60	355.00	0.59	48.80	37.90	0.60	355.00	0.59
C25	48.58	30.65	0.64	281.45	0.45	48.90	30.65	0.64	275.00	0.45
C26	33.48	29.84	0.44	242.74	0.69	33.66	29.84	0.44	235.00	0.69
C27	43.55	31.45	0.49	351.13	1.65	43.33	31.45	0.49	355.00	1.65
C28	53.61	41.94	0.22	316.29	1.51	54.78	41.94	0.22	355.00	1.51
C29	35.16	49.19	0.39	285.32	1.70	34.93	49.19	0.39	275.00	1.70
C30	60.32	41.13	0.47	269.84	0.74	61.00	41.13	0.47	275.00	0.74
C31	13.35	33.06	0.62	304.68	1.56	13.64	33.06	0.62	275.00	1.56
C32	10.00	27.42	0.33	250.48	1.22	9.84	27.42	0.33	235.00	1.22

Label	Outer diameter D (mm)	Steel tube thickness t (mm)	Concrete Cylindrical Strength fc (N/mm2)	Applied Load Napp (N)	Steel yield strength fy (N/mm2)	Length L (m)
C1	508	10	48.39	5040819	355	6.51
C2	139.7	6.3	42.74	588879	235	4.42
C3	457	20	47.58	3716189	275	9.15
C4	168.3	10	35.48	1354429	275	3.37
C5	177.8	5	29.03	277694	275	3.99
C6	168.3	6.3	45.97	1182099	355	5.93
C7	610	14.2	39.52	4423124	275	4.11
C8	323.9	20	25.00	3155658	355	9.39
C9	406.4	20	32.26	6863047	355	5.65
C10	457	12.5	40.32	5769852	275	10.70
C11	177.8	16	45.16	1491717	355	4.39
C12	193.7	5	26.61	635002	355	1.57
C13	244.5	16	34.68	1373149	275	2.94
C14	323.9	8	28.23	2585205	235	10.17
C15	508	8	37.10	5491521	275	8.10
C16	323.9	6.3	43.55	3199629	235	7.71
C17	610	20	50.00	12735358	275	6.55
C18	355.6	14	44.35	3863056	355	2.14
C19	355.6	6.3	25.81	1963138	275	7.67
C20	244.5	4	46.77	2020099	275	3.49
C21	508	16	36.29	3538990	355	9.87
C22	177.8	6.3	33.87	465715	275	6.92
C23	457	8	38.71	2541750	235	10.37
C24	610	12.5	37.90	11170160	355	6.39
C25	244.5	5	30.65	1498539	275	2.17
C26	168.3	5	29.84	525931	235	2.65
C27	273	6.3	31.45	1740096	355	8.67
C28	219.1	4	41.94	524612	355	5.52
C29	139.7	4	49.19	448288	275	4.55
C30	610	10	41.13	7790140	275	7.61
C31	193.7	14.2	33.06	1803354	275	7.49
C32	139.7	14.2	27.42	520677	235	4.66

The selection of Diameter and thickness is based on the table of standards given in Euro Code 3 (2005) and the selection is by the nearest ratio of D/t from LHS output and the values given in the standard section of EC3. The length and the applied load of the CFST column were calculated based on the relationship given in Euro Code 4 (2004).

Appendix B

Axial deformation vs time plot for the LHS samples

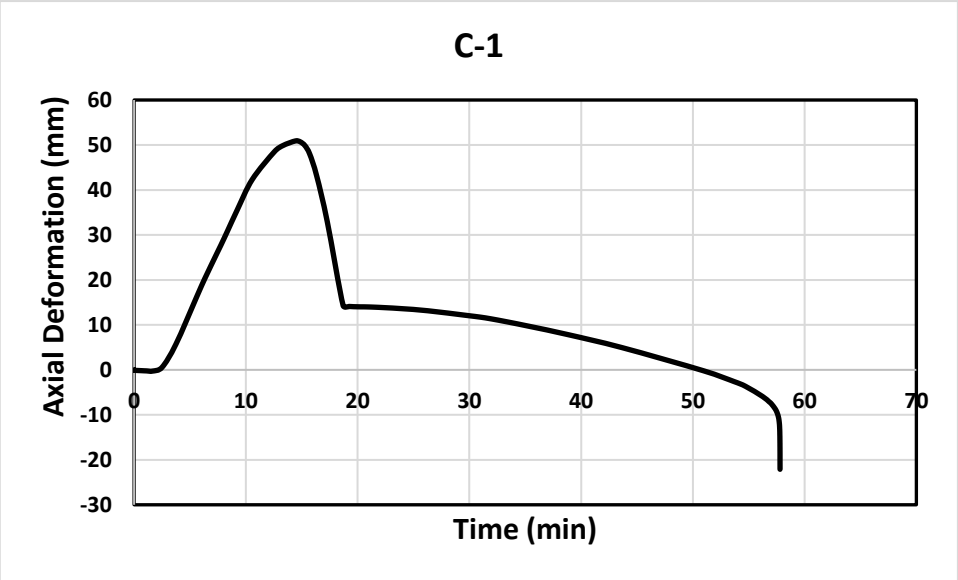

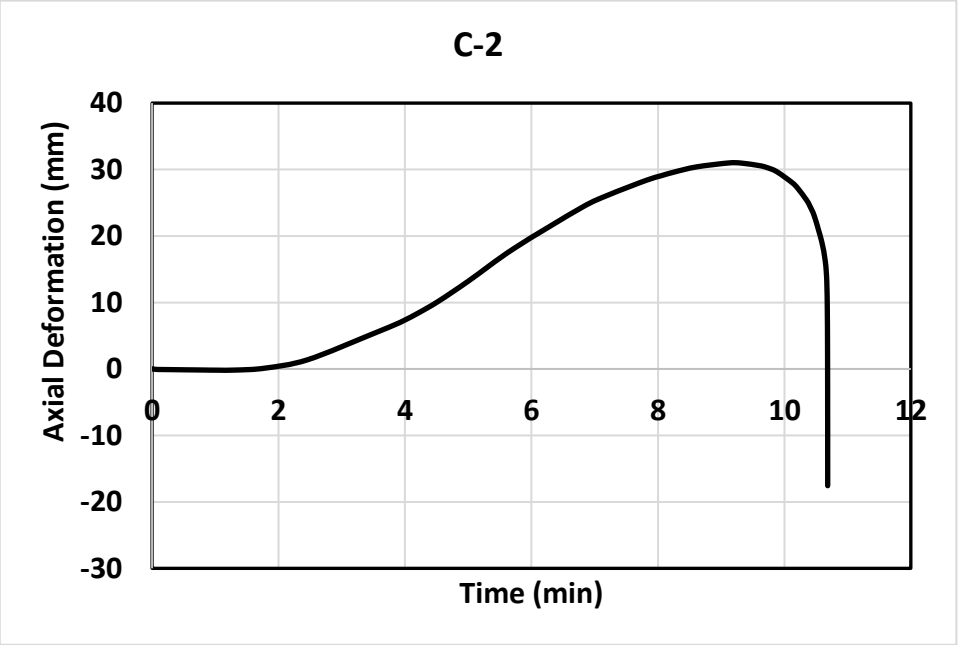

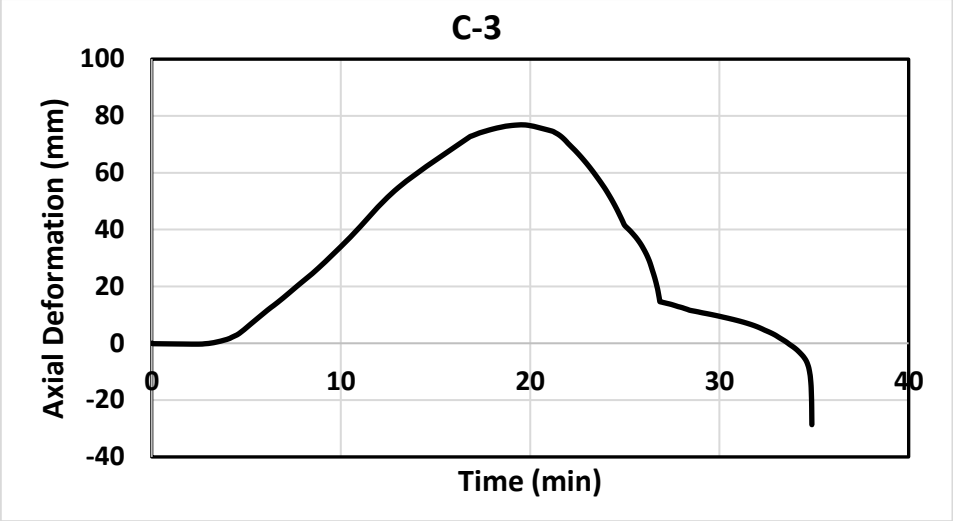
C-3
Axial Deformation (mm)
100
80
60
40
20
0
-20
-40
0
10
20
30
40
Time (min)

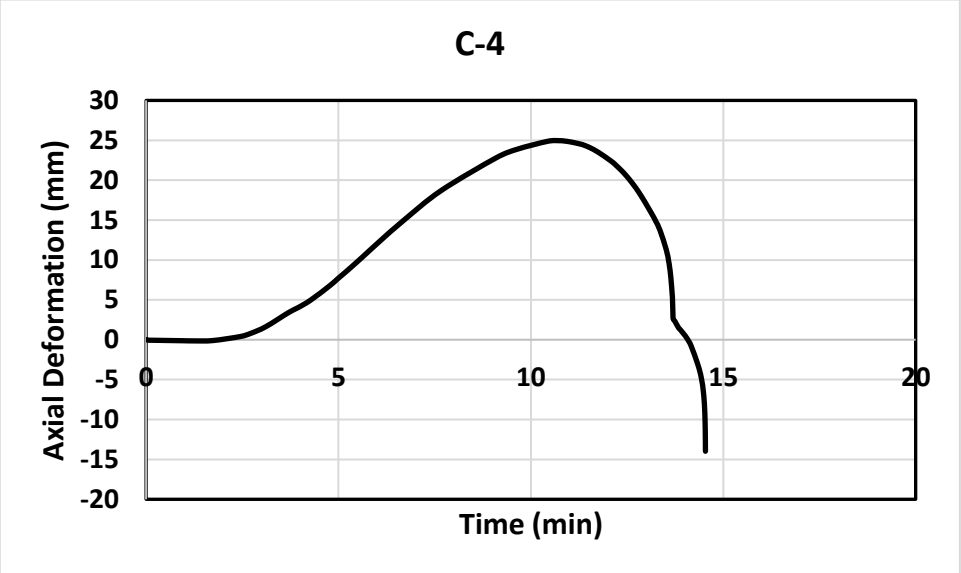
C-4
Axial Deformation (mm)
30
25
20
15
10
5
0
-5
-10
-15
-20
0
5
10
15
20
Time (min)

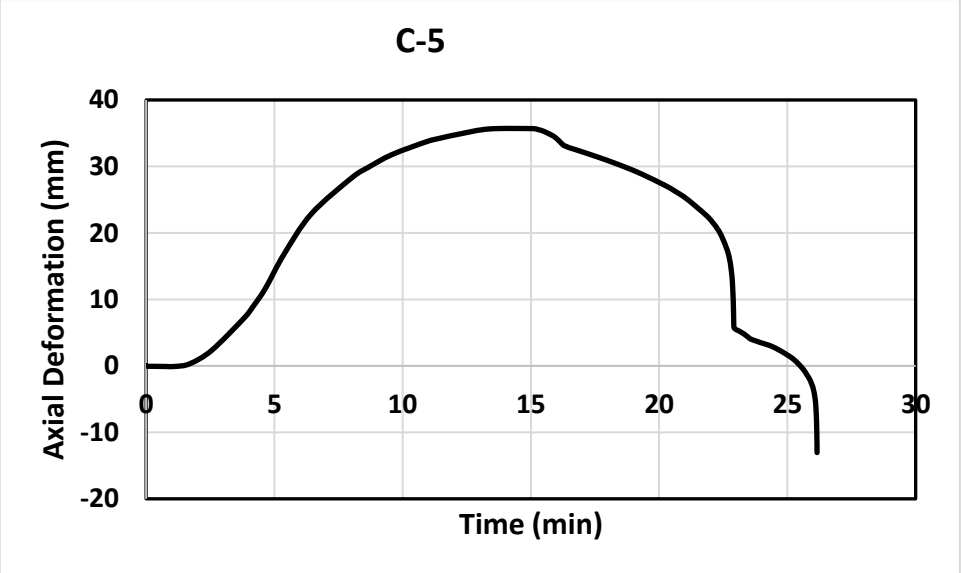
C-5
Axial Deformation (mm)
40
30
20
10
0
-10
-20
0
5
10
15
20
25
30
Time (min)

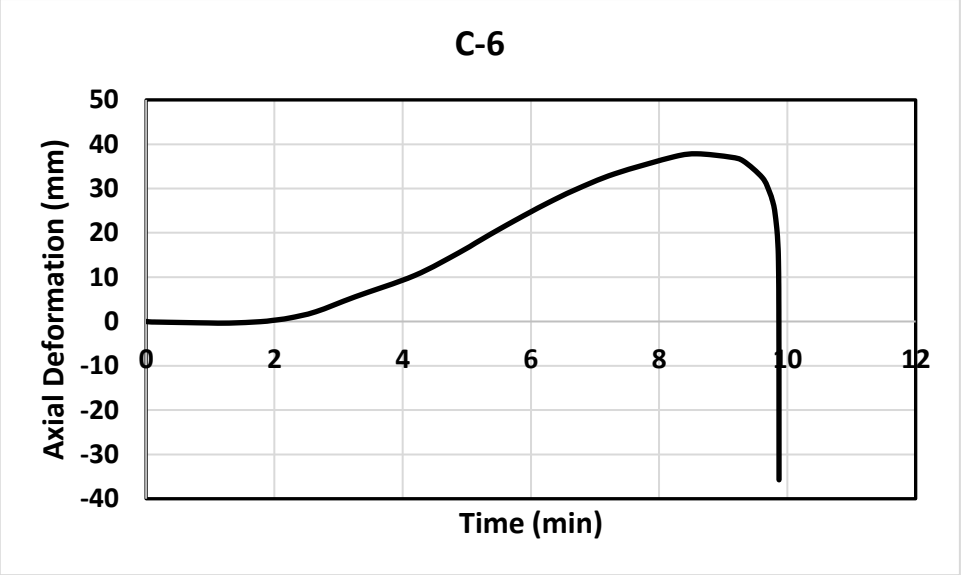
C-6
Axial Deformation (mm)
50
40
30
20
10
0
-10
-20
-30
-40
0
2
4
6
8
10
12
Time (min)

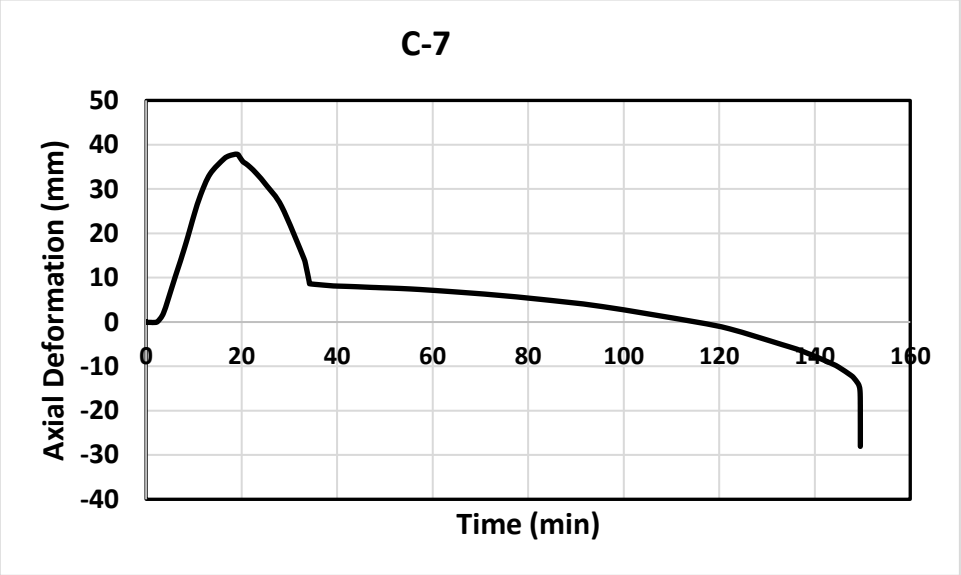
C-7
Axial Deformation (mm)
50
40
30
20
10
0
-10
-20
-30
-40
0
20
40
60
80
100
120
140
160
Time (min)

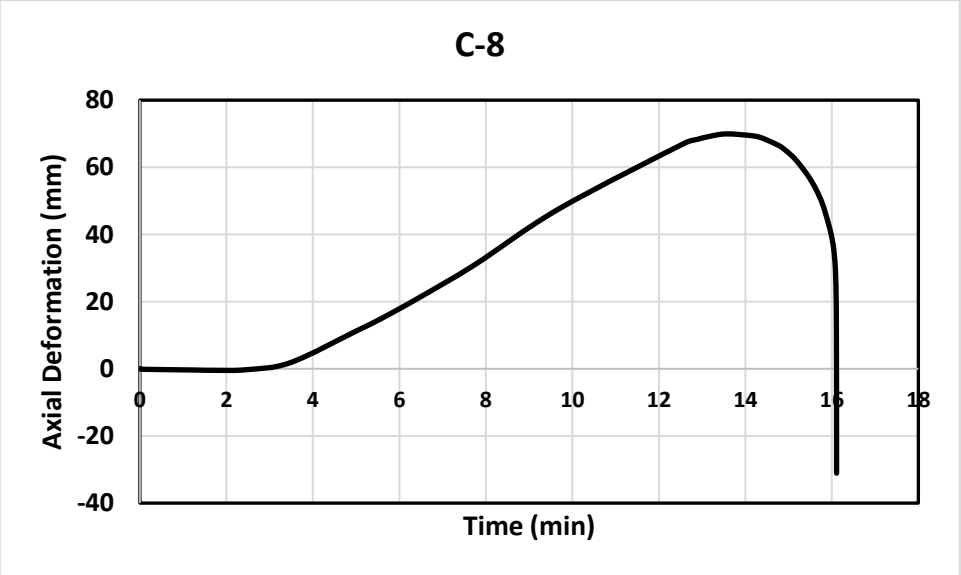
C-8
Axial Deformation (mm)
80
60
40
20
0
-20
-40
0
2
4
6
8
10
12
14
16
18
Time (min)

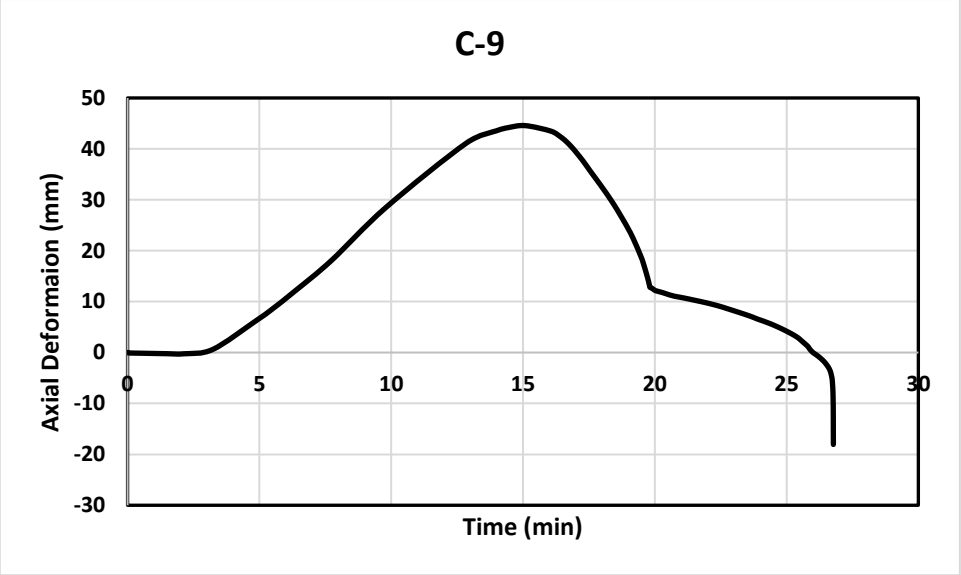
C-9
Axial Deformaion (mm)
50
40
30
20
10
0
-10
-20
-30
0
5
10
15
20
25
30
Time (min)

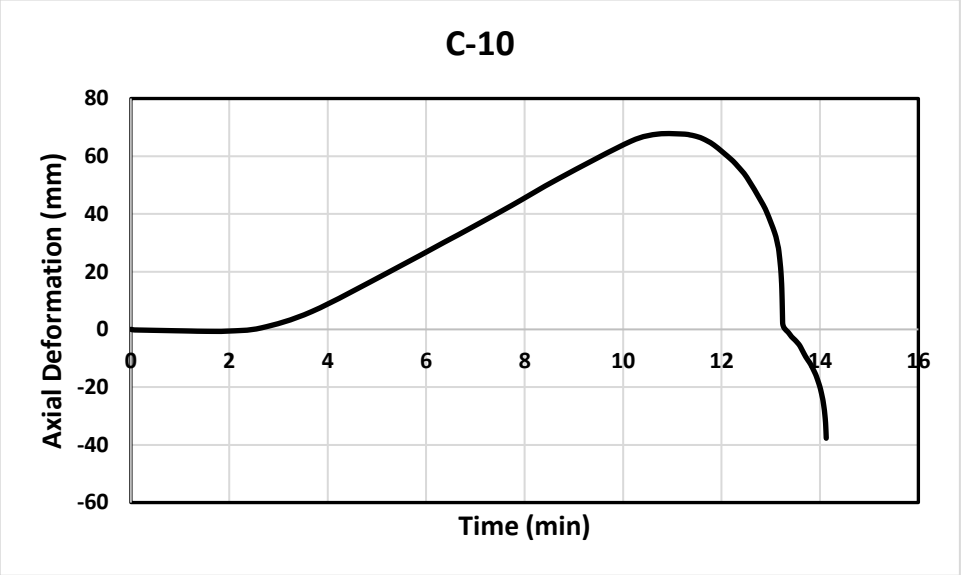
C-10
Axial Deformation (mm)
80
60
40
20
0
-20
-40
-60
0
2
4
6
8
10
12
14
16
Time (min)

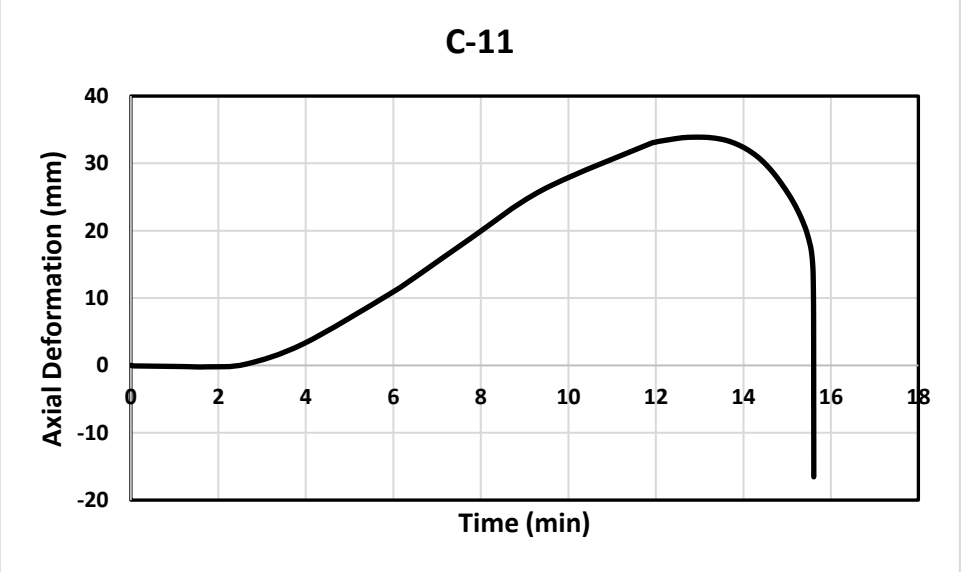
C-11
Axial Deformation (mm)
40
30
20
10
0
-10
-20
0
2
4
6
8
10
12
14
16
18
Time (min)

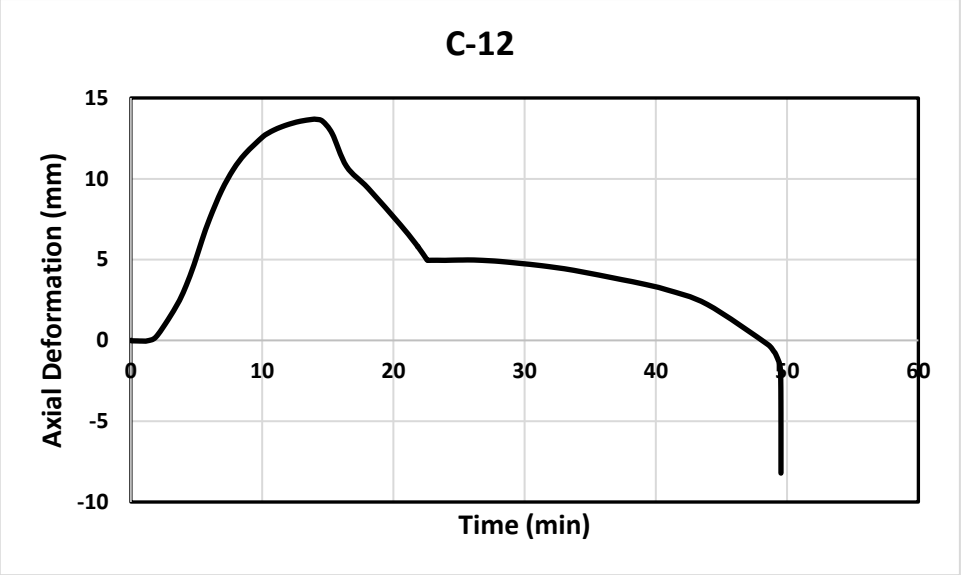
C-12
Axial Deformation (mm)
15
10
5
0
-5
-10
0
10
20
30
40
50
60
Time (min)

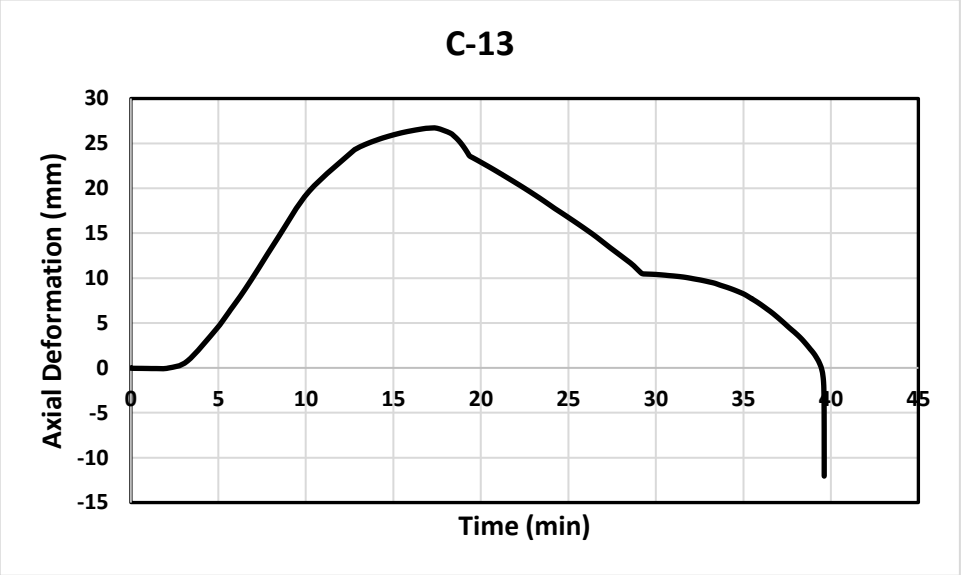
C-13
Axial Deformation (mm)
30
25
20
15
10
5
0
-5
-10
-15
0
5
10
15
20
25
30
35
40
45
Time (min)

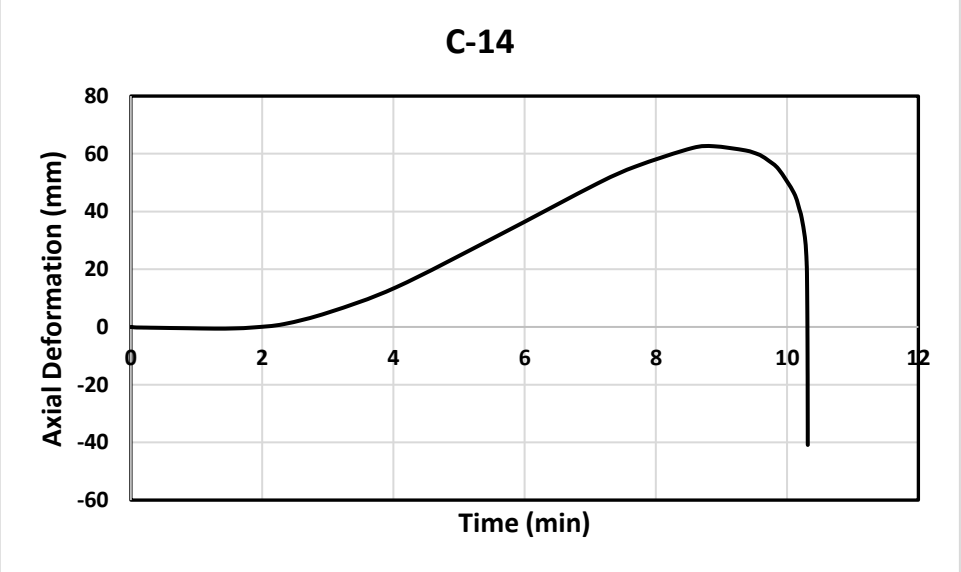
C-14
Axial Deformation (mm)
80
60
40
20
0
-20
-40
-60
0
2
4
6
8
10
12
Time (min)

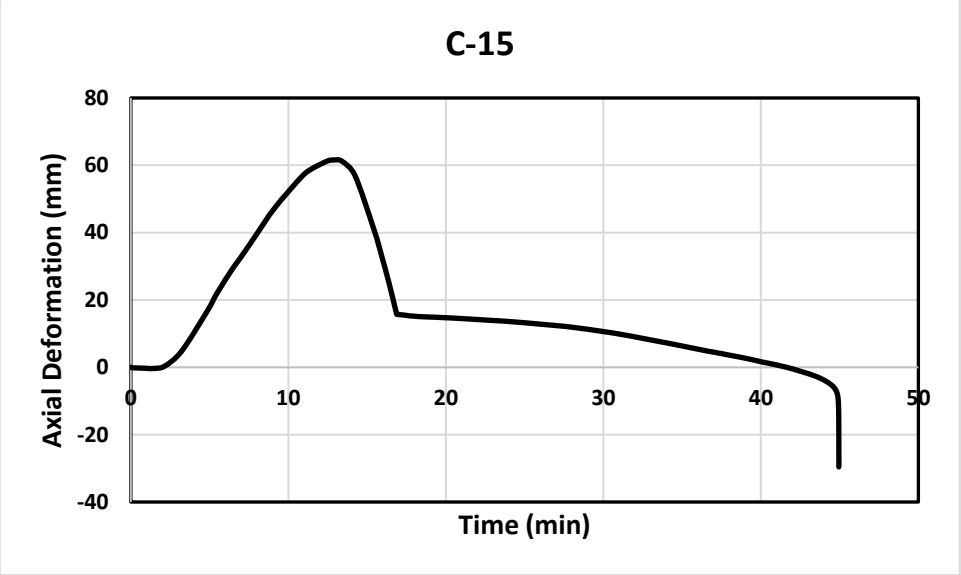
C-15
Axial Deformation (mm)
80
60
40
20
0
-20
-40
0
10
20
30
40
50
Time (min)

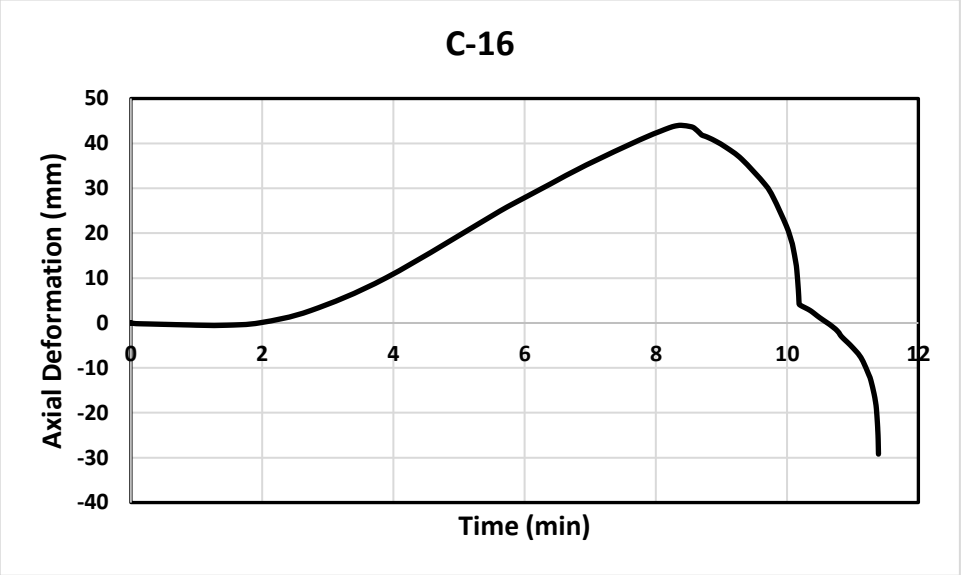
C-16
Axial Deformation (mm)
50
40
30
20
10
0
-10
-20
-30
-40
0
2
4
6
8
10
12
Time (min)

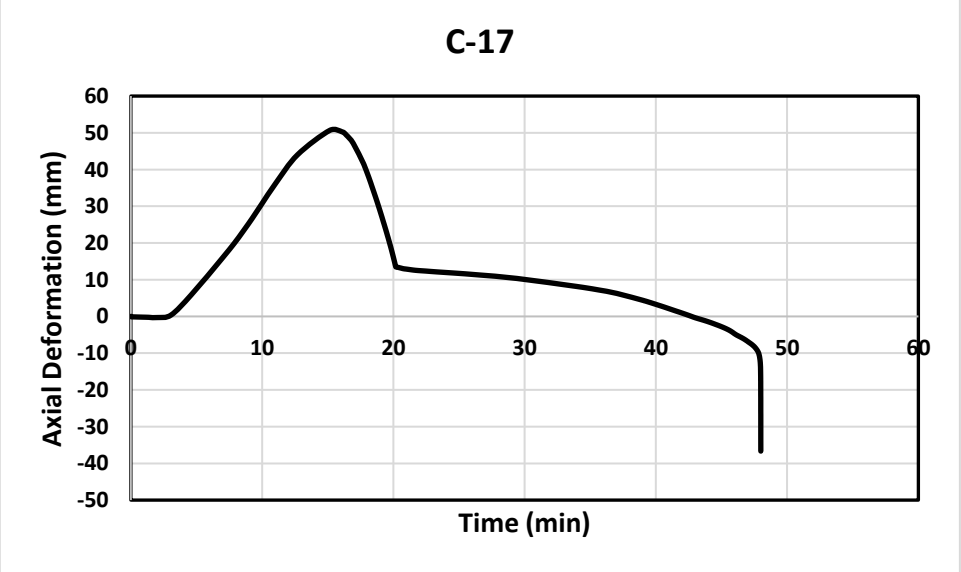
C-17
Axial Deformation (mm)
60
50
40
30
20
10
0
-10
-20
-30
-40
-50
0
10
20
30
40
50
60
Time (min)

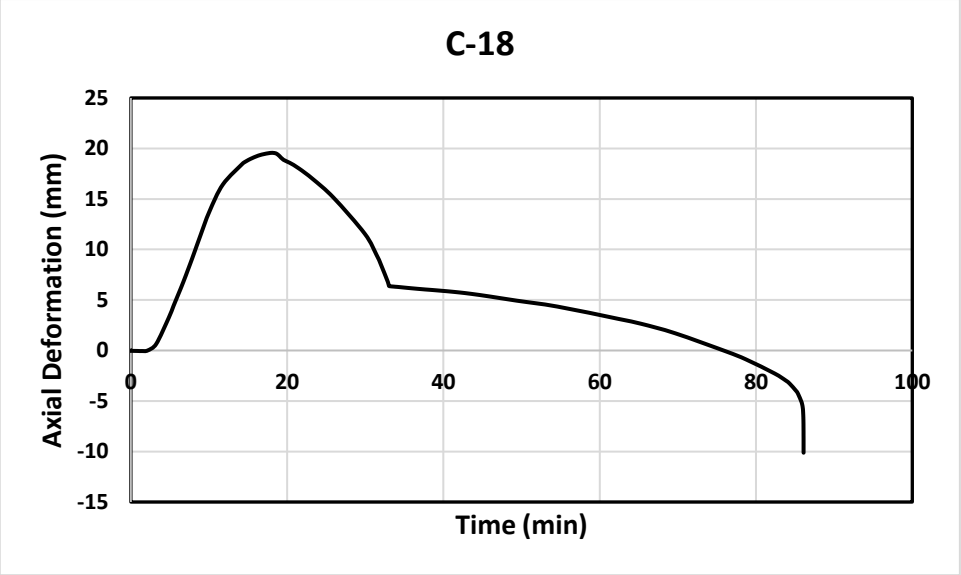
C-18
Axial Deformation (mm)
25
20
15
10
5
0
-5
-10
-15
0
20
40
60
80
100
Time (min)

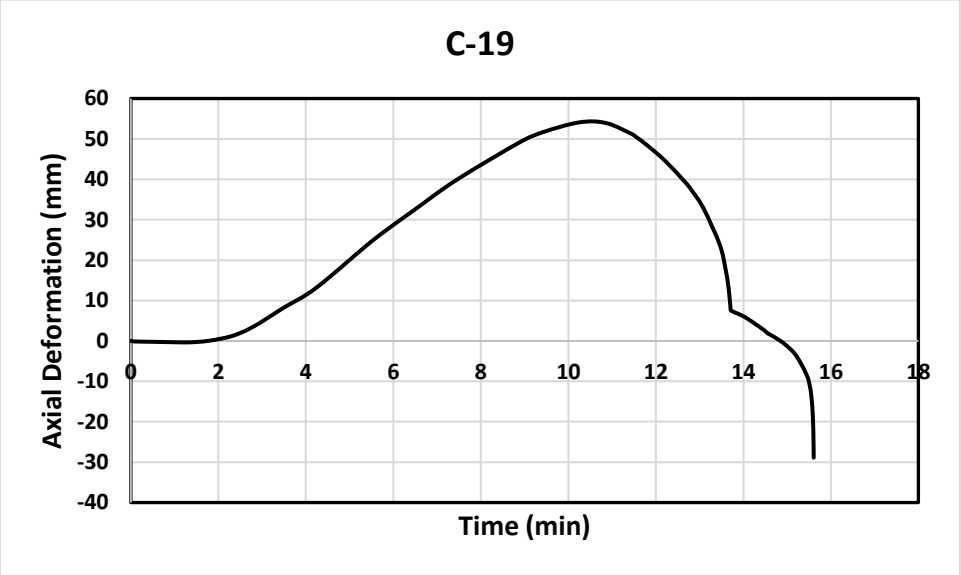
C-19
Axial Deformation (mm)
60
50
40
30
20
10
0
-10
-20
-30
-40
0
2
4
6
8
10
12
14
16
18
Time (min)

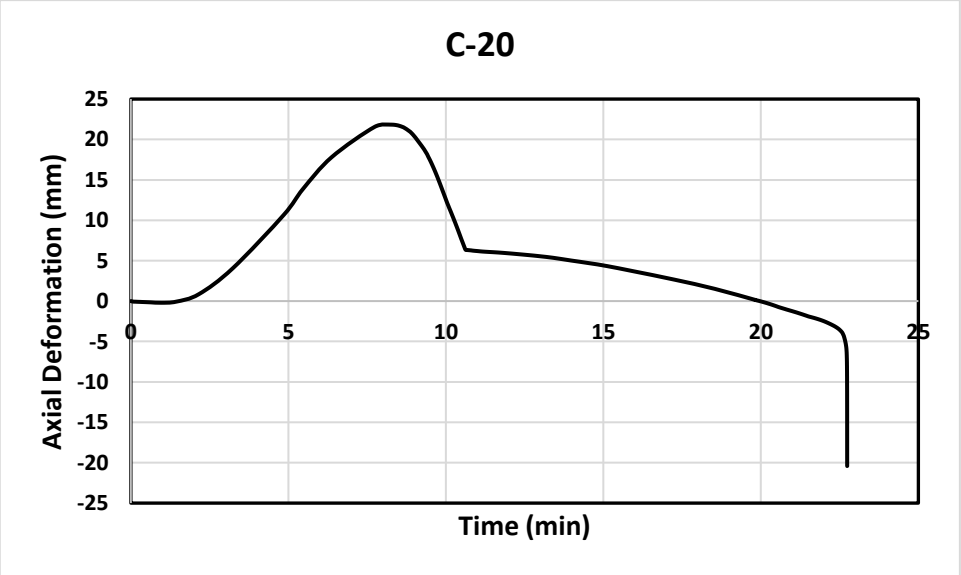
C-20
Axial Deformation (mm)
25
20
15
10
5
0
-5
-10
-15
-20
-25
0
5
10
15
20
25
Time (min)

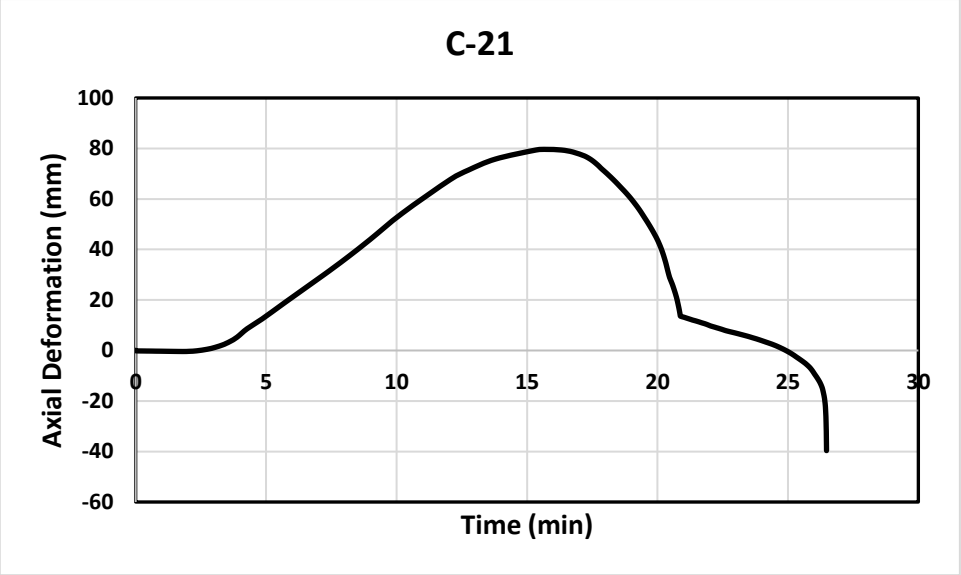
C-21
Axial Deformation (mm)
100
80
60
40
20
0
-20
-40
-60
0
5
10
15
20
25
30
Time (min)

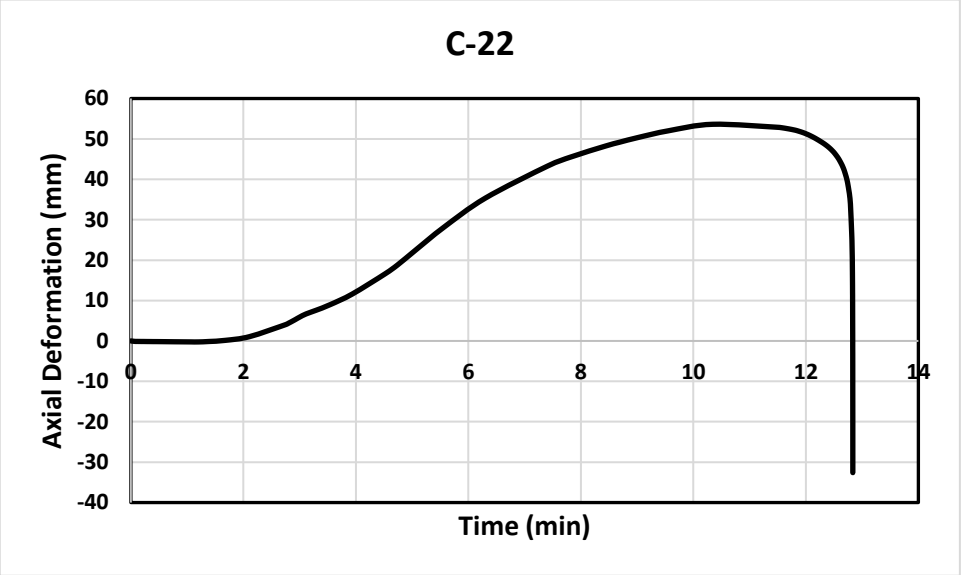
C-22
Axial Deformation (mm)
60
50
40
30
20
10
0
-10
-20
-30
-40
0
2
4
6
8
10
12
14
Time (min)

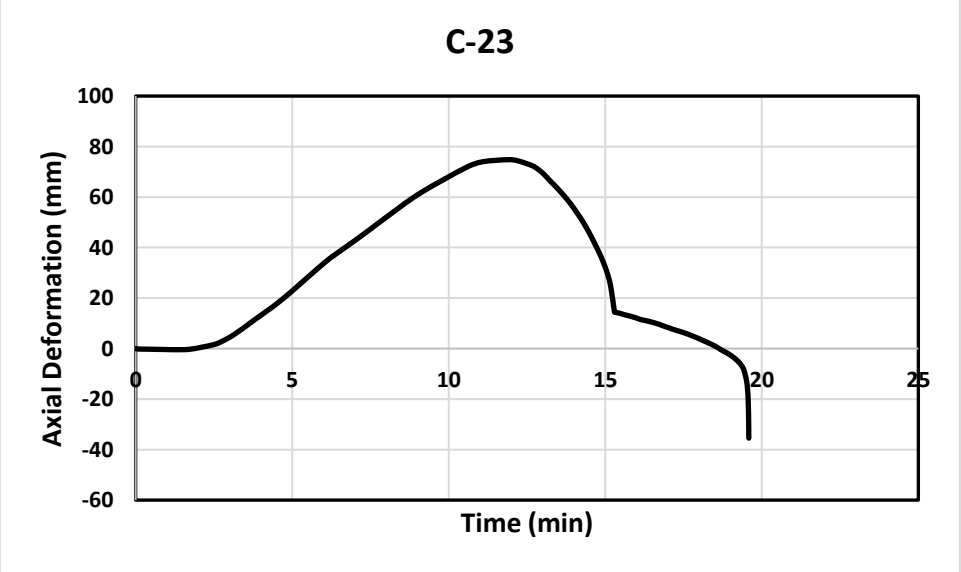
C-23
Axial Deformation (mm)
100
80
60
40
20
0
-20
-40
-60
0
5
10
15
20
25
Time (min)

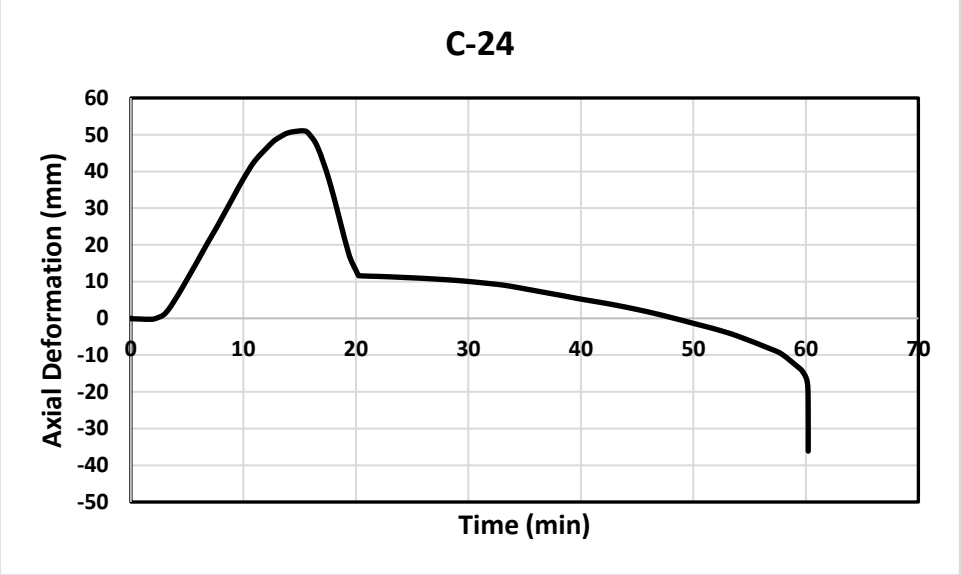
C-24
Axial Deformation (mm)
60
50
40
30
20
10
0
-10
-20
-30
-40
-50
0
10
20
30
40
50
60
70
Time (min)

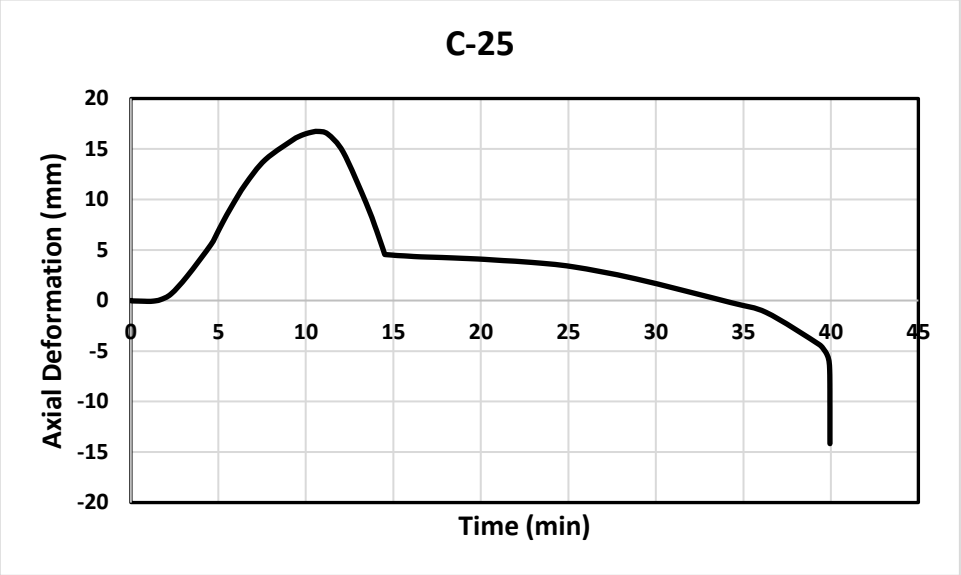
C-25
Axial Deformation (mm)
20
15
10
5
0
-5
-10
-15
-20
0
5
10
15
20
25
30
35
40
45
Time (min)

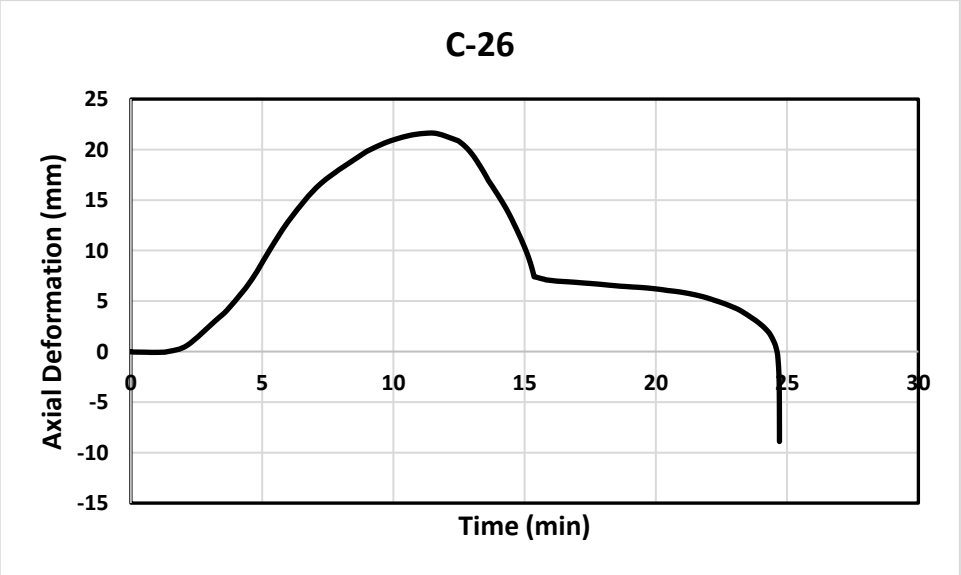
C-26
Axial Deformation (mm)
25
20
15
10
5
0
-5
-10
-15
0
5
10
15
20
25
30
Time (min)

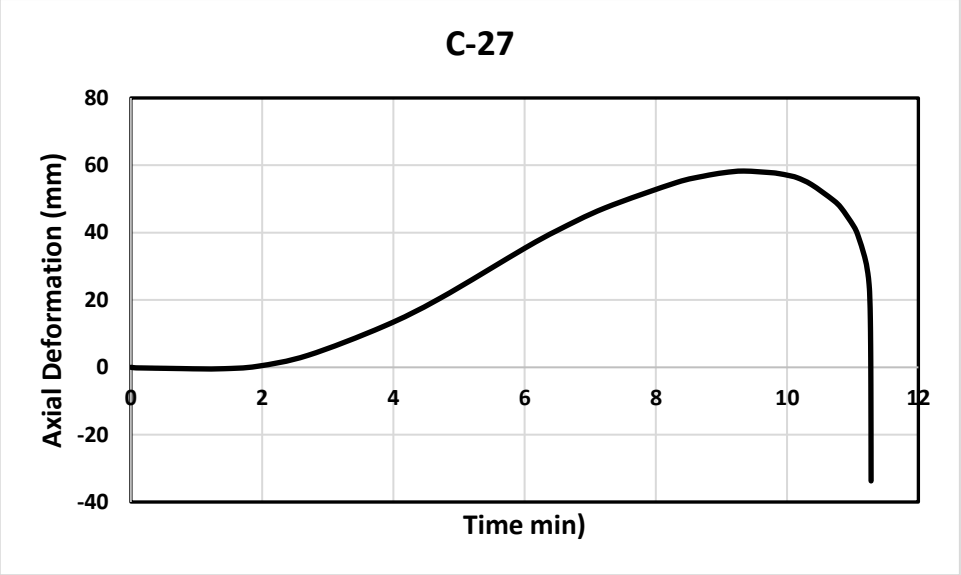
C-27
Axial Deformation (mm)
80
60
40
20
0
-20
-40
0
2
4
6
8
10
12
Time min)

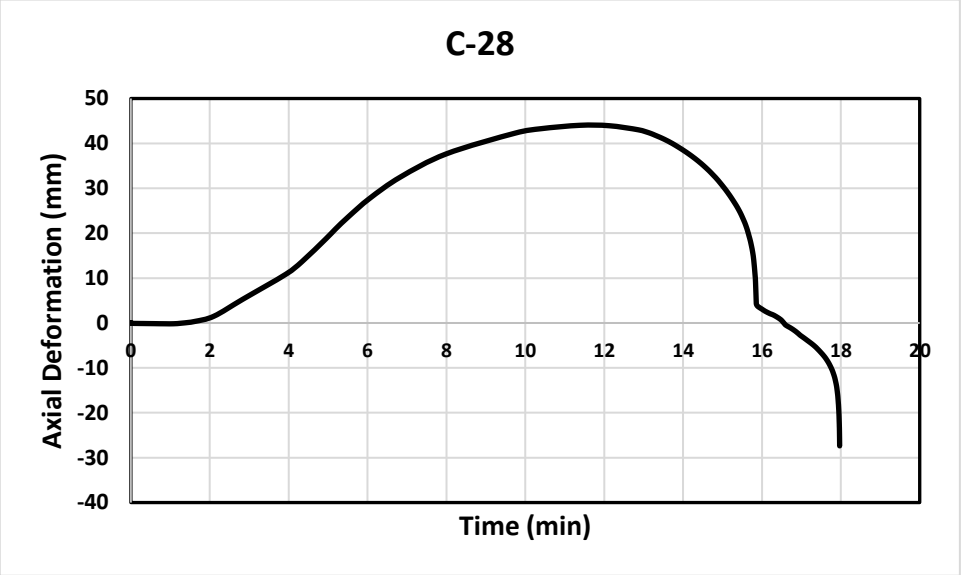
C-28
Axial Deformation (mm)
50
40
30
20
10
0
-10
-20
-30
-40
0
2
4
6
8
10
12
14
16
18
20
Time (min)

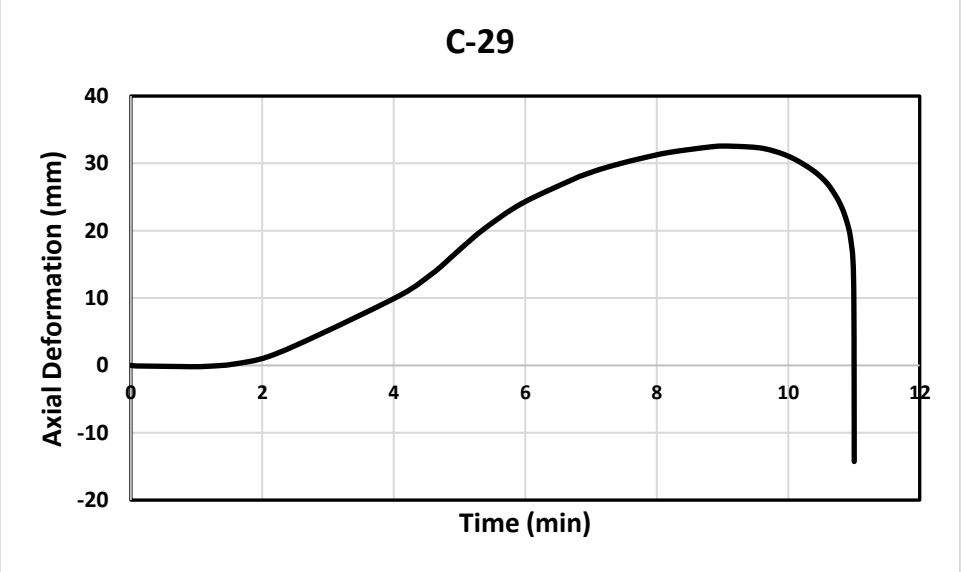
C-29
Axial Deformation (mm)
40
30
20
10
0
-10
-20
0
2
4
6
8
10
12
Time (min)

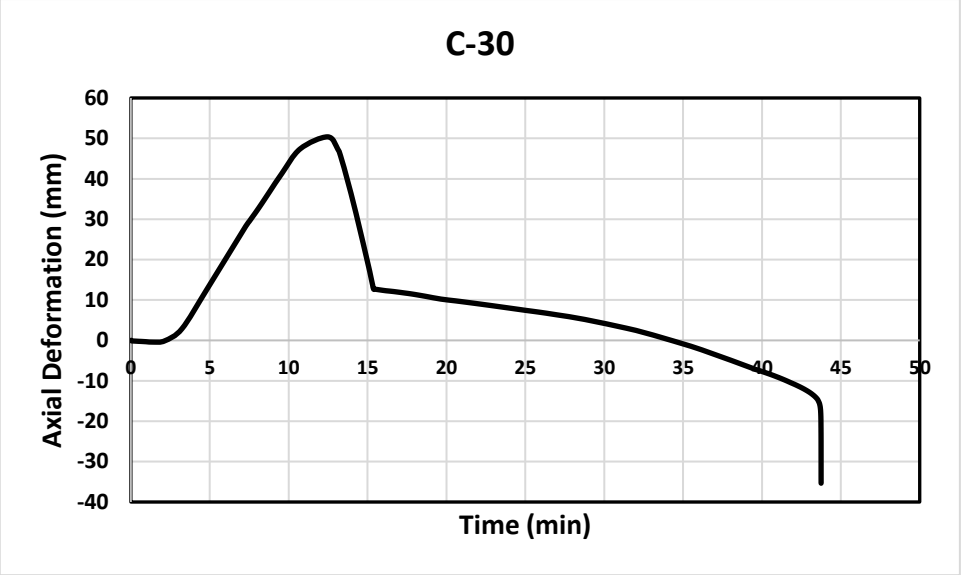
C-30
Axial Deformation (mm)
60
50
40
30
20
10
0
-10
-20
-30
-40
0
5
10
15
20
25
30
35
40
45
50
Time (min)

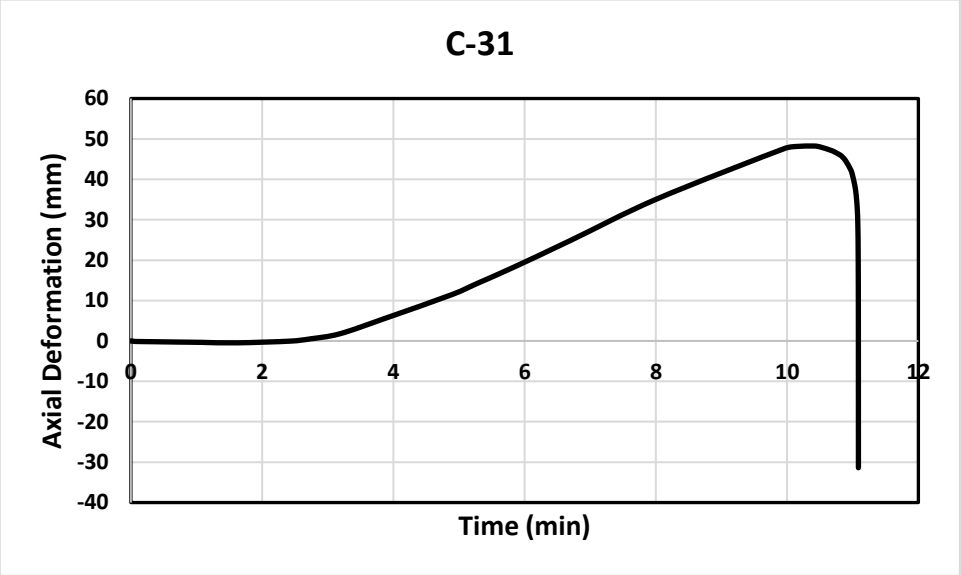
C-31
Axial Deformation (mm)
60
50
40
30
20
10
0
-10
-20
-30
-40
0
2
4
6
8
10
12
Time (min)

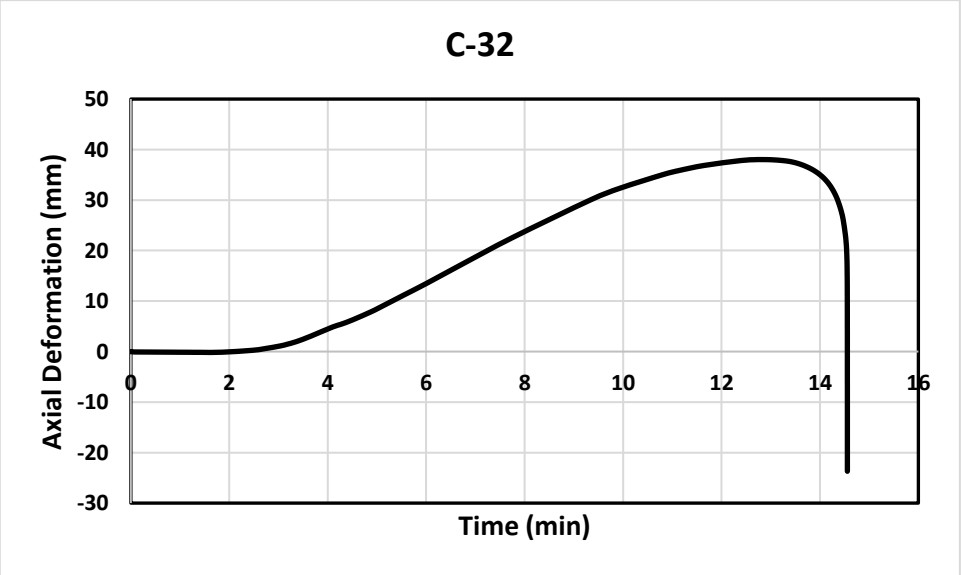
C-32
Axial Deformation (mm)
50
40
30
20
10
0
-10
-20
-30
0
2
4
6
8
10
12
14
16
Time (min)